Building and characterizing low sulfide instrumented waste rock piles:

Pile design and construction, particle size and sulfur characterization, and

initial geochemical response

by

Lianna Jane DeGeer Smith

A thesis
presented to the University of Waterloo
in fulfillment of the
thesis requirement for the degree of
Master of Science
in
Earth Sciences

Waterloo, Ontario, Canada, 2009

Author's declaration

I hereby declare that I am the sole author of this thesis. This is a true copy of the thesis, including any required final revisions, as accepted by my examiners.

I understand that my thesis may be made electronically available to the public.

Abstract

A rigorous laboratory and field study to measure and compare low sulfide waste rock and drainage characteristics at various scales has been designed and implemented. The field study was constructed at the Diavik diamond mine in the Northwest Territories, Canada. Three well-instrumented, 15 m high test piles and three sets of 2 m scale experiments were constructed from run of mine waste rock. Diavik waste rock is comprised of granite and metasedimentary biotite schist country rock. The biotite schist contains the sulfide minerals, principally pyrrhotite. Diavik segregates waste rock based on sulfur content. One test pile contains waste rock with 0.035 wt. % S, within the operational sulfur target of < 0.04 wt. % S for lower sulfur waste rock designation. The second pile contains waste rock with 0.053 wt. % S, lower than the operational sulfur target of > 0.08 wt. % S for the higher sulfur waste rock designation. The third pile contains a core of 0.082 wt. % S waste rock which is within the operational sulfur target of > 0.08 wt. % S for the higher sulfur waste rock. The third pile has been re-contoured and capped by a 1.5 m of till and 3 m of lower sulfide waste rock as per the current reclamation plan for the higher sulfide waste rock pile. The test piles were built using standard end-dumping and push-dumping methods. Instrumentation was installed at the base of each pile and on four angle of repose tip faces, as well as in the covers of the third pile. Instrumentation was selected to measure matrix flow, pore water and bulk pile geochemistry, gas-phase oxygen and carbon dioxide concentrations, temperature evolution, microbiological populations, permeability to air, and thermal conductivity, and to resolve mass and flow balances. Instruments were designed to permit measurements at multiple scales. During pile construction samples of the < 50 mm fraction of waste rock were collected. The samples were analysed for sulfur content and particle size distribution. Particle size distributions for the

lower and higher sulfur waste rock are similar but the higher sulfur waste rock has a higher proportion of fines. Particle size distributions for both waste rock types suggest the piles have rock-like characteristics rather than soil-like characteristics. Sulfur concentrations vary with the scale of measurement: concentrations of smaller size fractions are higher than larger size fractions. Acid-base accounting using standard methods and site-specific mineralogical information suggest that the waste rock is acid generating. However, when acid-base accounting is compared to effluent pH and alkalinity, the data suggest these calculations may be conservative. Drainage effluent from the higher sulfide test pile was measured for field parameters (pH, Eh, alkalinity) and dissolved cations, anions and nutrients. The geochemical equilibration model MINTEQA2 was used to interpret potential geochemical controls on solution chemistry. The pH decreases to < 5, concomitant with the minimum alkalinity of < 1 mg L^{-1} (as total $CaCO_3$), suggesting all available alkalinity is consumed by acid-neutralizing reactions. Sulfate concentrations reach 1995 mg L^{-1}. Calculated saturation indices of Al (oxy)hydroxides and Al hydroxysulfate species, and pH suggest Al oxyhydroxide dissolution is buffering pH at times. Concentrations of Fe (< 0.37 mg L^{-1}), Fe (II) and calculated saturation indices of Fe(III) (oxy)hydroxide species suggests that Fe is predominantly Fe(III) and Fe is being controlled by secondary mineral precipitation. The dissolved trace metals Mn (<19.2 mg L^{-1}), Ni (<10.4 mg L^{-1}), Co (<1.8 mg L^{-1}), Zn (<0.9 mg L^{-1}), Cd (<0.015 mg L^{-1}) and Cu (<0.05 mg L^{-1}) show increasing trends in the effluent water. No dissolved trace metals appear to have secondary mineral controls. Elevated SO_4, Al, Fe dissolved metals Ni, Co, Zn, Cd and Cu, and depressed pH values suggest sulfide mineral oxidation is occurring in the test pile containing 0.053 wt. % S.

Acknowledgements

Dedication

It is with inexpressible gratitude that I dedicate this thesis to my parents, Mary and Bill, for

their unwavering support for my adventures here, there and everywhere.

Table of Contents

Appendices

List of Tables

List of Figures

Chapter 1: Introduction

Mining waste rock stockpiles are large, heterogeneous, unsaturated piles. When the waste rock contains sulfide minerals acid mine drainage (AMD) can develop when the sulfide minerals are exposed to atmospheric oxygen. In subaerial environments sulfide minerals oxidize and release acidity, sulfate, and dissolved metals to water draining through the waste material. The generation of AMD can persist for hundreds of years or longer (e.g. Nordstrom and Alpers, 1999; Moncur et al., 2005) and is a concern for mining companies because of potential environmental impacts, and monitoring and treatment costs.

AMD generation is controlled by coupled physical and biogeochemical processes that control mineral weathering rates and physical hydrologic flow. Studies of physicochemial processes in mine tailings have defined physical and biogeochemical controls on AMD production (e.g. Blowes and Jambor, 1990; Blowes et al., 1991; Al et al., 1997; Johnson et al., 2000; Moncur et al., 2005; Gunsinger et al., 2006). However, the coupled AMD processes occurring within waste rock pile systems are more difficult to characterize. Waste rock piles are physically and geochemically heterogeneous with internal structures created during dump construction, particle sizes ranging from silt to boulders, variable saturation, variable geochemical composition and variable reactivity of the particles. These heterogeneities influence pile permeability and thermal regimes, which in turn influence oxygen transport within the pile, transient flow regimes, microbiologically-mediated sulfide oxidation rates, mineral weathering rates, and spatial and temporal solute loadings in drainage.

Recent waste rock pile characterization studies have advanced the understanding of the physicochemical processes occurring in waste rock piles. Strömberg and Banwart (1994) developed a geochemical model for leachate genesis and element cycling for the pyritic waste

dump at the Aitik mine in Sweden and successfully compared results to drainage water composition from the dump. The same authors conducted large column experiments to determine weathering kinetics (Strömberg and Banwart, 1999a) and acid-consuming processes (Strömberg and Banwart, 1999b) in Aitik waste rock. Linklater et al. (2005) used a numerical coupled chemistry and transport model that included gas and heat transport, water infiltration, and geochemical reactions to reproduce observed field data at the Aitik waste dump. Lefebvre et al. (2001a) provided conceptual models for multiphase transfer processes in pyritic waste rock from the Doyon mine in Canada and the Norhalde mine in Germany with a focus on oxygen transport and heat transfer processes associated with AMD. A follow-up study successfully applied numerical simulations to the same dumps (Lefebvre et al., 2001b). Sracek et al. (2004) collected and analysed leachate samples from the unsaturated and saturated zone of the Doyon mine dump. Conclusions included that goechemical and physical processes associated with AMD are strongly coupled, and strong spatial and temporal variations in dump geochemical and physical behaviour are due to waste rock texture and mineralogy. Nichol et al. (2005) describes a flow and tracer test on 5 m high waste heaps at the Cluff Lake mine, Canada with conclusions of highly variable flow and transport properties, and difficulties in measuring and quantifying wetting front velocities, net infiltration and contributions of different flow mechanisms to outflow. Stockwell et al. (2006) deconstructed, sampled and characterized a 12 m high waste heap at the Key Lake mine, Canada. Difficulties with the Key Lake study included the inability to develop a field-based soil-water characteristic curve or discern a correlation between pore water chemistry and the tendency for preferential flow. Difficulties were attributed to waste rock compositional and textural heterogeneity. Although these waste rock studies have advanced waste dump characterization, each study illustrates the

complexity in characterizing unsaturated waste dumps and the need for additional studies, including laboratory and field comparisons, to form a body of literature that covers a range of geochemical and physical properties of mine waste material at various scales.

A rigorous waste rock pile study is underway at the Diavik diamond mine in the Canadian Arctic as part of a complementary laboratory and field research program. Three instrumented waste rock piles ("test piles") and three sets of 2 m scale experiments were constructed. The overall goals of the program are to (1) characterize the flow, thermal, and gas transport regimes, and the geochemical and microbiological processes in low sulfide waste rock piles in a continuous permafrost environment; and (2) to quantitatively assess the application of small-scale laboratory column experiments in the prediction of the effluent quality of unsaturated waste rock stockpiles. The field portion of the study consists of three test piles and three sets of 2 m scale experiments that were constructed from 2005 to 2007. Instrumentation was selected to measure matrix flow, pore water and bulk pile geochemistry, gas-phase oxygen and carbon dioxide concentrations, temperature evolution, microbiological populations, waste rock permeability to air, and thermal conductivity, as well as to resolve mass and flow balances. Monitoring is expected to continue beyond 2010. The laboratory portion of the study consists of 36 humidity cells that were initiated in 2005 (Blowes et al., 2007).

1.1   Site description and background

The test piles were constructed at the Diavik diamond mine in the Northwest Territories, Canada (Figure 1-1). The Diavik diamond mine is an operating open-pit and underground diamond mine that is located on a 20 km^2 island within the lake Lac de Gras. The Diavik site is located in the Arctic desert region of central Canada, an area of continuous

permafrost. Winter conditions persist from September through May with an average annual ambient temperature of -8.5 °C, an average maximum temperature of 18 °C occurring in July and an average minimum temperature of -31 °C occurring in January/February. Average precipitation for the area is 280.3 mm, about 60% of which occurs as snow (Environment Canada, 2008).

The Diavik kimberlite ore occurs as pipes hosted in Archean granite and pegmatite granite country rock. The granite and pegmatite granite are massive and moderately to coarsely crystalline and contain metasedimentary biotite schist xenoliths. The region is cut by a series of Proterozic diabase dikes (Blowes and Logsdon, 1998). Static tests conducted during the feasibility stage indicated that the granite and pegmatite granite had similar compositions, contained only trace sulfide minerals, and would be non acid generating with very low potential to leach metals during weathering. The biotite schist contains locally disseminated pyrrhotite [$Fe_{1-x}S$]. Static tests indicated the biotite schist is potentially acid generating because of the pyrrhotite content, very low carbonate content, and a silicate mineral assemblage that provides little neutralization potential (Blowes and Logsdon, 1998). The diabase dikes are considered geochemically insignificant because of their very low abundance.

During mining, Diavik segregates the waste rock based on sulfur content before it is excavated and stockpiled. Waste rock is categorized as Type I (<0.04 wt % S), Type II (0.04 to 0.08 wt % S) or Type III (>0.08 wt % S). Type I waste rock is comprised of granite and is considered environmentally benign. Little Type II rock is produced and is comprised primarily of granite with minimal biotite schist. Type II rock is considered to have low or no acid-generating potential. Type III rock is comprised of predominantly granite with a greater amount of biotite schist. The biotite schist content causes the Type III rock to be potentially

acid generating. Each rock type is stockpiled in a designated containment area. Type I rock only is used for construction material and excess Type I stockpiled. The permanent stockpiles will contain up to 200 Mt of waste rock, of which up to 40% will be Type III waste rock. The current closure and reclamation plan for the Type I pile is contouring the slopes to 18.4° (3H:1V) for geotechnical stability. The Type II pile plan includes contouring the slopes to 18.4° (3H:1V) and covering the area with 4 m of Type I. The Type III pile is planned to be re-contoured to 18.4° (3H:1V), capped with a 1.5 m thick low permeability layer of till to act as barrier to water and oxygen infiltration, and covered with 3 m of Type I rock to act as the freeze-thaw layer (DDMI, 2006).

The contoured and layered Type III closure plan, as well as uncovered piles of Type I waste rock and Type III waste rock resting at the angle of repose of waste rock (38°) form the basis of the test piles research program. The three test piles are referred to as the Type I pile (uncovered test pile of Type I waste rock), the Type III pile (uncovered test pile of Type III waste rock), and the Covered pile (re-contoured and capped test pile based on the current closure plan for the Type III dump).

1.2   Scope

This thesis consists of five chapters and describes the design and construction of the test piles (Chapter 2), the particle size and sulfur characteristics of the test piles (Chapter 3), and the initial geochemical response of the Type III test piles during the first field season (Chapter 4). Each chapter is written in the form of an article to be submitted to a refereed journal and provides an abstract, introduction, site description, methods, results and discussion, and summary and conclusions. Chapter 1 provides a global introduction and Chapter 5 compiles the overall summaries and conclusions. As a consequence of this format, there is

some repetition in the introductory material provided in each of the chapters. Additional

authors will be acknowledged for chapters submitted to the refereed journal, and the chapters

will be modified slightly to reflect changes due to additional authorship.

1.3 Figures

Figure 1-1: Location of Diavik diamond mine

Chapter 2: Design and construction of field-scale instrumented waste rock piles in the Canadian Arctic

2.1   Overview

The physicochemical processes that affect acid mine drainage (AMD) in unsaturated waste rock piles and the capabilities of small-scale laboratory experiments to predict AMD from waste rock are not well understood. A rigorous laboratory and field study to measure and compare low sulfide waste rock and drainage characteristics at various scales has been designed and constructed. This paper describes the design and construction of three well-instrumented waste rock piles ("test piles") and 2 m scale field experiments at the Diavik diamond mine in the Nortwest Territories, Canada. The test piles are comprised of granitic and sulfide-bearing metasedimentary waste rock excavated during open pit mining operations. One test pile contains waste rock with a target sulfur content of <0.04 wt. % S; the second test pile contains waste rock with a target sulfur content of >0.08 wt. % S; and the third test pile consists of the higher sulfide waste rock re-sloped and capped with a low permeability till layer and a low sulfide waste rock cover. The test piles are approximately 15 m high with bases of 50 m by 60 m for the first two piles and 80 m by 125 m for the third pile. Instrumentation was selected to measure matrix flow, pore water and bulk pile geochemistry, gas-phase oxygen concentration, temperature evolution, microbiological populations, waste rock permeability to air, and thermal conductivity, as well as to resolve mass and flow balances. Instrument locations were selected to characterize coupled physicochemical processes at multiple scales and the evolution of those processes over time. A sufficient number of each instrument type survived the pile construction process to allow adequate characterization of the physicochemical processes occurring at various scales in the test piles.

2.2   Introduction

Waste rock is excavated during ore recovery and is commonly stockpiled at mine sites in large, heterogeonous, unsaturated waste rock piles. Waste rock contains concentrations of sulfide minerals that are not economic to recover. When sulfide minerals contained in mine wastes are exposed to atmospheric oxygen and water, acid mine drainage (AMD) develops as bacterially-mediated sulfide minerals oxidation releases acidity, sulfate and dissolved metals to the water draining from the waste materials. The generation of AMD can continue for hundreds of years (Nordstrom and Alpers, 1999; Moncur et al., 2005) and can be a costly environmental concern for mining companies.

AMD from waste rock piles is controlled by the geochemical characteristics of the waste rock that affect mineral weathering rates and the physical hydrologic processes that control unsaturated flow (Smith et al., 1995; Strömberg and Banwart, 1999; Lefebvre et al., 2001a; Smith and Beckie, 2003). Mineral weathering rates in waste rock are governed primarily by oxygen supply, transport limitations at the particle scale and the rate of reaction on the particle surface, which may be catalyzed by bacteria (Blowes et al., 1991). Sulfide mineral reaction rates are temperature-dependent due to bacterial activity and reductions in reaction rate with decreasing temperature have been found to follow Arrhenius behaviour (e.g. Janzen et al., 2000; Benner et al., 2002).

Advective-convective oxygen supply depends on the pile permeability, geometry and thermal regime (Ritchie, 1994, 2003). Particle scale oxygen transport at a mineral surface may be limited by the diffusion of reactants through alteration rims surrounding the waste rock particle, as described conceptually and mathematically by the shrinking core model (Levenspiel, 1972; Cathles, 1979; Davis and Ritchie, 1986, 1987; Davis et al., 1986; Wunderly

9

et al., 1996; Lefebvre et al., 2001b; Mayer et al., 2002, 2003). The transport and release of dissolved constituents from the oxidation zone is controlled by the physical hydrogeologic processes that control unsaturated flow through the pile. These processes include diffusion, flow through the porous matrix and preferential flow through more permeable pathways. The interaction between these flow and transport processes is complex because of waste pile heterogeneity (Nichol et al., 2005), structure and geometry (Lamontagne et al., 1999; Lefebvre et al., 2001a). Transient flow conditions can result in spatial variations in flow patterns and flow intensities, which lead to spatial variability in flushing rates and, thus, variability in drainage solute and metal loadings (Velbel, 1993; Nichol et al., 2005). Smith and Beckie (2003) identified the limited insight into these processes that control water flow through unsaturated waste rock as the greatest source of uncertainty in predicting metal and solute loadings in drainage.

Physical and geochemical properties and heterogeneities in unsaturated waste rock piles are complex and may not be adequately represented by limited laboratory testing programs. Therefore, laboratory results may not accurately predict drainage quality for full-scale waste dumps. Kinetic tests that attempt to characterize field conditions include humidity cell tests and column experiments. Humidity cells provide estimates of weathering rates by exposing crushed rock to repeated wetting and drying cycles to accelerate mineral oxidation, alteration and secondary mineral formation (ASTM, 2000; Lapakko, 2003). Leaching column experiments vary in design (e.g. Strömberg and Banwart, 1999; Bennett et al., 1999) but can provide information such as acid, sulfate and metal loadings in the leachate from crushed rock samples. However, laboratory experiments lack large-scale heterogeneities and structures observed in the field which can alter the biogeochemical and physical hydrologic regimes that

10

affect in situ mineral weathering rates. The small volumes (~1 kg) of rock crushed to < 10 mm in diameter used in standard laboratory tests (e.g. ASTM, 2000) cannot capture grain size influences or structural heterogeneities observed in waste rock piles. Humidity cell and column experiments have been found to over predict mineral weathering rates by two or more orders of magnitude (Velbel, 1993; Malström et al., 2000). In northern regions, these complexities are compounded by annual freeze-thaw cycles which affect mineral weathering rates and water transport, and accelerate physical weathering.

Mining companies conventionally use laboratory experiments to predict drainage quality and the potential environmental impacts of waste rock pile drainage. Resolving the scale-dependence of weathering rates will help mining companies and regulators design and evaluate waste management and reclamation plans with greater confidence. Field-scale experiments are needed to evaluate the accuracy and applicability of approaches used to scale laboratory experiment results to make predictions for full-scale facilities.

Three instrumented waste rock piles ("test piles") and three sets of 2 m scale experiments were constructed in the Canadian Arctic as part of a complementary field and laboratory research program. The overall goals of the program are to (1) characterize the flow, thermal, and gas transport regimes, and the geochemical and microbiological processes in waste rock piles in a continuous permafrost environment; and (2) to quantitatively assess the application of small-scale laboratory experiments in the prediction of the effluent quality of unsaturated waste rock stockpiles. This paper describes the design and construction of field-scale, well instrumented waste rock piles and 2 m scale experiments at an operating mine, and discusses the effectiveness of the construction methods.

2.3 Site description and background

The test piles were constructed from 2004 to 2007 at the Diavik diamond mine, an operating open-pit and underground diamond mine. The mine is located 300 km northeast of Yellowknife, Northwest Territories, Canada in the treeless "barren lands" of the Canadian Arctic (Figure 2-1). The mine is located on a 20 km^2 island located within the oligotrophic lake Lac de Gras which forms the headwaters of the Coppermine River. The ore bodies are located beneath Lac de Gras. A series of water-retaining dikes were constructed around the ore bodies to permit open-pit mining.

The Diavik site is located in the Arctic desert region of central Canada, an area of continuous permafrost. Winter conditions persist from September through May and a thin 1.5 m to 5 m thawed layer develops in the ground surface in warm months. The mean annual air temperature in the area (1998 to 2007) is −8.5 ºC, with average maximum temperatures of 18 ºC occurring in July and minimum temperature of −31 ºC occurring in January/February. The area receives little precipitation: an average of 280.3 mm for 1999-2006 with about 60% occurring as snow (Environment Canada, 2008). The prevailing winds are northerly to easterly with an average speed of 4.75 m s^{-1} (17 km h^{-1}) recorded for 2006 (DDMI 2007).

The Diavik mine started production in 2003 and approximately 10 million carats of gem-quality diamonds are extracted annually from three diamondiferous kimberlite pipes accessed by two open pits. Underground infrastructure is being developed to access the lower reaches of the same pipes. Diavik kimberlite ore occurs as pipes hosted in Archean granite and pegmatitic granite country rock that is massive and moderately to coarsely crystalline. The granite contains metasedimentary biotite schist xenoliths. The region is cut by a series of Proterozoic diabase dikes (Blowes and Logsdon, 1998). The granite and pegmatitic granite

country rock contain only trace sulfides and are considered non-acid generating with very low potential to leach metals during weathering. Although the diabase dikes contain trace sulfides this rock is considered geochemically insignificant because of its very low abundance. The biotite schist is potentially acid generating as it contains locally disseminated pyrrhotite ($Fe_{1-x}S$) and other minor sulfides. The biotite schist contains little carbonate and the silicate mineral assemblage provides little neutralization potential (Blowes and Logsdon, 1998).

Waste rock excavated during operations is analysed for sulfur content and segregated into Type I (<0.04 wt % S), Type II (0.04 to 0.08 wt % S) or Type III (>0.08 wt % S). Type I is comprised primarily of the non-acid generating granite. The Type I rock is used primarily for construction material, with only minor volumes stockpiled. Type II rock is comprised predominantly of granites with minimal biotite schist and is considered to have low or no acid generating potential. Type III rock is comprised of granites and a greater amount of biotite schist. Due to the biotite schist content, Type III rock is considered potentially acid generating. Each waste rock type is stockpiled in a designated containment area. At the end of the mine life up to 200 Mt of waste rock, up to 40 % of which may be Type III, will be stockpiled in 60 to 80 m high permanent piles covering 3.5 km^2. Diavik proposes to implement a progressive reclamation strategy for the Type II and Type III waste dumps based on engineered dry covers (DDMI, 2006). The Type II pile is planned be contoured to 18.4° (3H:1V) slope and capped with 4 m of Type I material such that the active freeze-thaw zone occurs within the Type I layer, allowing permafrost to form in the Type II core. The Type III pile is planned be contoured to 18.4° (3H:1V) slope, capped with a 1.5 m low permeability layer of till as a barrier to water and oxygen infiltration, and covered with a 3 m Type I layer to act as the active freeze-thaw layer. The 18.4° slope angle was chosen to ensure geotechnical stability and to

ensure a safe working slope for standard mining equipment. The Type III pile layered cover design and feasibility are based on studies and numerical simulations that indicate a layer with a low oxygen diffusion coefficient would reduce the sulfur oxidation rates in the core of the pile (ANSTO, 1998).

The current contoured and layered Type III closure plan and uncovered piles of Type I waste rock and of Type III waste rock resting at the angle of repose form the basis for the test pile research program. The three test piles are referred to as the Type I pile (uncovered test pile of Type I waste rock), the Type III pile (uncovered test pile of Type III waste rock), and the Covered pile (Figure 2-2). The Covered pile is based on the Type III dump closure plan with contoured slopes, till cover and clean Type I waste rock cover.

2.4   Test piles design and construction methods

2.4.1   Design basis

The test pile dimensions were based on preliminary thermal modelling using the two-dimensional finite difference reactive transport code SULFIDOX (Brown et al., 1999; Brown et al., 2001; Linklater et al., 2005). SULFIDOX modelling conducted by the Australian Nuclear Science and Technology Organization (ANSTO) simulated gas and water transport; kinetically controlled sulfide oxidation, including the heat generated by sulfide oxidation; heat transfer; and ice formation and melting in a Type III rock pile (Blowes et al., 2006) . Based on modelling results, the pile dimensions were set to be 15 m high to ensure that thermal conditions at the top of the pile would not affect the stability of the permafrost at the pile base. The dimensions of the pile bases were determined by the slope angles for a 20 m wide crest. A minimum 20 m wide crest was required for equipment access. The Type I and Type III pile

bases were 50 m by 60 m, determined by the 38º (1.3H:1V) angle of repose of waste rock; and the Covered pile base was 80 m by 125 m, based on contoured 18.4º (3H:1V) slopes and a 24 m wide crest.

Preliminary SULFIDOX modelling results also were used to determine the location of the instrumentation planes within the pile. Simulated oxygen concentrations indicated that near ambient O_2 levels will persist throughout the piles when oxidation rates are $<10^{-9}$ kg O_2 m^3 s^{-1} but an oxygen gradient would develop with lower concentrations in the core of the pile when a higher oxidation rate of 10^{-8} kg O_2 m^3 s^{-1} was applied. Thermal profiles changed from the surface inward in response to seasonal temperature oscillations. Even at the highest oxidation rates considered (10^{-8} kg O_2 m^{-3} s^{-1}) the heat generated by sulfide oxidation was not sufficient to affect the thermal behaviour of the test piles. To capture the potential oxygen gradients and seasonal fluctuations in the temperature regime, four instrumentation planes were selected along angle of repose tip face slopes spaced 5 m apart and 5 m from the final slope surface.

Past studies of full-scale waste rock piles have analysed data collected from instruments installed in vertical boreholes drilled post-construction or from sampling points external to the waste dump (e.g. Harries and Ritchie, 1981, 1983; Lefebvre et al., 1993; Ericksson et al., 1997; Tan and Ritchie, 1997). Two separate studies constructed smaller-scale field experiments by methods other than standard waste dump construction methods to study the physical mechanisms of water movement (Nichol, 2005; Stockwell, 2006).

The Diavik test piles were constructed by standard waste dump construction methods and instrumentation was installed on the base of the piles, four angle of repose tip faces, and the transition between the access ramp and the piles. Instruments were installed on the angle of repose tip faces with the intention of assessing the influence of the construction method on the

thermal and physicochemical behaviour of the piles. Additional instrumentation was installed in the till and Type I layers of the Covered pile to monitor cover performance. Instrument distributions were designed to contribute to the characterization of coupled physicochemical processes and the evolution of those processes over time, contribute to the characterization of mineral weathering rates at various scales, and to constrain numerical model input parameters for low sulfide, unsaturated waste rock piles in which discontinuous zones of ice may form. Instrumentation was selected to measure matrix flow, pore water geochemistry, gas-phase oxygen concentration, temperature evolution, microbiological populations, waste rock permeability to air and thermal conductivity, as well as to resolve mass and flow balances.

Figure 2-2 illustrates the test pile site plan. Figures 2-3 through 2-5 illustrate the instrument distribution on each of the pile bases; the instrument line access at the crest of each pile; and the distribution of instruments on the most heavily instrumented face for each pile, respectively. Figure 2-6 illustrates the vertical distribution of the probes that measure matrix flow and pore water geochemistry.

2.4.2 Instrumentation

A basal drain system was installed on an impermeable liner at the base of each pile to capture all drainage water that flows to the base of the piles. The basal drainage system for all piles consists of a high density polyethylene (HDPE) impermeable liner installed on a graded, engineered base and a perforated 150 mm (6 in) schedule 40 PVC drain line that sits directly on the liner to collect and convey the drainage to discharge points (Figure 2-7). A lined 0.5 m berm surrounds the perimeter of each test pile to ensure all infiltration reports to the basal drain system and a 0.3 m crush layer covering the liner and PVC drain line protects the basal drain system. The PVC drain line is heat-traced with mineral insulated (MI) heating cable set to

maintain temperatures between 5 and 10 ºC. The Type I and Covered pile basal drainage systems collect water diagonally across the pad at a 1.4% grade, draining at a low point in the southwest and northwest corners, respectively. The Type III pile drainage system was modified to capture drainage in the active zone if permafrost forms within the core: water is directed from the centre of the pad to the perimeter at 0.5% grade and discharges from two low points at the northwest and southwest corners. Drain lines extending from the base of the piles are not perforated and are housed in 200 mm (8 in) nominal insulated HDPE pipe for mechanical protection and to minimize heat loss to the environment. All drainage is directed to instrumentation huts for continuous measurement of flow and geochemical parameters.

A series of three basal lysimeter clusters were located on the 0.3 m thick crush layer at the base of each pile. Each cluster consists of two 2 m by 2 m lysimeters and two 4 m by 4 m lysimeters (Figure 2-7) that drain to individual flow measurement and geochemical sampling points located in instrumentation trailers. The lysimeter walls are between 0.6 and 1.0 m high to prevent wicking effects. The entire lysimeter box was lined with HDPE liner to capture all water reporting to the lysimeter area. Beneath the liner the lysimeter base is graded at 1% to a corner drain, and was built in layers: 150 mm (6 in) crush bulk fill roughly graded; 16 mm (0.63 in) clean crush or 20 mm (2 in) minus crush graded to the drain; 100 mm (4 in) thick Styrofoam brand insulation (R40); and a 0.2 m esker sand layer. Self-regulating heating cable rated at 2.4 W m^{-1} (8 W ft^{-1}) was installed within the sand layer to ensure that any water reporting to the lysimeter base would flow to the drain and the insulation layer was installed to ensure the heat from the heat trace was directed upward towards the lysimeter base. Thermistors were installed to monitor heat released from the heating cable to the pile base.

A 37.5 mm (1.5 in) compression fitting sealed the drain to the HDPE liner and silicone sealant was applied to ensure the seal was water-tight. A 0.15 m slotted and screened 37.5 mm (1.5 in) schedule 40 PVC pipe was inserted into the compression fitting to prevent fines from entering the drain line. Each drain line consists of 37.5 mm (1.5 in) schedule 40 PVC pipe installed at 0.5 to 1.5% grade. Each drain line is heat-traced with MI cable and contains 6.25 mm (0.25 in) outside diameter (OD) low density polyethylene (LDPE) or nylon tubing that can be used to periodically flush the drain lines of secondary mineral precipitates. The drain lines for each cluster are housed in a 200 mm (8 in) nominal HDPE insulated pipe from the lysimeter to the instrumentation trailer for mechanical protection and to minimize heat loss to the pile and environment.

Two basal lysimeter clusters were located under the crest of the pile and one cluster was located beneath the batter where a vertical flow path from the surface of the pile to the base would be shorter. Waste rock fill for the basal lysimeters ensures textural and compositional consistency with the pile material thereby reducing the possibility of a capillary break or anomalous geochemical reactivity caused by fill material. The basal lysimeters are designed as part of the examination of the scale-up effects in flow variability and solute loadings between the bulk flow at the base, the different sized basal lysimeters, and soil water solution samplers (SWSS). SWSS are used to collect pore water samples in the pile interior.

The basal lysimeters and basal drains permit the calculation and comparison of the flux-averaged solute loads and spatial variability in flow for three different measurement scales. SWSS provide point measurements of pore water solute loadings by extracting pore water using applied suction from an area of influence of centimetres to tens of centimetres around the probe tip. Solute masses measured in SWSS samples are considered point measurements rather

than flux-averaged or volume-averaged concentrations because heterogeneities in the host medium can cause variability in pore water velocities, and pore water bypassing the matrix material (i.e. in preferential flow paths) may contain a solute mass significantly different from matrix pore water masses (Parker and van Genuchten, 1984; Litaor, 1988). Nichol et al. (2005) note that samples obtained from SWSS represent the flux-averaged concentration of the pore water based on the flux caused by the applied suction rather than the flux resulting from wetting front movement within the waste rock pile. SWSS, basal lysimeter and basal drain samples are analysed for pH, Eh, EC, TDS, acidity/alkalinity, anions, major ions, and trace metals. The relationship between SWSS point measurements and flux-averaged concentrations from the different-sized basal lysimeters and the basal drain will be determined as field data is collected.

Calibrated time-domain relfectometer (TDR) probes provide volumetric water content of waste rock within an area of influence of a few centimetres. TDR probes measure the dielectric permittivity of the waste rock, which can be used to calculate volumetric water content. TDR methods, limitations and probe designs for waste rock studies are discussed by Nichol et al. (2002; 2003). Point measurements of volumetric water content through space and time can be used to monitor wetting front propagation through the waste rock pile in which discontinuous zones of ice may form, and may indicate the locations and/or transient nature of any preferential flow paths. The velocity of the wetting front movement calculated using volumetric water contents measured by a series of TDR probes at various depths can be compared to the flow measured in each of the different-sized basal lysimeters and the basal drains.

TDR probe and SWSS distributions were selected to align vertically above the basal lysimeters. Probes were located on Face 1 and 2 of the Type I and Type III piles, and Face 2 and 3 of the Covered pile (Figure 2-6). SWSS were co-located within 0.5 m of TDR probes to correlate matrix flow and pore water chemistry. Co-located TDR probes and SWSS, which can also act as in-pile tensiometers, may permit matric suction measurements at the same location as moisture content measurements with the objective of determining site-specific soil-water characteristic curves necessary for flow interpretation and flow and reactive transport modelling. Resolving in-situ soil-water characteristic curves for waste rock have been problematic and have not been determined successfully in previous waste rock pile studies (Stockwell et al., 2006; Marcoline, 2007).

The TDR probes installed in the test piles were built using a design described by Nichol et al. (2002; 2003). SWSS were Hoskin Scientific model e-127-1920F1L12-B02M2. TDR probes and SWSS require hydraulic contact with matrix material to provide reliable readings and samples. To ensure the probes were surrounded with fine-grained material Nitex nylon screen commonly used for hydrogeological piezometer installations was sewn into bags, the probes were placed in the bags, and the bags were filled with either Type I (for the Type I pile) or Type III (for the Type III and Covered piles) waste rock screened to < 25 mm fraction. The nylon screen bags for the TDR probes had dimensions larger than the anticipated area of influence of 0.05 m of the probe. SWSS Nitex nylon screen bag dimensions were sized to be 0.175 m by 0.325 m to ensure good hydraulic contact between the tip and matrix material. TDR probe cable and SWSS tubing were strung through a common 50 mm (2 in) flexible PVC protective conduit that contained either MI or self-regulating heating cable for each profile the Type I and Type III piles. Tubing from each SWSS profile installed in the Covered pile was

strung through a common 50 mm (2 in) flexible PVC protective conduit that contained MI heating cable. Cables from TDR probes installed in the Covered pile were strung through individual flexible 25 mm (1 in) PVC conduits.

Internal pile gas compositions contribute to the determination of O_2 gas transport mechanisms, O_2 consumption rates from the oxidation of sulfide minerals, and CO_2 production rates from the dissolution of carbonate minerals. Measured O_2 consumption rates can be used to determine sulfide mineral oxidation rates if sulfide oxidation is assumed to be the only process consuming O_2 (Linklater et al., 2005). Gas sampling lines were located on the pile bases, on all instrumentation faces, and on the boundaries between the access ramp and the piles. Gas sampling lines consist of either nylon tubing 3.13 mm OD and 0.58 mm wall thickness, or low density polyethylene tubing 0.63 mm (0.25 in) inside diameter (ID) strung through flexible and/or rigid PVC conduit. The conduit was used to ensure the gas sampling tubes were not crushed or damaged during construction. Holes 25 mm (1 in) in diameter were drilled in the protective conduit at the designated sampling intervals, the gas sampling tubing was strung through each access port, and spray foam insulation was injected into the port annulus to prevent airflow within the conduit.

Gas sampling lines were installed with a high density, >200 sample points per pile, to provide redundancy and for detailed spatial measurements to capture any influence of compositional or textural heterogeneity on sulfide oxidation rates. Gas sampling lines were located immediately adjacent to SWSS (Figure 2-5 and Figure 2-6) such that O_2 concentrations could be determined for geochemical equilibrium and reactive transport modelling. Boundary gas composition information is provided by basal gas sample lines installed at the base and transition face.

Three basal thermistor strings were installed beneath each of the Type I and Type III piles, and two strings were installed beneath the Covered pile. The basal thermistors have sensors at 1 m intervals and were installed in vertical boreholes 10 m into bedrock and in 25 m long horizontal trenches within the crushed kimberlite or esker sand beneath the HDPE liner (Figure 2-3). An additional thermistor string was installed 10 m into bedrock about 100 m to the northeast of the Type I test pile as a control for bedrock thermal profiles. Basal thermistor strings provide thermal profiles beneath each pile and provide boundary condition information for thermal transport simulations. Thermistor strings located on tip faces monitor internal pile temperatures, and thermistor strings located in the till layer of the Covered pile monitor the thermal condition of the upper till layer (Figure 2-5). Near-surface thermistor sensors, including strings installed in the Type I cover of the Covered pile, monitor the development of the active layer as the ambient temperatures fluctuate. All thermistors were connected to dataloggers to continuously record temperatures at 12 hr intervals. The thermistor strings installed within the pile and cover layers were protected by 50 mm (2 in) flexible PVC conduit with 25 mm (1 in) diameter holes drilled above and below the sensor to improve sensor response time. Additional holes 150 mm above and below the sensors were injected with spray foam insulation to prevent air-flow within the conduit between sensors. Sensor spacing varies for all thermistor strings with typical spacings of 1 to 3 m within the pile and 1 to 5 m in the covers of the covered pile (Figure 2-5). Thermistor data will allow the determination of spatial and temporal variations in permafrost formation, as well as the quantification of thermal contributions from exothermic sulfide oxidation reactions. Spatial and temporal fluctuations in permafrost formation may play an important role in the hydrologic flow regime within the

pile by activating, deactivating or altering preferential flow paths,and thus transport of sulfide oxidation reaction products, within the piles.

Thermal conductivity measurements will be combined with temperature measurements to quantify seasonal heat fluxes, the rate of heat generation from sulfide oxidation, and to monitor seasonal convective heat transport. Pile thermal conductivity depends on the composition of the pile including local moisture content and waste rock heterogeneity. Thermal conductivity access ports consisted of 75 mm (3 in) schedule 40 PVC pipe and were located on all faces to maximize the spatial distribution of measurements. The access ports allow a thermal conductivity probe to be lowered to discrete depths within the piles. The probe is a linear heat source and temperature measurement system, and is described in detail in Tan and Ritchie (1997). The probe heat source is activated for several hours and the associated temperature responses are monitored during the heating and cooling phases. The resulting data are analyzed to provide a measurement of the thermal conductivity of the pile (Blackford and Harries, 1985). Alternate methods of determining thermal conductivity values measure waste rock pile thermal diffusivity and use thermal capacity of pile material to estimate thermal conductivity, but these methods may not adequately predict interior pile thermal conductivity values (Ritchie, 2003).

Air permeability probes were located on the tip face with the highest density of instruments (Face 1 in the Type I and Type III piles and Face 2 in the Covered pile). Air permeability probes consist of 75 mm (3 in) perforated plastic balls connected to one 0.635 cm (0.25 in) OD and one 0.953 cm (0.375 in) OD nylon tube with Swagelok fittings. N_2 gas is forced through the probe via the 0.635 cm (0.25 in) tube into the pile over a range of flow rates, the rise in gas pressure is measured through the 0.953 cm (0.375 in) tube and the

permeability is calculated (ADI and ANSTO, 1997; Bennett and Ritchie, 1993). Instrument lines and fittings were protected by 25 mm (1 in) and 50 mm (2 in) flexible PVC conduit, respectively. As with the gas sampling lines, spray foam insulation was injected at the top and bottom of the conduit to reduce airflow within the conduit. Air permeability tests are conducted periodically using an automated datalogging instrument to control and monitor N_2 flow rate and monitor gas pressure. Waste rock permeability to air can provide insight into O_2 replenishment mechanisms to the pile interior. Rapid O_2 replenishment compared to O_2 consumption rates by sulfide mineral oxidation increases the spatial extent of active sulfide oxidation (ADI and ANSTO, 1997).

Microbiology access ports were designed to determine if the chemolithotropic bacteria groups *Thiobacillus* and *Acidithiobacillus* populate waste rock piles with internal temperatures below 0 ºC. Bacterially-mediated oxidation of pyrrhotite, the predominant sulfide mineral in Diavik waste rock, can be described by the reaction:

$$Fe_{1-x}S + (2 - \tfrac{1}{2}x)O_2 + xH_2O \rightarrow (1-x)Fe^{2+} + SO_4^{2-} + 2xH^+ \tag{1}$$

Leduc et al. (1993) and Hubert et al. (1994) have shown that some isolates of the mesophile Fe-oxidizing bacteria *Thiobacillus ferrooxidans* can grow and oxidize Fe at temperatures as low as 2 ºC. Although the viability and activity of these bacterial populations in permafrost environments is not well constrained, these populations may be important to sulfide mineral oxidation in Diavik waste rock. Microbiology access ports consisted of 0.5 m long well screens threaded to 50 mm (2 in) schedule 40 PVC conduit. The medium for microbiological colonization is museum-grade crushed pyrite. Approximately 10 g of crushed pyrite was placed in nylon screen bags. The pyrite bags were autoclaved and remained sealed until installation. During installation the pyrite bags were lowered down the conduits to the

screened intervals. Five pyrite bags per interval were installed on separate leads. One pyrite

bag was extracted from each depth immediately post-construction and one will be extracted

annually thereafter to determine the extent of bacteria colonization and to infer biogeochemical

effects on water quality. Microbiology growth media are located at 2 m, 5 m, 8 m and 11 m

depth on Face 1 of the Type I pile; 2m, 4 m , 6 m and 10 m depth on Face 1 on the Type III

pile; and 5 m, 7 m , 8.5 m and 10.5 m depths on Face 2 of the Covered pile (Figure 2-5).

2.4.3   Construction methods

The foundations of each pile consisted of waste rock fill overlain by crushed kimberlite

(for the Type I pile base) or esker sand (for the Type III and Covered pile bases). The crushed

kimberlite and esker sand was graded to predetermined grades to ensure all infiltrating

meteoric water would be directed to the design discharge points. An impermeable HDPE liner

was installed on the graded foundation to capture all water infiltrating to the base of the piles.

For protection during pile construction of the Type I and Covered piles, the HDPE liner was

covered with geotextile and 0.3 m thick layer of Type I 50 mm (2 in) crush with fine fractions;

the Type III pile HDPE liner was covered with a 0.3 m thick layer of Type I 50 mm crush that

did not contain fine fractions. A 2 m thick protective layer of waste rock was placed by a dozer

on the crush layer for additional protection of basal instrumentation during pile construction.

Haul trucks and dozers end-dumped and push-dumped waste rock from the top of the

access ramp onto and across the completed pile bases to the design station of each

instrumentation face. During pile construction the < 50 mm fraction of the waste rock was

sampled as representative matrix material from the loads dumped by haul trucks at the crest of

the pile, as well as from each instrumentation face. On each instrumentation face instruments

were installed according to the design distribution by lowering the instruments from the top of

the pile to the base or, for thermistor installation only, raised from the pile base to the crest

(Figure 8a). Sample and instrument locations on the face were accessed using a 41 m (125 ft)

man-lift and surveyed using a global positioning system (GPS). To protect the face instrument

lines during pile construction, while also ensuring consistent waste rock properties, an

excavator covered the face instrument lines with waste rock to a thickness of 0.5 to 1 m (Figure

2-8b). After the instrument lines were covered, haul trucks and dozers continued dumping and

pushing waste rock to the next instrumentation face.

Instrument lines terminating at the crest of the pile were covered by HDPE covers and

buried beneath 0.5 m of waste rock for protection before pushing to the next tip face resumed.

After pile construction was completed, the instrument lines were excavated and extended to the

surface to permit data logging and/or manual measurements.

The Covered pile Type III waste rock core was re-sloped by a dozer to a 18.4° (3H:1V)

slope. A dozer placed a 1.5 m layer of till on the Type III core. Crest instruments were

extended and re-buried in the till layer to allow mining equipment access to the crest of the pile

to place the 3 m Type I cover. Due to limited equipment availability the instruments buried in

the till were not excavated until December and January, after the till had frozen. An excavator

fitted with a chisel tip exposed the buried instrument lines. Unfrozen till was placed around the

lines and additional instruments were installed in the till layer to complete the 1.5 m till layer.

Additional instruments also were installed in the T1 layer of the crest. An excavator placed the

3 m Type I cover on the crest to complete the Covered pile.

2.4.4   Construction of 2 m scale experiments

In addition to the three piles, 2 m scale experiments were constructed in a dedicated

research area to collect flow and geochemistry data for the active freeze-thaw zone and to

provide an additional scale for measuring physicochemical processes. Four 2 m diameter, 2 m high HDPE tanks were installed on a graded bench bedded with esker sand. The tanks were installed such that the top of the tanks were level with the ground surface. A single layer of boulders (0.3 m) were hand-placed on the bottom of the tanks to protect the tanks from punctures during filling by an excavator. The tanks continuously drain via 37.5 mm (1.5 in) PVC pipe with heating cable to an instrumentation trailer for flow and geochemistry measurements. Two tanks and the adjacent area were filled with < 2 m Type III waste rock to simulate the Type III pile. Two more tanks and the adjacent area were filled with < 2 m Type I waste rock. The surrounding area was filled to grade with Type I waste rock to emulate the smooth topography of the pile crests.

An additional two tanks were designed to mimic the covered pile active layer. The tanks were installed within a "pocket" about 20 m by 20 m by 20 m deep of Type III material to ensure the tanks were surrounded below and around with Type III waste such that the tanks would be exposed to any thermal influence exerted by the surrounding Type III waste rock. Vertical standpipes of 50 mm (2 in) schedule 40 PVC pipe with slotted ends were installed in the two tanks to permit periodic water level measurements and geochemical sampling. Each tank was filled with <2 m Type III waste rock. The surrounding Type III waste rock was re-contoured to a 18.4° (3H:1V) slope, covered with 1.5 m of till and 3 m of Type I rock as per the Covered pile design.

2.4.5 Instrumentation trailers

The basal drains, all basal collection lysimeters, and the Type I and Type III 2 m scale experiments drain to heated instrumentation trailers. The drainage is directed through a series of flow-through cells which allow for periodic collection of geochemical samples, continuous

pH measurements, and continuous EC measurements. Tipping bucket rain gauges maintain a continuous record of flow from each of the discrete sample areas (Figure 2-9).

2.5   Results and discussion

Full-scale dump construction methods were applied effectively for test pile construction. Standard end-dumping and push-dumping methods were used to construct the test piles to ensure consistency with the full-scale dump construction. Instrument lines installed on the tip faces were covered with waste rock delivered during pile construction to ensure consistent material composition and grain size distribution of the < 0.5 m fraction. During pile construction a traffic surface was created on the crest of the pile as is observed on full-scale waste dumps. However, excavating the instruments disrupted the crest traffic surface. The excavations were backfilled with the spoil material to maintain the original grain size distribution and waste rock composition. The disruption of the crest may have increased the crest permeability. Similarly, the permeability of the 0.5 m cover over the instrument lines may be different from the permeability of the test pile and/or the full-scale waste dump because the material was placed with an excavator rather than by end-dumping methods.

Initial indications of construction effectiveness for the Type I and Type III piles are supported by the number of instrument lines that survived the construction phase. Instrument survival rates varied with the type of instrument. In the Type I and Type III piles, TDR probes had the lowest survival rate at 40% and 46%, respectively. SWSS survival was 44% in the Type I pile and 61% in the Type III pile. Gas sampling lines, thermal conductivity ports, thermistor strings and air permeability probes all had > 80% survival (Table 2-1).   The construction method for the face instruments was tested prior to pile construction by installing test instruments on an angle of repose face and using standard mining equipment to place and

28

dump material, as per the conceptual construction method. These successful trials contributed to the high instrument survival rates during pile construction. Also contributing to the high survival rate of tip face instruments was the flexible PVC conduit protecting the instrument cables and tubing.

Basal collection lysimeter drain lines were tested after the lysimeters and drain lines were installed and no failures were identified. The post-construction success rate will be determined as water infiltrates the pile and reports to the basal collection lysimeter system.

The low survival rate of SWSS on Face 1 of the Type III pile, the first series of instruments to be installed during this study, probably was caused by the tubing leads being pulled from the probe and/or the porcelain cups being crushed. For subsequent SWSS installations, epoxy was applied to the probe connections and the SWSS were sufficiently covered by a protective cover of waste rock. Low TDR probe functionality may not be caused primarily by the construction method, but rather the probe functionality was not verified before installation in the Type I and Type III piles. Probe function for probes installed in the Covered pile was confirmed prior to installation: 10 of the 11 TDR probes installed in the Covered pile survived.

Face 2 instruments on the Type III pile had a low survival rate compared to other faces. Face 2 instrument lines were inadequately covered with waste rock placed by an excavator before end-dumping and push-dumping continued. During construction it was suspected that the TDR probes on Face 2 had a high probability of failure as a result of the inadequate cover thus additional TDR probes and co-located SWSS were installed on Face 3 of the Type III pile.

Covered pile instrument survival rates are lower because of difficulties in recovering instrument lines buried in the frozen till layer. Instrument lines buried in the till were

uncovered and extended through the till and Type I covers during the winter because suitable excavation equipment was not available earlier in the construction season. Instrument recovery from the till layer required the use of an excavator fitted with a chisel tip. Some instrument lines were abandoned during this excavation step. Furthermore, extending instrument leads in cold weather was challenging because SWSS tubing, gas lines, thermal conductivity conduit and protective conduit become rigid and brittle in the sub -40°C ambient temperatures experienced during the instrument recovery phase. Many instrument lines cracked or shattered during excavation or when handled as the instruments were extended. This type of failure was the primary cause of the low survival rates of the SWSS, gas sampling lines and thermal conductivity access ports in the Covered pile.

The Type I pile had a lower density of instruments installed within the pile but the survival rates are comparable to those of the Type III pile. The instrument survival rates of the Type I, Type III and Covered piles are anticipated to be sufficient to monitor the pile physicochemical and thermal evolution of Type I waste rock, Type III waste rock and the current Diavik closure option for the Type III full-scale dump, respectively.

2.6   Conclusions

Three large-scale waste rock piles were constructed in the Canadian arctic to measure water flow, thermal conductivity, gas evolution and transport, and geochemical and microbiological processes. One pile was constructed from granite waste rock classified as non-acid generating. The second pile was constructed from potentially acid-generating waste rock consisting of granite rock with some amount of biotite schist. The third pile was constructed from the potentially acid-generating waste rock that was contoured and capped with low

permeability till and clean waste rock, as per the current reclamation plan for the Diavik Type III dump.

The types of instruments installed within the piles can provide measurements to quantify coupled physicochemical process occurring in waste dumps and the evolution of those processes over time. Quantifying the coupled processes will contribute to characterizing ARD development from low-sulfide waste rock piles in a permafrost environment and to permit a comparison of field-scale results to the 2 m scale experiments and laboratory predictions.

Initial results of instrumentation tests indicate that construction methods were effective. Overall construction effectiveness and the value of instrumentation on the angle of repose tip faces will be evaluated as measurements and samples from tip face instrumentation are collected as part of the monitoring phase, and compared to previous waste dump instrumentation projects.

2.7   Tables

Table 2-1: Internal pile instrument distribution and survival rates for each test pile. Individual gas sampling ports were not rated for survivability because of the transient nature of blockages (e.g. ice). Long-term integrity of individual gas ports will be identified over time.

Instrument	Type I Pile		Type III Pile		Covered Pile	
	No. Installed	No. Survived	No. Installed	No. Survived	No. Installed	No. Survived
TDR	10	4	28	13	11	10
SWSS	25	11	44	27	20	6
Air permeability probes	6	6	6	6	8	3
Gas sampling lines	30	29	30	25	34	28
Thermal conductivity ports	12	11	12	12	12	3
Thermistor strings	10	10	10	10	24	12
Microbiology access ports	3	3	3	3	3	0

2.8   Figures

Figure 2-1: Location of Diavik diamond mine

Figure 2-2: Site plan for the test piles field study

Type I/Type III
Instrumentation
Trailer

Type I pile

N

Type III pile

Upper Collection
Lysimeters

Access Ramp

UCL
Instrumentation
Trailer

Covered pile

Covered Pile
Instrumentation
Trailer
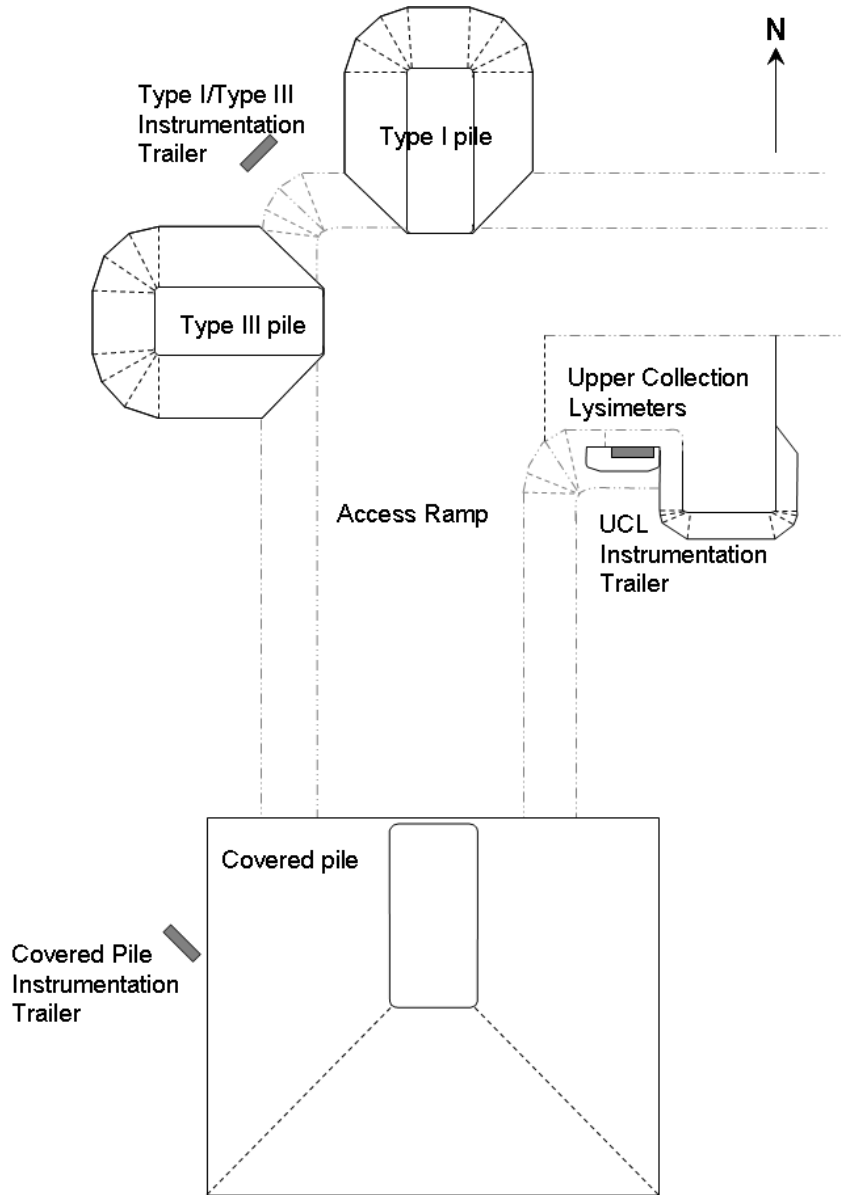
Legend for Figures 2-3 to 2-6:

◇	Gas sample point	⊗	Air permeability probe
○	Thermal conductivity port (plan view)	⊕	Thermistor bead
⫽	Thermal conductivity port (cross section)	—	Impermeable liner
●	TDR probe	⋰	Basal drain line
●	SWSS	⟋	Basal collection lysimeter drain line
◉	Microbiology access ports	☐	Basal collection lysimter (BCL)

Figure 2-3: Pile instrument base dimensions and instrument configuration for (a) Type I pile; (b) Type III pile; and (c) Covered pile

(a)
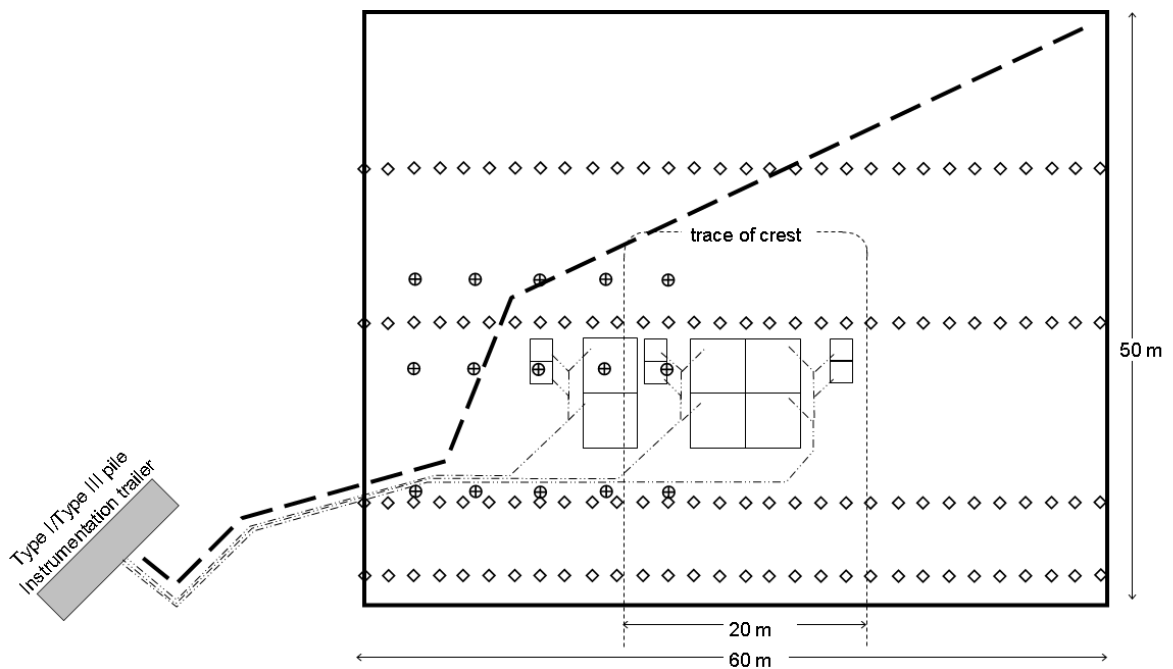
(b)
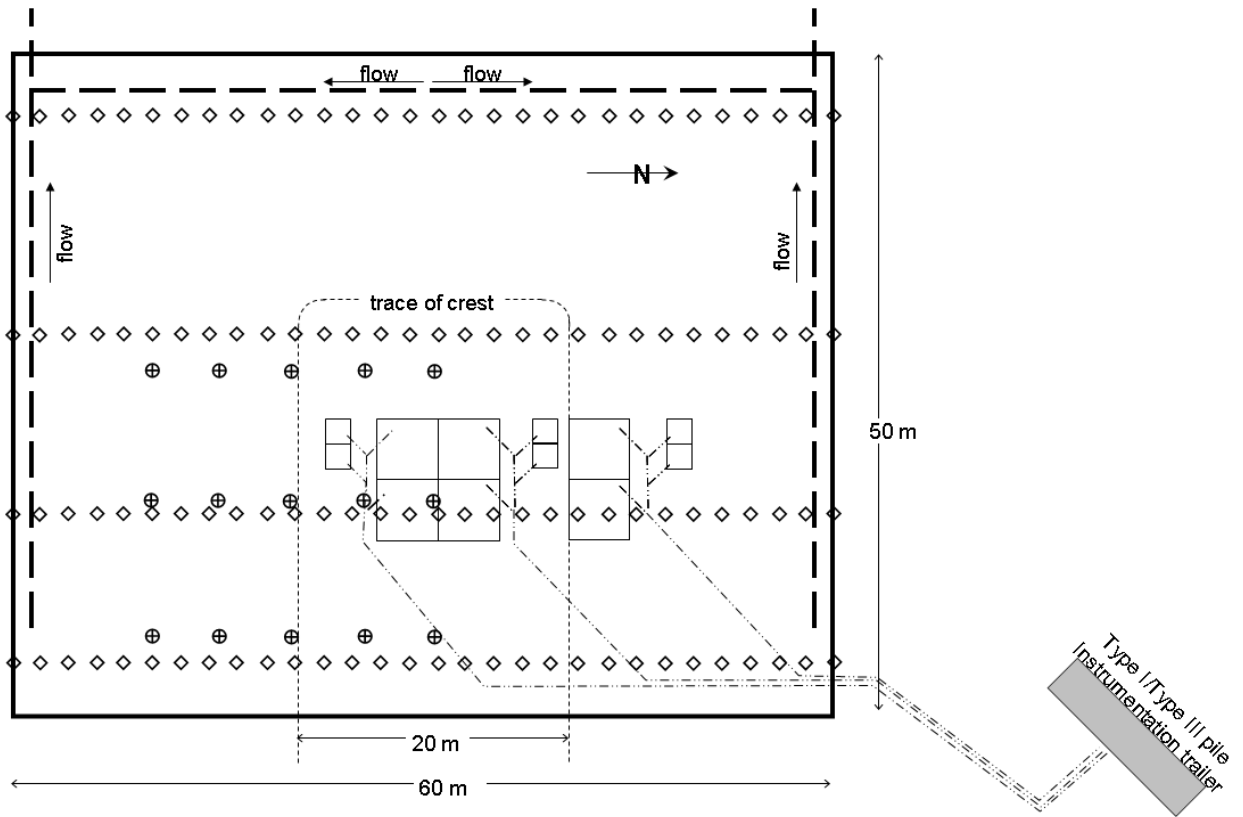
(c)
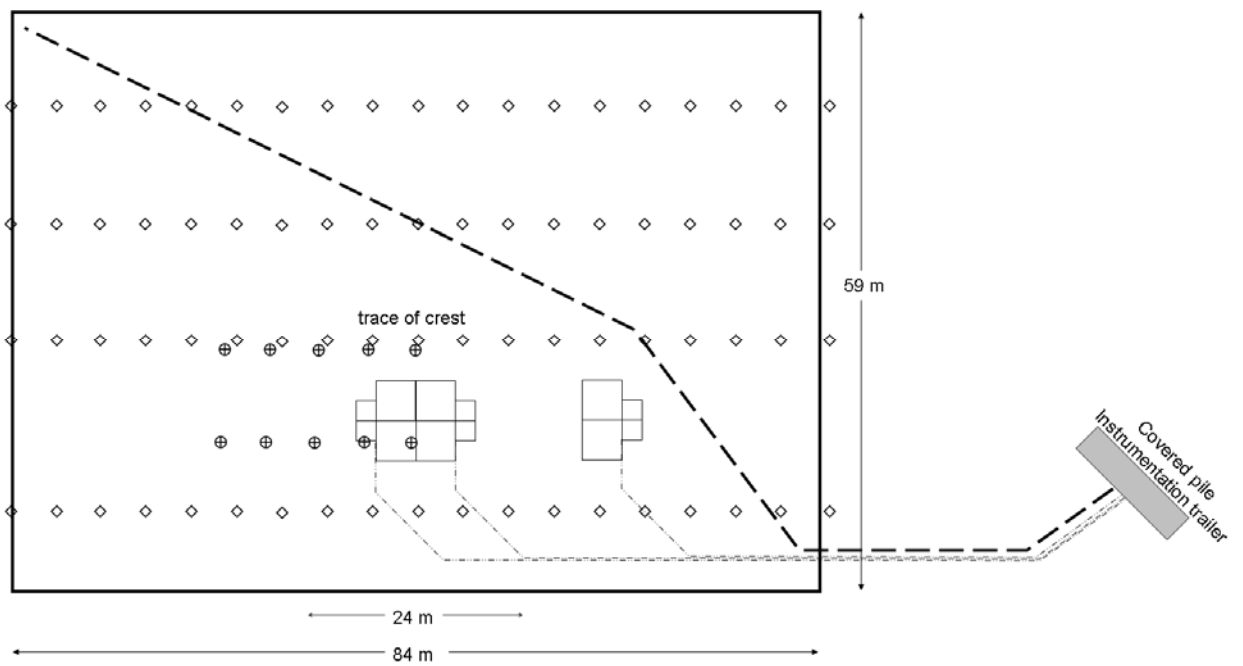
Figure 2-4: Plan view of instrument distribution at crest for (a) Type I pile; (b) Type III pile; and (c) Covered pile

(a)
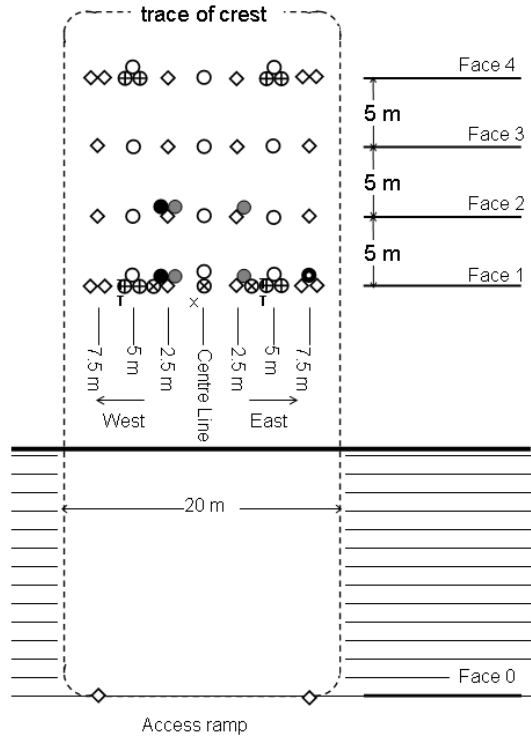
(b)
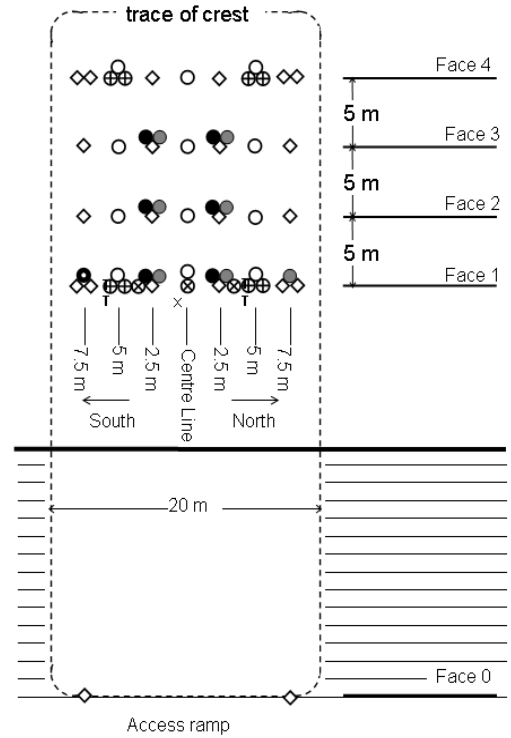
(c)
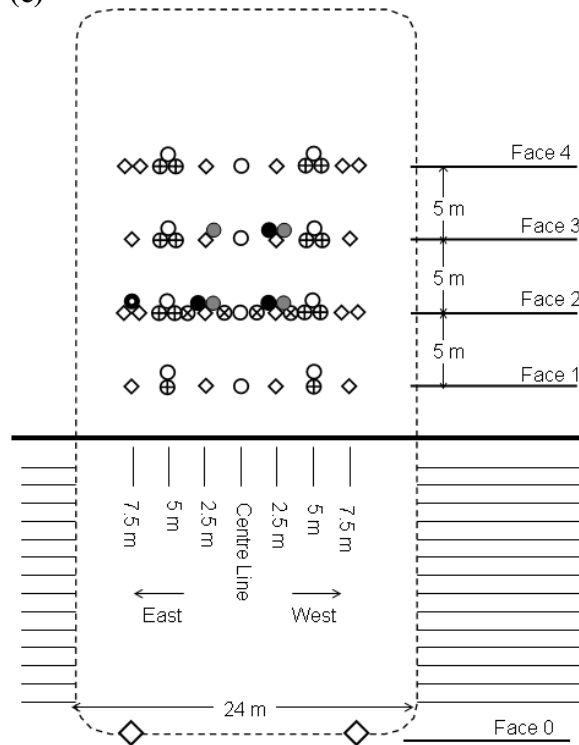
Figure 2-5: Cross sectional view of interior pile instrument distributions and dimensions for the most heavily instrumented face of (a) Type I pile; (b) Type III pile; and (c) Covered pile

(a)
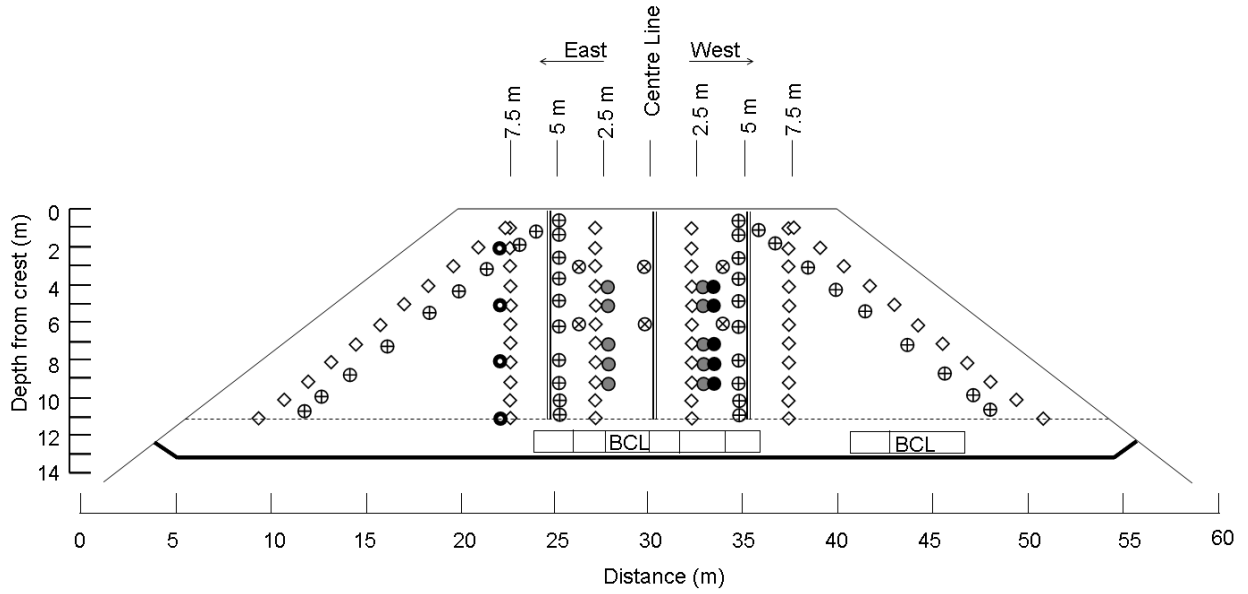
(b)
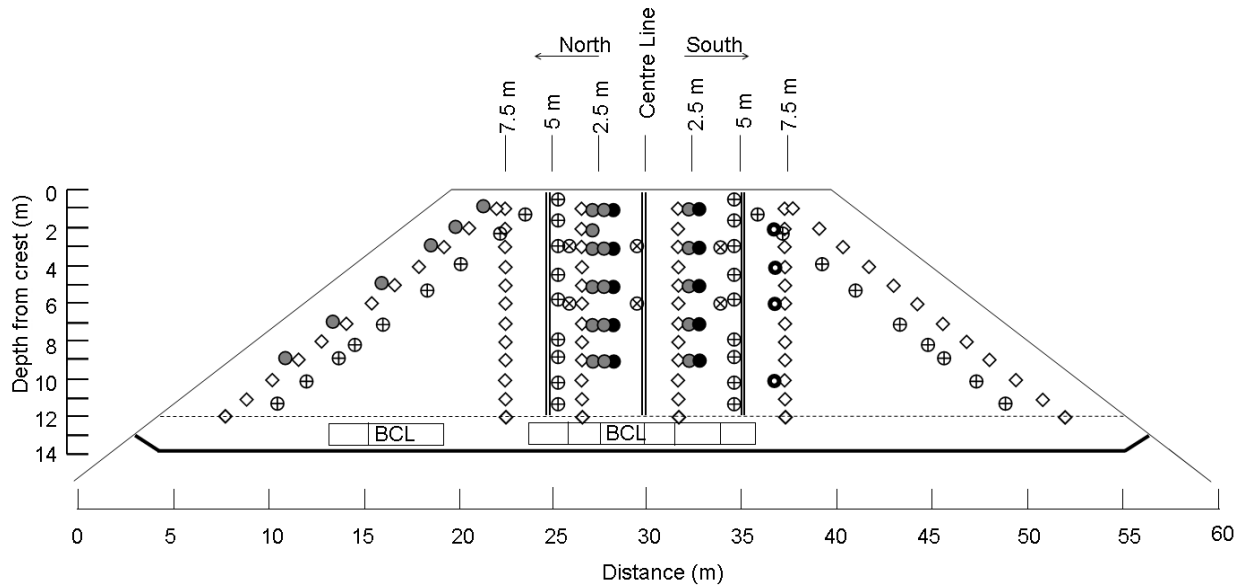
(c)
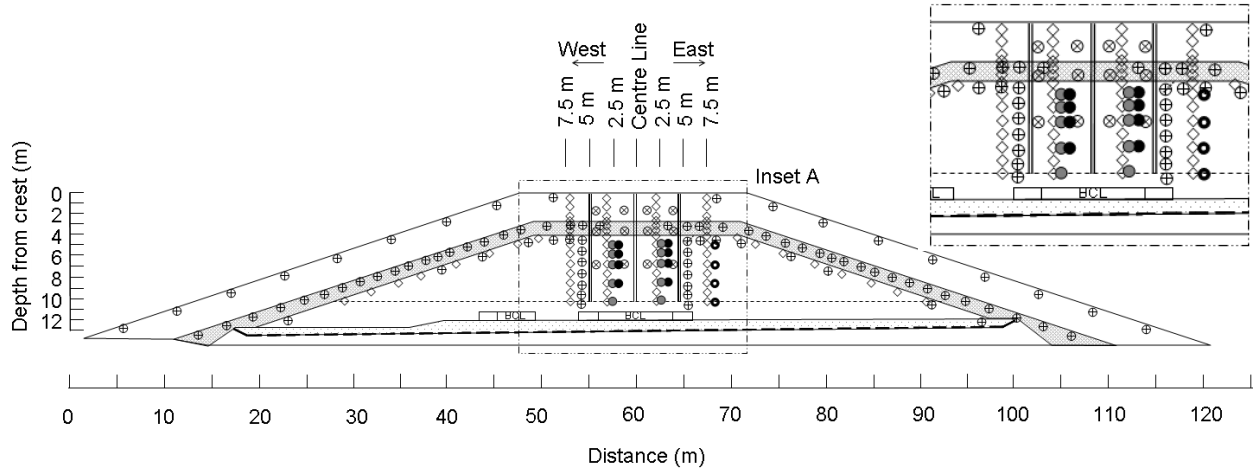
Figure 2-6: Profile view of vertical alignment of TDR and SWSS in the (a) Type I pile; (b) Type III pile; and (c) Covered pile.

(a)
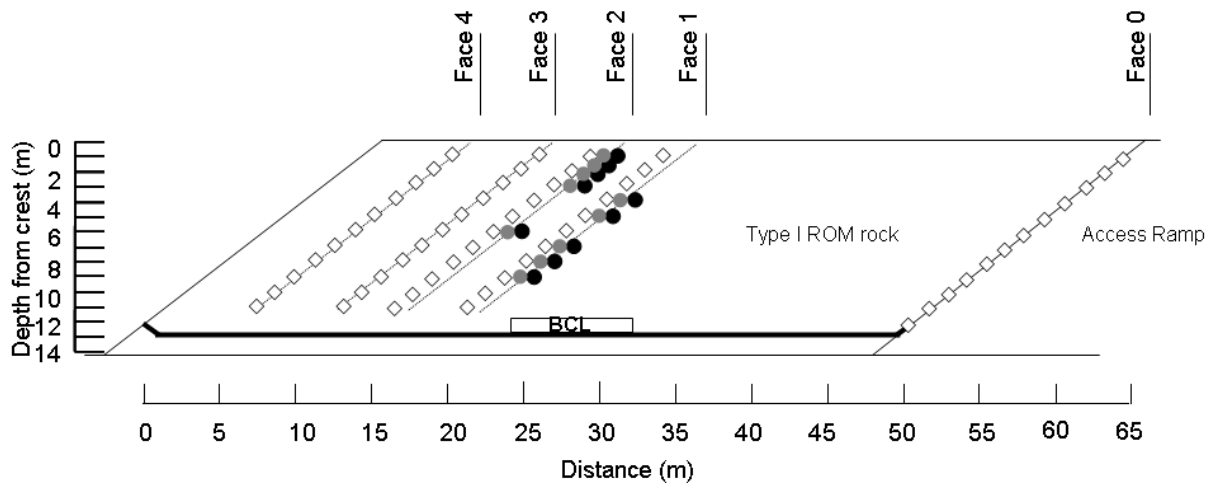
(b)
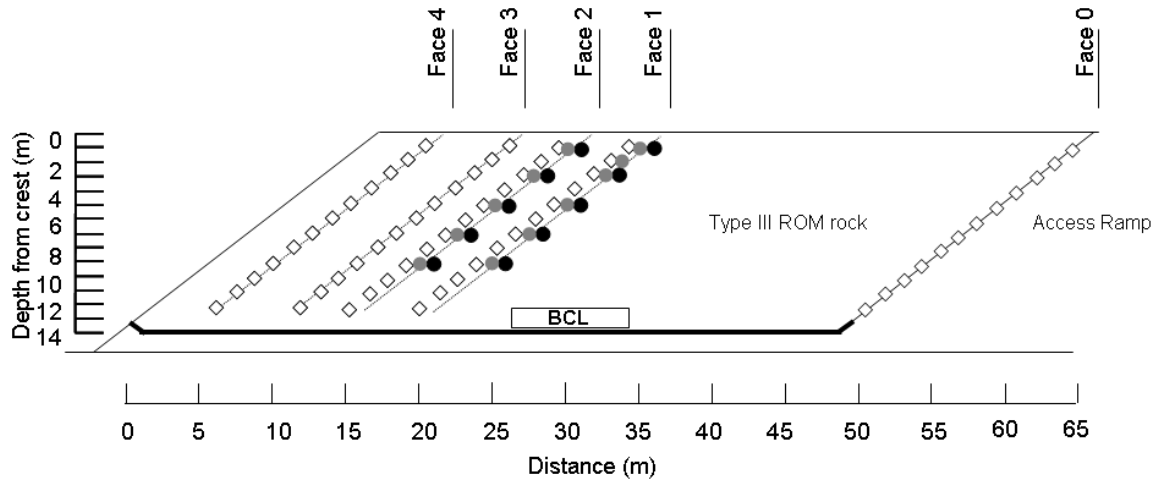
(c)
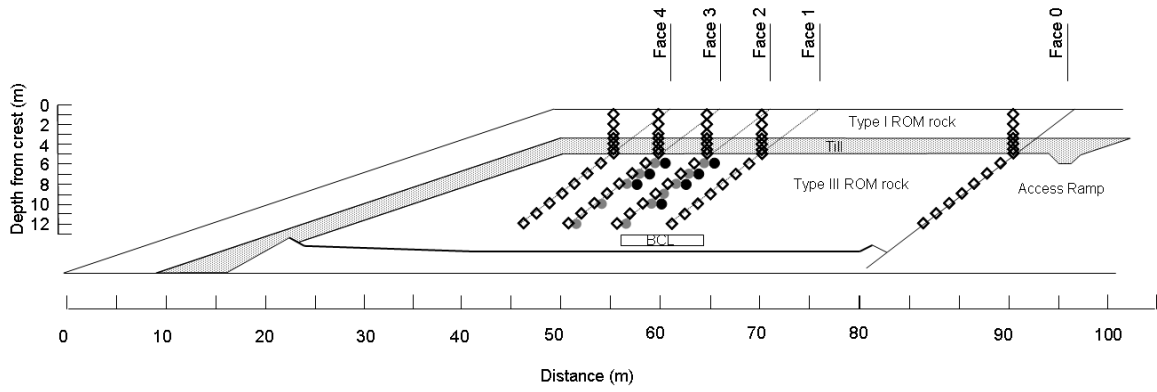
Figure 2-7: (a) Basal drain system on (b) Clusters of basal collection lysimeters. Larger boxes are 4 m by 4 m; smaller boxes are 2 m by 2 m. Individual lysimeter drain lines are housed in a 200 mm (8 in) nominal black HDPE pipe for each cluster for mechanical and thermal protection.

(a)   **(b)**

Figure 2-8: (a) Type III pile, Face 1 instrument installation. (b) Excavator placing 0.5 m thick run of mine rock cover over face instrument lines

(a)   **(b)**

Figure 2-9: Instrumentation trailer measurement configuration for sample collection, continuous pH measurement, continuous electrical conductivity measurement, and flow measurements; (a) schematic drawing; (b) photo of actual set-up.
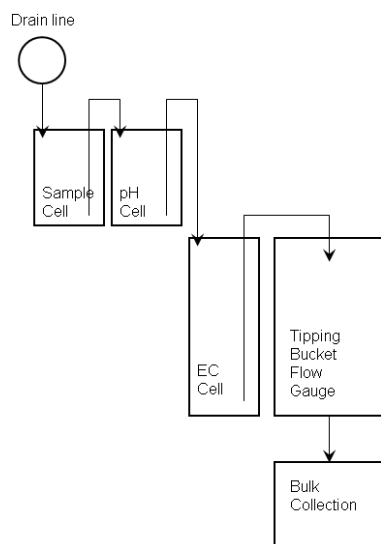
(a)   **(b)**

Chapter 3: Particle size and sulfur characteristics of low sulfide waste rock

3.1   Overview

Three 15 m high instrumented waste rock piles ("test piles") were constructed at the Diavik diamond mine in the Northwest Territories, Canada to measure and compare low sulfide waste rock and drainage characteristics at various scales. The test piles are part of a complementary field and laboratory research program. During test pile construction samples of the < 50 mm fraction of waste rock were collected from two types of waste rock that are segregated during mining operations based on sulfur concentration. The samples were analysed for sulfur content and particle size distribution. One test pile contains waste rock with an average of 0.035 wt. % S, within the operational sulfur target of < 0.04 wt. % S for the lower sulfur waste rock type. The second pile contains waste rock with an average of 0.053 wt. % S, lower than the operational sulfur target of > 0.08 wt. % S for the higher sulfur waste rock type. The third pile has a low permeability till layer and a low sulfide waste rock thermal layer covering a core of average 0.082 wt. % S waste rock which is within the operational sulfur target of > 0.08 wt. % S for the higher sulfur waste rock. Particle size distributions for the lower and higher sulfur waste rock are similar, but the higher sulfur waste rock has a higher proportion of fines. Particle size distributions for both waste rock types suggest the piles have rock-like characteristics rather than soil-like characteristics. Sulfur determinations for discrete particle sizes of the < 10 mm fraction illustrate higher sulfur concentrations in smaller particles for both the lower sulfur waste rock and the higher sulfur waste rock. Similarly, sulfur concentrations calculated for the > 10 m scale are lower than those calculated for the < 50 mm scale. Acid-base accounting using standard methods and site-specific mineralogical

information suggest that the waste rock is acid-generating. However, when acid-base accounting is compared to effluent pH and alkalinity the data suggest these calculations may be conservative.

3.2   Introduction

Large, heterogeneous, unsaturated stockpiles of mining waste can expose residual sulfide minerals to the atmosphere and result in acid mine drainage (AMD). AMD is characterized by drainage with elevated acidity, sulfate and dissolved metal levels that are released by bacterially-mediated sulfide mineral oxidation. AMD is controlled by coupled physical and biogeochemical processes that control mineral weathering rates and hydrologic flow in mine waste stockpiles. Waste rock piles are physically and geochemically heterogeneous with internal structures created during dump construction, particle sizes ranging from silt to boulders, variable saturation, variable geochemical composition and variable reactivity of the particles.

Fundamental AMD-generation processes influenced by grain size include mineral weathering and fluid flow (water and air). Sulfide mineral oxidation depends on the supply of oxygen to the mineral site and the available reactive sulfide mineral surface area in the pile, which is a function of total available sulfide-mineral mass and the particle-size distribution. Particle size affects the pile permeability, which is one control on the rate at which oxygen and water move through the pile. Particle size also affects the rate at which oxygen (and other reactants and products) diffuses through a particle to reach a reaction site. This transport-limited process can be described conceptually and mathematically by the shrinking core model (Levenspiel, 1972; Cathles, 1979; Davis and Ritchie, 1986, 1987; Davis et al., 1986; Wunderly et al., 1996; Lefebvre et al., 2001a; Mayer et al., 2002, 2003). In a series of batch reactors of

discrete particle size fractions, Strömberg and Banwart (1999) determined that there is a difference in sulfide mineral weathering rates between larger and smaller particles. Sulfide mineral availability to oxidation is a major control on environmental mass loading of acidity, sulfate and metals, as well as AMD persistence.

Reaction product and dissolved constituent loads are transported by infiltrating water. Matrix flow and flow channelization in unsaturated waste rock piles can result in spatially and temporally variable drainage volume and mass loadings, and may account for the difference in weathering rates observed in the field and in the laboratory (Vebel, 1993; Nichol et al., 2005; Stockwell et al., 2006). Textural and compositional waste rock heterogeneity, pile structure and pile geometry influence each physicochemical process and the coupling between these processes in unsaturated waste rock piles (Lamontagne et al., 1999; Lefebvre et al., 2001b; Nichol et al., 2005).

This paper describes the particle size, sulfur distributions and acid-base accounting results for 15 m high instrumented waste rock piles ("test piles"). This characterization study is part of a rigorous waste rock pile study with laboratory and field research components to evaluate the physicochemical evolution of unsaturated waste rock piles and laboratory column experiments (Chapter 2). Three 15 m test piles were constructed at the Diavik diamond mine, Northwest Territories, Canada (Figure 2-1), where the average annual ambient temperature is -8.5 °C and temperatures fluctuate from an average maximum of 18 °C in July to an average minimum of -31 °C in January/February (Environment Canada, 2008). The Diavik mine is an operating open-pit and underground diamond mine. The kimberlite ore bodies are hosted in Archean granite and pegmatitic granite country rock that is massive and moderately to coarsely crystalline. The granite contains metasedimentary biotite schist xenoliths. The region is cut by

a series of Proterozoic diabase dikes (Blowes and Logsdon, 1998). Static tests conducted during the baseline geochemistry study indicate that the granite and pegmatitic granite country rock contain only trace sulfides and are considered non-acid generating with very low potential to leach metals during weathering. The biotite schist contains locally disseminated pyrrhotite and other minor sulfide minerals, and little carbonate. The biotite schist is considered potentially acid generating because of the low neutralization potential (NP). The silicate mineral assemblage was found to contribute little to the NP. The diabase dikes also were found to contain trace sulfides but this rock type is considered geochemically insignificant because of its very low abundance.

As part of the Diavik operational waste rock management program waste rock is segregated into Type I (target of <0.04 wt. % S), Type II (target of 0.04 to 0.08 wt. % S) or Type III (target of >0.08 wt. % S). Type I is comprised primarily of granite. Type II rock is comprised predominantly of granite with minimal biotite schist. Type III rock is comprised of granite with a greater amount of biotite schist. Due to the biotite schist content Type III rock is considered potentially acid generating. During open pit production Diavik classifies the waste rock by analyzing sulfur from samples of vertically integrated cuttings from each hole drilled for blasting. Sulfur analysis results are analysed for each blast pattern. Mineable units of waste rock within a blast pattern are delineated based on sulfur distributions and each waste rock type is hauled to a designated stockpile or construction area. At the end of the mine life up to 200 Mt of waste rock, up to 40 % of which could be Type III, will be stockpiled in a 60 to 80 m high permanent pile covering up to 3.5 km^2.

The three instrumented waste rock test piles were constructed of run of mine waste rock. One test pile consists of Type I waste rock, one consists of Type III waste rock and the

third consists of Type III material that has been re-contoured and capped by a till layer and a Type I later ("Covered pile"), after the current closure plan for the Type III dump (Chapter 2).

3.3   Characterization methods

During test pile construction samples of the < 50 mm fraction were taken to measure the particle size distribution and the sulfur content of the matrix material. Samples were collected from most haul truck loads delivered to the test piles as the instrumentation faces were being constructed (Figure 3-2). Each particle size sample was 5 to 10 kg and each sulfur sample was 2 to 5 kg. Samples also were collected directly from the instrumentation face as instruments were being installed. Particle size samples collected directly from the face are not considered representative and are not included in the data set. Instrumentation faces were characterized by large cobbles and boulders, with few locations available for unbiased sampling of the < 50 mm fraction (Figure 3-3). Most of the samples collected from the face were composite samples, consisting of finer material scraped from larger boulders from several locations within about 2 m of the target sample location.

All sulfur samples that were collected were analyzed to determine the sulfur content. Samples were dried in an oven at 105°C for 2 to 4 hours. Cooled samples were crushed and homogenized. Aliquots of 0.26 +/- 0.01 g of pulverized samples were analysed using a LECO IR-432 Sulfur Determinator. The equipment was calibrated using seven calibration standards with the three closest to the average sulfur content used for calibration. A minimum of seven sulfur blanks were analyzed per day. Sulfur standards were analyzed every tenth sample and sample duplicates were analyzed randomly.

Randomly selected particle size samples were analyzed according to ASTM standard D422-63 (ASTM, 2002). Samples were split using a riffle splitter or the coning and quartering

method. Samples were sieved using either a standard sieve set (12", 6", 3", 1½", ¾", ½", 3/8", #4, #`10, #20, #40, #60, #100, #200, and a pan for smaller size fractions) or a metric sieve set (40 mm, 28 mm, 20 mm, 14 mm, 10 mm, 5 mm, 2.5 mm, 1.25 mm, 0.625 mm, 0.315 mm, 0.160 mm, 0.080 mm, and a pan for smaller size fractions). To compare results between sieve sets the standard sieve set data were interpolated to correspond to the size fractions of the metric sieve sizes.

Size fractions of selected particle size samples were retained and analyzed for sulfur and carbon content. Each fraction (5 mm, 2.5 mm, 1.25 mm, 0.625 mm, 0.315 mm, 0.160 mm, 0.080 mm and pan) was pulverized using a four-position Fritsch Pulverisette Analysette planetary ball mill and analyzed for sulfur and carbon content using an Eltra CS-2000 Carbon/Sulfur Determinator. Each sample was analyzed in duplicate. Sulfur standards were analyzed every 10 to 15 samples with two to four standards analyzed each time; the two most similar results were used for calibration.

Laboratory column effluent was sampled weekly and analyzed at the University of Waterloo for a range of parameters (Moore, 2009). The pH was measured on unfiltered aliquots using an Orion Ross combination electrode (model 815600) calibrated with standard buffer solutions of pH 10, 7 and 4. Alkalinity was measured for aliquots filtered through 0.45 um cellulose-acetate syringe filters. Alkalinity was measured using a Hach digital titrator and bromocresol green/methyl red indicator (Moore, 2009). Type I and Type III waste rock used in the column experiments were collected in 2004 and 2005. Two split samples from each waste rock type collected in each year were analyzed for wt. % C and wt. % S at two separate external laboratories, for a total of four analyses on each waste rock type collected in each of 2004 and 2005.

3.4   Results and Discussion

3.4.1   Particle size distribution

The particle size distributions are similar between piles, and between Type I and Type III material, including the Type III pile and Covered pile Type III core (Table 3-1, Figure 3-4). The Type I pile shows the greatest variation in particle size between faces compared to the Type III pile and the Covered pile core. The Type III pile is slightly finer than the Type I pile and Covered pile core. The d10 results, the diameter of particle that 10 % of the material is finer than, illustrates that Type III material has a greater proportion of fine particles compared to the Type I material. This distribution may be lithogically controlled. Biotite schist contained in Type III material is more friable than granite and because Type III material also contains a substantial portion of granite, the larger particle sizes are likely controlled by the granite fraction of the samples. The reactivity of discrete particle sizes of Diavik waste rock were not evaluated as part of this study.

Average test pile permeability to air is 1.4×10^{-9} m^2, which is on the high end for the range measured at other waste rock piles (Amos et al., 2009), and CO_2 and O_2 internal pile gas compositions remain at atmospheric levels (<0.01 vo. % CO_2 and 20.9 vol. % O_2 respectively), suggesting macroscale O_2 supply would not limit sulfide mineral oxidation. Sulfide mineral availability to oxidation is a major control on environmental mass loading of acidity, sulfate and metals, as well as AMD persistence.

A single larger-scale (92 kg) particle size measurement was obtained by Diavik for Type I material for size fractions <900 mm (Figure 3-5). Dawson and Morgenstern (1995) defined < 20 % of material passing the 2 mm sieve (i.e. d20 = 2 mm) as the division between a waste rock pile that behaves in a "soil like" manner compared to a "rock like" manner. The

smallest sieve used for the 92 kg sample was 2.5 mm, through which 14.3 % of the sample passed, indicating that a Type I waste rock pile would behave in a rock like manner. Rock like pile characteristics influence pile physicochemical processes including hydrology and, thus, solute flushing. Rock like piles may have a larger contribution of flow from macropore or channelized flow than from matrix flow. However, macropore flushing in the test piles seems to be limited to high intensity rainfall events (Neuner et al, 2009).

3.4.2   Sulfur distribution

During operations, Diavik determines mineable units of waste rock type based on sulfur concentrations of depth-integrated samples of blast hole cuttings from each blast hole in a blast pattern. Blast pattern run of mine waste rock sulfur concentration was averaged from best available data of blast hole assay results, blast pattern configurations, and the number of loads from each pattern delivered for each construction face (Appendix B). Waste rock delivered to build the test piles was classified by Diavik as part of Diavik waste rock management procedures and is considered representative of waste rock moved to the Type I and Type III Diavik waste rock dumps during the same time periods as pile construction.

The Type I pile average sulfur concentration of the < 50 mm fraction is 0.035 wt. % S (n= 242, σ=0.019), towards the high end of the Type I waste rock designation (Figure 3-6). Face 3 and Face 5 have the highest average wt. % S, though the averages are within the Type I target range. Individual Type I pile samples ranged from 0.0028 wt. % S to 0.26 wt. % S. Blast pattern averages for all faces of the Type I pile fall within one standard deviation of the average for the < 50 mm samples. Blast pattern information for Face 4 was not available.

The Type III pile average sulfur concentration of the < 50 mm fraction is 0.053 wt. % S (n=270, σ=0.037), within the Type II waste rock designation. Individual samples from the

Type III pile ranged from 0.0085 wt. % S to 0.27 wt. % S. Only the Face 1 average of the Type III pile is within the Type III waste rock designation. The average wt.% S of the base, Face 3, Face 4 and Face 5 are within the Type II waste rock designation and Face 2 is within the Type I waste rock designation. Blast pattern averages for all the Type III pile faces, except Face 2, fall within one standard deviation of the < 50 mm sample average (Figure 3-6).

The Covered pile core (Type III material) average sulfur concentration of the <50 mm fraction is 0.082 wt. % S (n=183, σ=0.053), at the lower end of the Type III waste rock designation. The Covered pile core sulfur concentration has the highest variability of all of the piles (individual samples range from 0.006 wt. % S to 0.38 wt. % S). The Covered pile core contains waste rock more representative of Type III target sulfur concentration. The Covered pile core was built after the Type III pile with waste rock from different blast patterns. Blast pattern averages for the Covered pile core fall within one standard deviation of the < 50 mm average for all faces except Face 3 (Figure 3-6). Results illustrate more variable sulfur concentrations for Type III material compared to Type I material, which emphasizes the variable nature of the Diavik waste rock sulfur content due to the spatially discontinuous sulfide-bearing biotite schist xenoliths.

3.4.3 Relationship between particle size and sulfur content

Blast pattern average sulfur concentrations are typically lower than the < 50 mm average sulfur concentration, but within one standard deviation. This trend may indicate a higher sulfur concentration in smaller size fractions. Sulfur analyses for discrete particle size fractions < 10 mm show a general trend of increasing sulfur concentration for smaller particle size for both Type I and Type III pile material (Covered pile material particle size fractions were not analyzed), suggesting the smaller size fractions could be more reactive (Figure 3-7).

However, the < 10 mm size fractions also showed decreasing carbon content with increasing particle size and Type I material with a slightly higher carbon content than Type III material (Figure 3-8).

Test pile sulfur mass calculated from the < 50 mm sample sulfur measurements from each pile face is higher compared to calculations using average blast pattern sulfur results (Table 3-2, Appendix B). Mass loadings estimated using the < 50 mm sample sulfur concentration would be higher than those calculated using blast pattern averages. Experiments to determine the reactivity of distinct grain size fractions were not conducted as part of this study. Results comparing sulfur concentrations of blast pattern averages, < 50 mm samples, and discrete particle size samples indicate that the reactivity of a range of particle sizes would need to be evaluated for sulfur concentration and reactivity to identify any discernable relationship between particle size and reactivity, and to predict more accurately environmental mass loadings and persistence of AMD.

3.4.4 Acid-Base Accounting calculations

Ratios of neutralizing potential (NP) and acid-generating potential (AP) are commonly used to infer AMD development potential of waste rock. Typically NP:AP less than 1:1 (i.e. NP:AP < 1) indicate potentially acid generating material, NP:AP between 3:1 and 1:1 (1 < NP:AP <3) indicate uncertain acid generating potential, and NP:AP greater than 3:1 (NP:AP > 3) indicate non-acid generating material.

The AP of each size fraction was calculated using a modified Sobek test (Sobek et al., 1978). The AP for each size fraction was calculated for two scenarios, following Jambor (2003). Both scenarios assumed that the analytically determined sulfur concentration consisted entirely of sulfide mineral. This assumption is consistent with previous mineralogical studies of

Diavik waste rock that showed negligible SO_4 content (Blowes and Logsdon, 1998). The first

set of AP calculations assumed the S content was entirely pyrite [FeS_2] and that the pyrite will

oxidize by the overall reaction (Blowes et al, 2003):

$$FeS_{2(s)} + \frac{15}{4} O_{2(aq)} + \frac{7}{2} H_2O_{(aq)} \rightarrow Fe(OH)_{3(s)} + 2SO_4^{2-} + 4H^+ \tag{1}$$
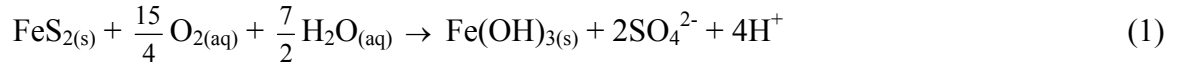
Pyrrhotite ($Fe_{1-x}S$) with the composition $Fe_{0.85}S$ [$Fe_{17}S_{20}$] was determined to be the

primary sulfide mineral in Diavik country rock (Jambor, 1997). The second set of AP

calculations assumed the S content was entirely pyrrhotite and that the pyrrhotite with

composition $Fe_{0.85}S$ will oxidize with oxygen as the primary oxidant by the overall reaction:

$$Fe_{0.85}S_{(s)} + 2.35\ O_2 + 1.85\ H_2O \rightarrow 0.85\ Fe(OH)_{3(s)} + SO_4^{2-} + 1.15\ H^+ \tag{2}$$

Pyrrhotite oxidation releases less acidity compared to pyrite oxidation for the overall reactions.

Although pyrrhotite can react 20 -100 times faster than pyrite (Blowes et al., 2003), kinetics

are not considered in AP calculated using the Sobek method. The AP calculated using pyrite

oxidation (AP(py)) for the discrete particle size fractions is more conservative compared to the

AP calculation using pyrrhotite oxidation (AP(po)). The AP(po) calculations are a linear shift

from AP(py) calculations. The shift is caused by fewer moles of H^+ released during pyrrhotite

oxidation.

The NP for the grain size fractions was calculated assuming that the analytically

determined carbon content consisted entirely of $CaCO_3$. This assumption is considered

reasonable based on the known mineralogical information (Jambor, 1997; Blowes and

Logsdon, 1998), NP values for minerals provided in the literature (Jambor et al., 2007), and

that previous studies on Diavik waste rock that illustrate that the silicate mineral assemblage

contributes little to the NP (Blowes and Logsdon, 1998). Calculated NP values have been

shown to be lower than values measured using the Sobek test, however measured and

calculated values have a close relationship for a variety of rock types (Jambor et al., 2007). Furthermore, calculating NP values from analytical determinations avoids many of the perceived deficiencies of the traditional Sobek method: e.g. over or under acidification (Jambor et al., 2007), particle size controls (White et al., 1999), ferrous iron effects (Skousen et al., 1997; Jambor et al., 2003; Weber et al., 2004), and empirical fizz relationships (Weber et al., 2004).

NP:AP(py) of the < 10 mm Type I material has a range of 0.14 to 5.03 and a mean of 1.16 (n=70, σ=1.13), which are lower compared to the Type I NP:AP(po) values that range from 0.25 to 8.75 with a mean of 2.01 (n=70, σ=1.98; Figure 3-9). Smaller particles generally have lower mean NP:AP ratios than larger particles (Figure 3-10). Type I mean NP:AP values for the < 0.315 mm fraction are < 1 for NP:AP(py) and <1.6 for NP:AP(po). For larger particle size fractions the mean NP:AP(py) is < 1.6 and the NP:AP(po) is < 2.7. These NP:AP(py) values suggest the < 0.315 mm fraction is potentially acid generating but the larger size fractions are of uncertain acid-generating potential. NP:AP(po) values suggest all size fractions are of uncertain acid generating potential, but the smaller size fractions approach the acid generating side of the zone of uncertainty whereas the larger size fractions are towards the non acid generating size of the zone of uncertainty.

Type III material has lower NP:AP ratios compared to Type I material and shows a similar trend of lower NP:AP values with smaller size fractions (Figure 3-10). NP:AP(py) values for < 10 mm fractions of Type III material range from 0.01 to 15.27 with a mean of 0.51 (n=243, σ=1.43). NP:AP(po) values are higher with a range of 0.02 to 26.56 and a mean of 0.89 (n= 243, σ=2.50). All Type III size fractions have NP:AP(py) < 0.95, whereas NP:AP(po) for the < 1.25 mm fraction are < 0.77 but >1.29 for the larger size fractions. The NP:AP(py)

values suggest all Type III material is acid generating. The NP:AP(po) values suggest the smaller size fractions are acid generating but the larger size fractions are of uncertain acid generating potential but approach the acid generating side of the zone of uncertainty.

AP and NP for waste rock used in the laboratory column experiments were calculated using the analytically determined wt. % S and wt. % C values, respectively, and the same assumptions that were applied to the field waste rock samples. The laboratory waste rock samples represent two sets of splits that were analyzed at two separate labs for a total of four data points. NP:AP ratios based on calculations from all data are presented. The NP:AP(py) calculations for the Type I column material collected in both 2004 and 2005 suggest that the material would have uncertain to acid generating potential. NP:AP(po) calculations have higher values, but also suggest uncertain to acid generating potential. Laboratory results from the same columns of Type I material show circumneutral pH levels (typically 5.5 > pH > 8.5) and low (2.8 – 17.1 mg L^{-1}), stable alkalinity levels (Moore, 2009). Column effluent pH and alkalinity values are better represented by NP:AP(po) calculations because the NP:AP(py) calculations suggest the column experiment would be acid generating whereas NP:AP(po) calculations suggest acid generation would be less (Figure 3-11). Type I column material from 2004 has an average S content of 0.018 wt. % S and the 2005 Type I material has an average S content of 0.019 wt. % S (Moore, 2009). Both the 2004 and 2005 Type I column material are within the Diavik Type I waste rock designation.

The 2004 Type III material has an average S content of 0.19 wt. % S and falls within the Diavik Type III waste rock designation. Both the NP:AP(py) and NP:AP(po) calculations for the Type III material collected in 2004 suggest the material would be acid generating with low neutralizing potential. NP:AP(po) calculations also suggest the material would be acid

generating but the extent of acid-generation would be less. The 2004 Type III room temperature column effluent becomes acidic and then stabilizes near pH 4. The NP values indicate little alkalinity in the 2004 Type III material. The column effluent data illustrates that little alkalinity is present initially and all of the available alkalinity is consumed within the first 20 weeks of the humidity cell test. After the alkalinity is depleted, the pH falls and then pH stabilizes (Moore, 2009; Figure 3-11).

Type III material collected in 2005 has an average S content of 0.041 wt. % S, at the boundary between Type I and Type II Diavik waste rock designations. NP:AP(py) calculations for the 2005 Type III material indicate that one sample would fall within the acid generating zone and three samples would fall within the zone of uncertainty. When NP:AP(po) calculations are applied, all three samples shift from the zone of uncertainty towards the non acid generating zone. Laboratory results show stable, slightly alkaline circumneutral pH levels and stable alkalinity levels. Of the Type I and Type III column samples, three of the 2005 Type III samples have the highest NP values. The humidity cell results from these 2005 Type III samples also exhibited the highest column effluent pH and alkalinity values. The 2005 Type III column effluent pH and alkalinity persist at relatively constant values and are consistent with the NP:AP(po) predictions (Figure 3-11).

The 2004 and 2005 Type I column material have similar NP:AP values and column effluent pH and alkalinity trends. The NP:AP(py) values predict uncertain to acid generating material whereas NP:AP(po) values also predict uncertain generating material, but with a lower acid generating potential. The Type I column effluent pH values are circumneutral and stable and the alkalinity values are low but stable. The 2004 Type III column material NP:AP values predict acid generating material, which is consistent with the low pH and alkalinity values of

the column effluent. The 2005 Type III column effluent has the highest pH and alkalinity levels of the columns, and is consistent with the NP:AP(po) calculations that indicate this material is non-acid generating. NP:AP ratios calculated for the material used in the laboratory experiments, together with the column pH and alkalinity results, indicate that NP:AP(po) calculations better predict acid generating potential compared to NP:AP(py) calculations according to the standard 1:1 and 3:1 boundaries for acid generating and non acid generating material, respectively. However, NP:AP(po) calculations appear to be conservative with respect to the acid generating potential of the Diavik waste rock.

3.5   Summary and conclusions

Grain size distributions of the Diavik test piles waste rock indicate the piles have rock-like characteristics. Sulfur content measurements vary with the scale of the measurement: concentrations determined on < 50 mm samples exhibit higher sulfur concentrations than blast pattern averages. The < 10 mm fraction shows decreasing sulfur concentrations with increasing particle size.

The NP:AP calculations, together with column effluent data, suggest that AP values calculated using site-specific pyrrhotite composition better predict the acid-generating behaviour of Diavik Type I and Type III material. However, the calculations suggest that samples with both NP > 0.02 and NP:AP(po) ratios of > 1.4 are likely to be non-acid generating. The differences in NP:AP(py) and NP:AP(po) values emphasize the importance of understanding site-specific mineralogy when predicting mass loadings and AMD persistence. As field-scale geochemistry results and hydrologic characterizations are obtained and compared to column experiments the degree of importance of variations in sulfide concentration and flow regimes to mass loadings will be determined.

The sulfur and particle size data presented in this paper provide a basis for further test pile characterization studies at various scales. Additional measurements are required to characterize better the relationships among particle size, sulfur content and acid-generating potential; as well as the propensity of the test piles for channelized flow.

3.6   Tables

Table 3-1: Average particle size and one standard deviation for the Type I, Type III and Covered test piles.

d	Type I pile (σ)	Type III pile(σ)	Covered pile (σ)
d10	0.49 mm (1.30 mm)	0.20 mm (0.10 mm)	0.25 mm (0.23 mm)
d30	3.70 mm (4.73 mm)	1.75 mm (1.76 mm)	3.37 mm (3.63 mm)
d50	11.24 mm (7.46 mm)	6.93 mm (4.94 mm)	11.16 mm (6.92 mm)
d60	16.06 mm (7.99 mm)	10.56 mm (4.60 mm)	16.86 mm (8.95 mm)

Table 3-2: Mass of sulfur in each pile calculated using the average sulfur concentration for the < 50 mm samples and blast pattern (BP) averages for each test pile face. Calculations were based on the as-built volume for each test pile face and a blasted waste rock density of 2.04 tonnes m^{-3}. The blasted waste rock density was obtained by Diavik from several field measurements.

	Mass of S (tonnes)					
Face	Type I pile		Type III pile		Covered pile core	
	< 50 mm	BP	< 50 mm	BP	< 50 mm	BP
Base	14.6	3.0	12.7	8.9	12.4	6.5
Face 1	3.8	3.4	23.6	18.0	20.0	17.0
Face 2	1.2	0.7	2.1	4.3	2.5	1.8
Face 3	1.5	0.6	1.7	1.4	12.2	4.6
Face 4	1.6	No data	3.5	3.4	6.0	4.0
Face 5	7.3	1.6	8.4	4.4	13.1	9.9
Pile Total	*30.0*		*51.9*	*40.4*	*66.3*	*43.7*

3.7   Figures

Figure 3-1: Location of Diavik Diamond Mine

Figure 3-2: Typical haul load from which < 50 mm size fraction was sampled for particle size and sulfur concentration. White square scale in photo is 0.5 m by 0.5 m.

Figure 3-3: Typical instrumentation face (a) entire face; and (b) instrumentation face sample area. Square scale in (a) is 0.5 m by 0.5 m and highlighted yellow with arrow for clarity; white square scale in (b) is 0.5 m by 0.5 m.

(a)

(b)

Figure 3-4: Particle size distributions of the <50 mm size fraction for the (a) Type I pile, (b) Type III pile, (c) Covered pile Type III core, and (d) till layer of the Covered pile

(a)

(b)

(c)

(d)
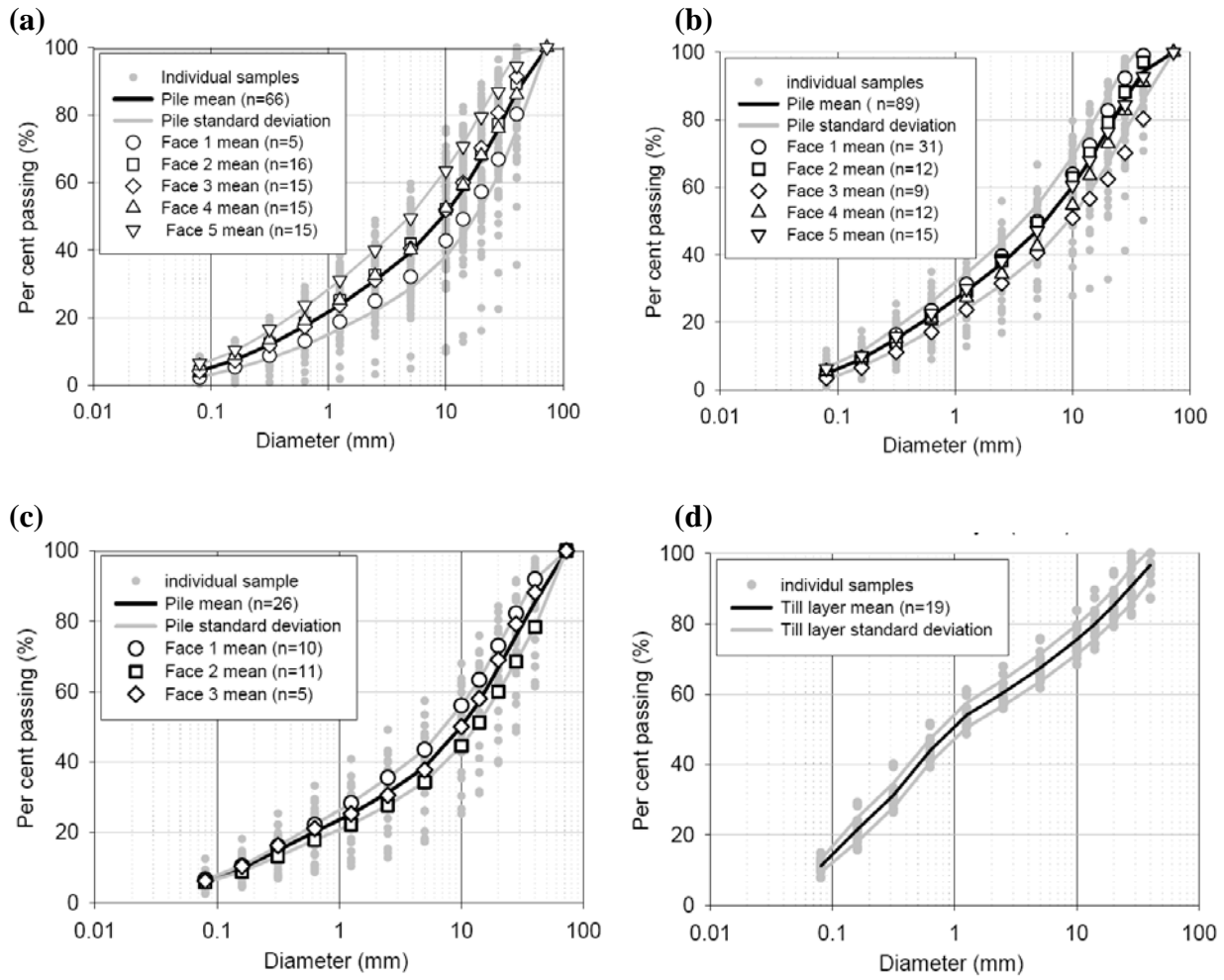
Figure 3-5: large scale (92 kg, < 900 mm) particle size distribution with the averaged cumulative distribution from the < 50 mm samples from the Type I pile, Type III pile and Covered pile core for comparison.
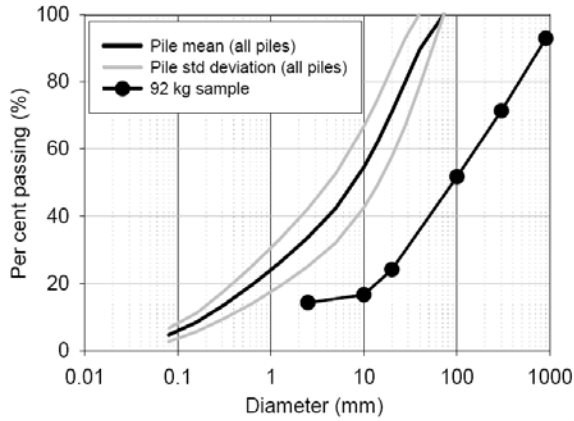
Figure 3-6: Sulfur distribution for (a) Type I pile, (b) Type III pile and (c) Covered pile core for < 50 mm sample sulfur concentrations (closed grey symbols) and blast pattern sulfur means (open symbols). Error bars on the mean sulfur concentration for the <50 mm fraction (closed symbols) indicate one standard deviation. The dashed line indicates the pile average concentration.
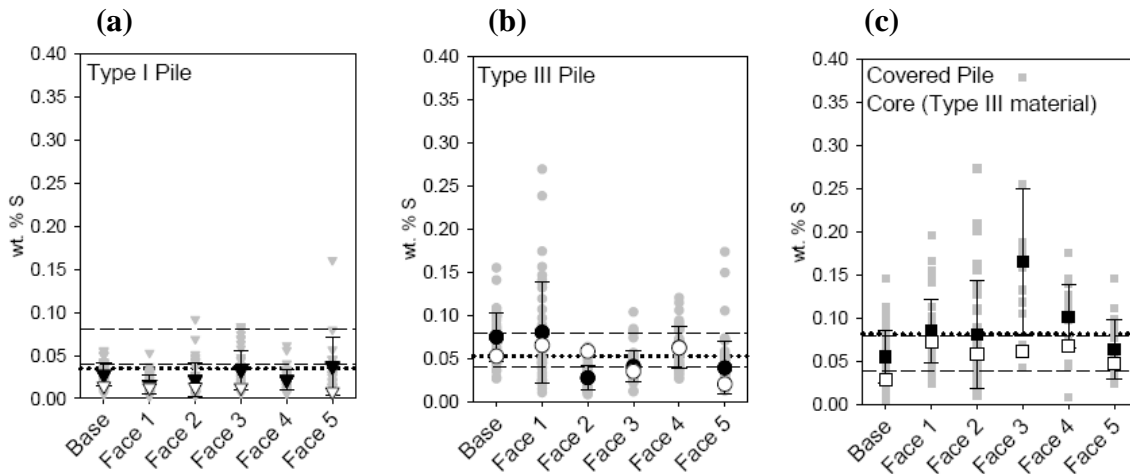
Figure 3-7: Sulfur distribution for discrete particle sizes for (a) Type I pile material and (b) Type III pile material. Solid line indicates average values and dotted line indicates test pile average.

(a)

(b)
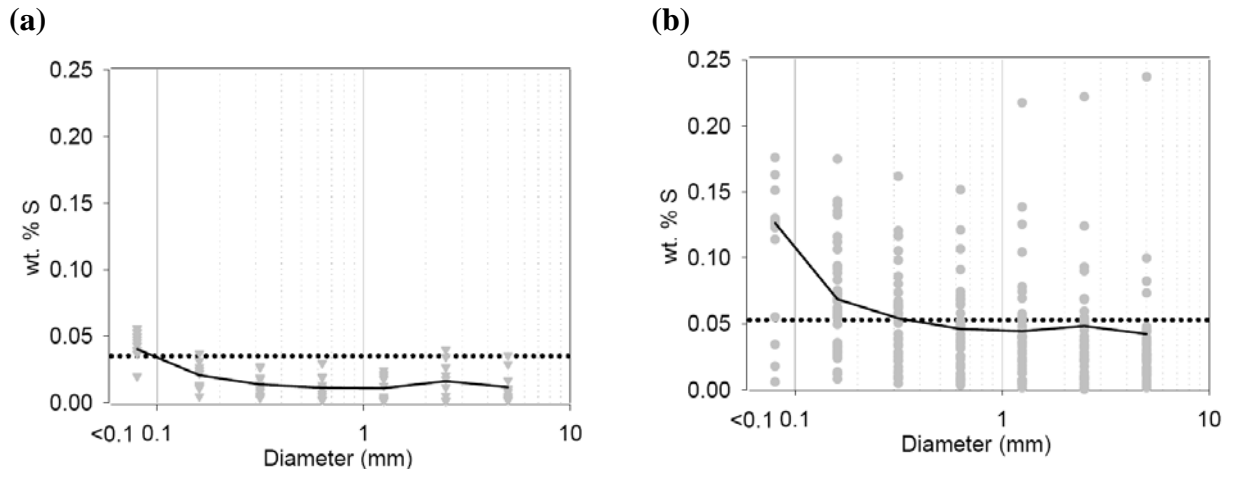
Figure 3-8: Carbon distribution for discrete particle sizes for (a) Type I pile material and (b) Type III pile material. Solid line indicates average value.

(a)

(b)
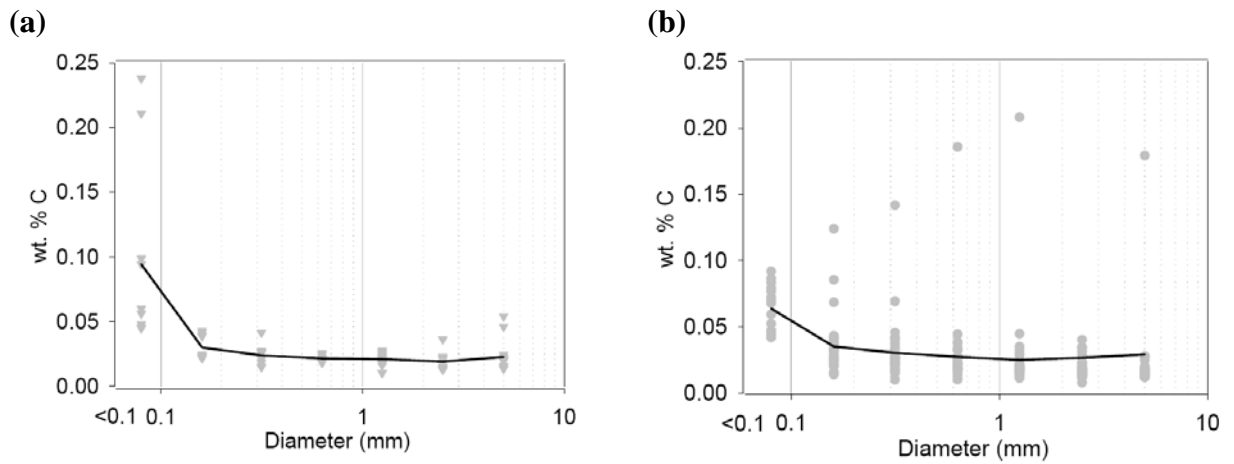
Figure 3-9: Comparison of NP:AP(py) (open symbols) and NP:AP(po) (closed symbols) ratios for all particle size fractions for (a) Type I pile material and (b) Type III pile material. The mean with one standard deviation is illustrated by error bars. Where the negative error bars indicated NP:AP < 0, the minimum NP value was assigned.

(a)   **(b)**
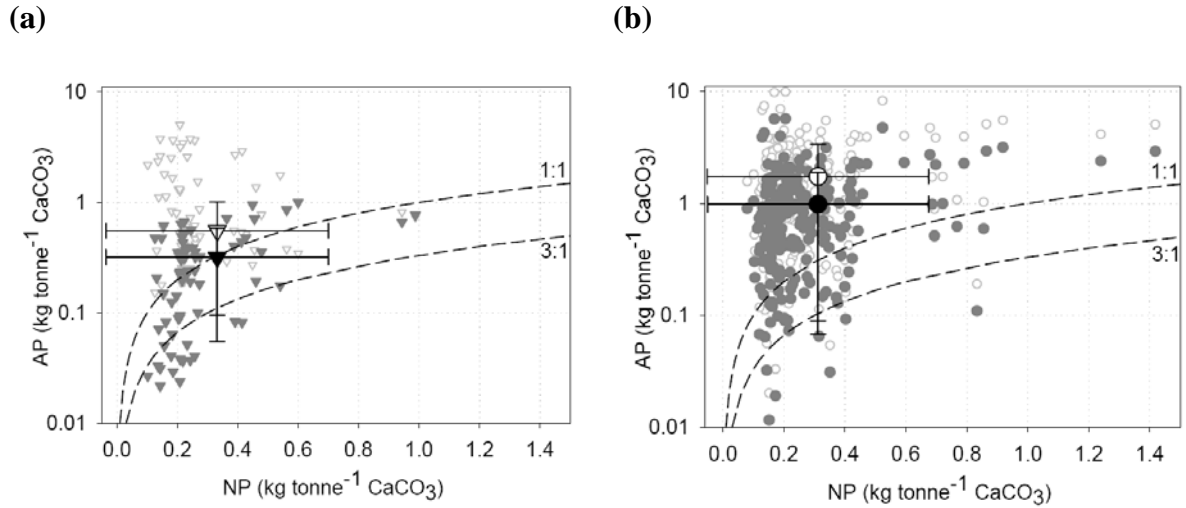
Figure 3-10: NP:AP for the <10 mm grain size fraction for (a) Type I NP:AP(py) (b) Type III NP:AP(py) (c) Type I NP:AP(po) and (d) Type III NP:AP(po). Error bars illustrate one standard deviation from the mean. Where error bars indicated NP:AP < 0, the minimum NP:AP value was assigned.

(a)   **(b)**

65

(c)

(d)
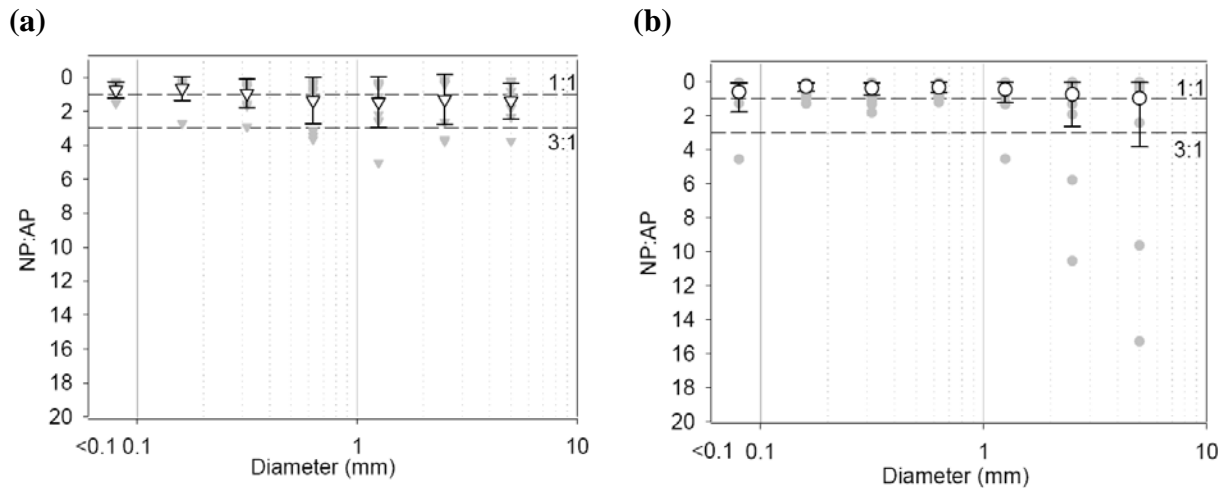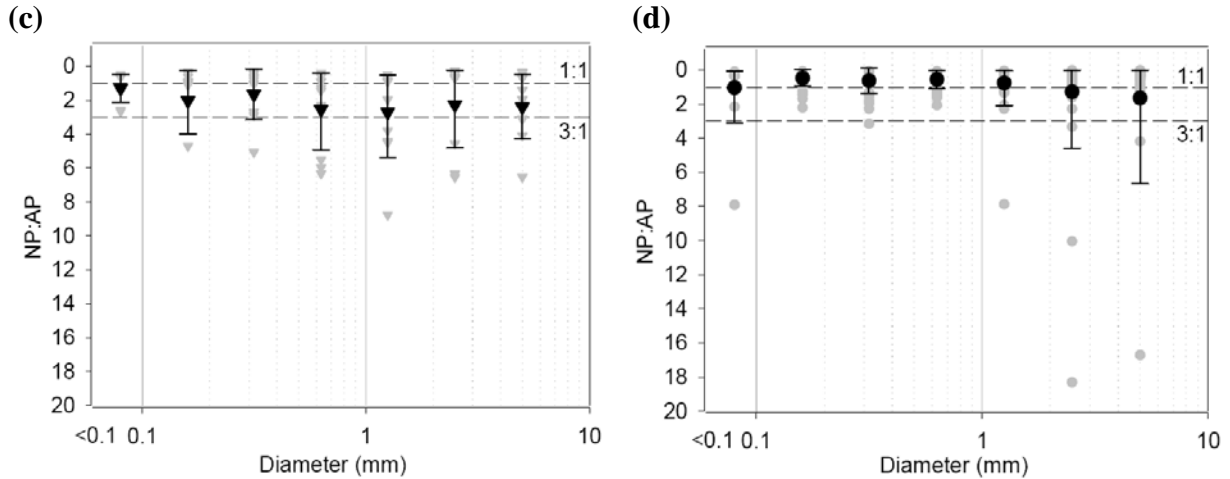
Figure 3-11: NP:AP ratios, mean pH and mean alkalinity for material used in the laboratory humidity cell experiments conducted at room temperature for (a) Type I material collected in 2004 with average 0.018 wt. % S; (b) Type I material collected in 2005 with average 0.019 wt. % S; (c) Type III material collected in 2005 with average 0.19 wt. % S; and (d) Type III material collected in 2005 with average 0.041 wt. % S. Open symbols represent NP:AP(py) and closed symbols represent NP:AP(py). Data presented represent two splits of the same sample analyzed for wt. % C and wt. % S at two different analytical laboratories.

(a)

(b)
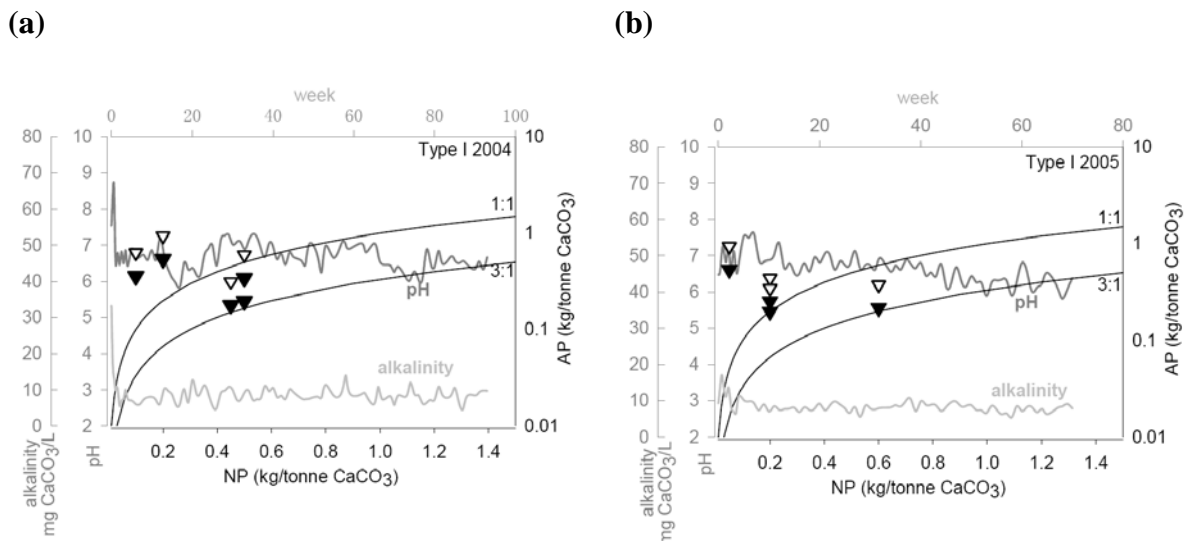
(c)
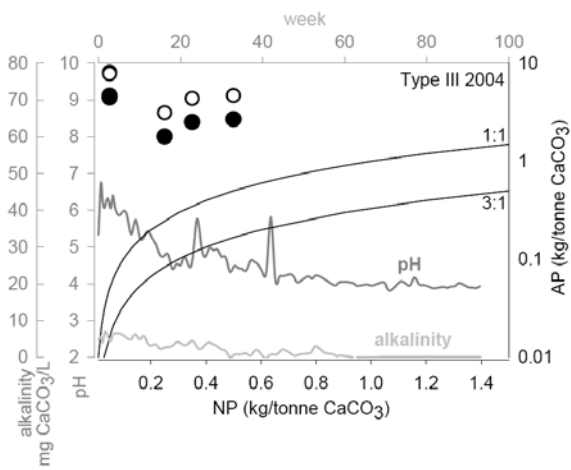
(d)
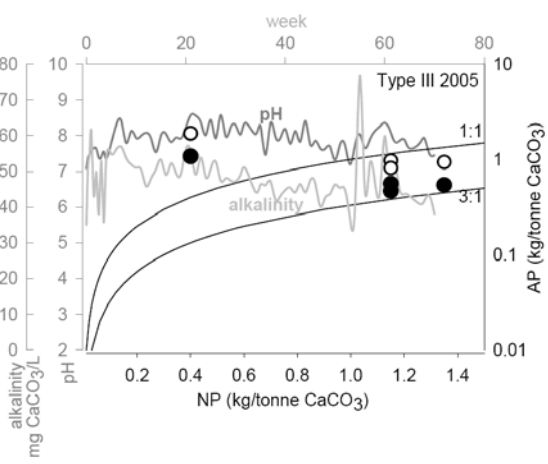
Chapter 4: Initial geochemical response from a low sulfide waste rock pile

4.1   Overview

Three 15 m high instrumented waste rock piles were constructed at the Diavik diamond mine in the Northwest Territories, Canada as part of a rigorous laboratory and field study to measure and compare low sulfide waste rock and drainage characteristics at various scales. This paper describes the geochemical response during the first field season of one of the test piles containing 0.053 wt. % S. Drainage effluent was measured at two sampling points for field parameters (pH, Eh, alkalinity), dissolved cations, anions, and nutrients. The geochemical equilibrium model MINTEQA2 was used to interpret potential geochemical controls on solution chemistry. The geochemical response from the first field season characterizes the initial flushing response of blasting residues and oxidation products derived from newly-exposed sulfides in waste rock exposed to the atmosphere for less than one year. Sulfate concentrations reach 1995 mg L^{-1} when ambient temperatures are higher, and decrease as ambient temperatures drop. The pH decreases to < 5, concomitant with minimum alkalinity of < 1 mg L^{-1} (as total $CaCO_3$), suggesting all available alkalinity is consumed by acid-neutralizing reactions. Concentrations of Al are <0.38 mg L^{-1} and concentrations of Fe are < 0.37 mg L^{-1}. Calculated saturation indices of Al and Fe (oxy)hydroxides and pH and alkalinity trends suggest Al and Fe oxyhydroxide dissolution is buffering pH at times. The dissolved metals Mn (<19.2 mg L^{-1}), Ni (<10.4 mg L^{-1}), Co (<1.8 mg L^{-1}), Zn (<0.9 mg L^{-1}), Cd (<0.015 mg L^{-1}) and Cu (<0.05 mg L^{-1}) show increasing trends in the effluent water. Manganese is released by aluminosilicate weathering, Ni and Co are released by pyrrhotite oxidation, Zn and Cd are released by sphalerite oxidation and Cu is released by chalcopyrite oxidation. No dissolved metals appear to have discrete secondary mineral controls. Changes in sulfate, pH

68

and metal concentrations indicate sulfide oxidation is occurring and effluent concentrations are influenced by ambient temperatures and, possibly, increasing flow path lengths that flush reaction products from previously unflushed waste rock.

4.2 Introduction

Mining wastes may contain concentrations of sulfide minerals that are economically insignificant but potentially environmentally damaging. Exposing these sulfide minerals to the atmosphere can cause acid mine drainage (AMD) as sulfide minerals oxidize and weather, and the reaction products are carried by infiltrating rain and snowmelt into the adjacent environment. AMD is characterized by low pH and increased sulfate and metals loads. Discharges of AMD from mines and mine tailings to surface water and groundwater have been well documented and continue to be an environmental concern world-wide (e.g. Blowes and et al., 1992; Moncur et al., 2005, 2006).

Many studies have focused on AMD generation from abandoned mine tailings (e.g. Blowes and Jambor 1990; Blowes et al., 1991, 1992; Al et al., 1997; Johnson et al., 2000; Blowes et al., 2003a, Moncur et al., 2005, 2006; Gunsinger et al., 2006), but fewer studies address AMD from physically and geochemically heterogeneous unsaturated waste rock piles (e.g. Strömberg and Banwart, 1999; Lefebvre et al., 2001; Nichol et al., 2005; Stockwell et al., 2006). Three instrumented waste rock piles ("test piles") were constructed at the Diavik diamond mine as part of a complementary field and laboratory research program with the objectives of characterizing the physicochemical response of unsaturated waste rock piles and to evaluate the effectiveness of laboratory column experiments for predicting large-scale waste rock pile behaviour (Chapter 2). This paper describes the geochemical response during the first field season of one test pile containing waste rock with an average sulfur concentration of

0.053 wt %. S. The geochemical response from this low sulfide waste rock pile is a result of a complex combination of physicochemical processes that control sulfide mineral oxidation reactions, acid neutralization, and the transport and attenuation of and reaction products.

The test piles were constructed at the Diavik diamond mines, Northwest Territories, Canada (Figure 4-1), an operating open-pit and underground diamond mine. The area receives little precipitation with an annual average of 280.3 mm for 1999-2006. About 60% of the precipitation occurs as snow. The mean annual air temperature of the area (1998 to 2007) is −8.5 ºC, with a maximum average temperature of 18 ºC occurring in July and minimum average temperature of −31 ºC occurring in January/February (Environment Canada, 2008). The prevailing winds are northerly to easterly with an average speed of 4.75 m s^{-1} (18 km h^{-1}) recorded for 2006.

Ore is mined from diamondiferous kimberlite pipes that were emplaced in the Archean granite and pegmatite granite country rock. The granite and pegmatite granite are massive and moderately to coarsely crystalline and are similar compositionally. The granite has no appreciable sulfide mineral content. Hosted in the granite are bitotite schist xenoliths with variable sulfur concentrations ranging from 0.02 to 0.42 wt. % S (Jambor, 1997). Static tests conducted during the feasibility stage indicated that the granite is environmentally benign whereas the biotite schist has low, but sufficient sulfide mineral concentrations to be considered potentially acid generating (Blowes and Logsdon, 1998).

During mining the waste rock is segregated based on sulfur content into Type I (target <0.04 wt % S), Type II (target 0.04 to 0.08 wt % S) or Type III (target >0.08 wt % S), and stockpiled in separate areas. Type I rock is comprised primarily of granite, Type II rock is comprised predominantly of granite with minimal biotite schist, and Type III rock is comprised

predominantly of granite with a greater amount of biotite schist. Type III rock is considered potentially acid generating because of the biotite schist content. At the end of mine life, up to 200 Mt of waste rock, up to 40% of which may be Type III, will be stockpiled in 60 to 80 m high permanent piles covering up to 3.5 km^2.

This paper describes the geochemistry of the effluent from the Type III pile basal drain system. The Type III pile has a base of 50 m by 60 m. It was constructed from freshly blasted Type III rock hauled directly from the open pit during test pile construction. The slopes rest at the angle of repose of waste rock (38°). The basal drain system consists of impermeable liner installed on graded base to collect all water draining to the base of the pile (Chapter 2), thus providing samples of the bulk water within the pile. The Type III basal drain configuration has two outflow points at the north basal drain (3BNXdrn15) and the south basal drain (3BSXdrn15; Figure 4-2), each with geochemical sampling and monitoring flow-through cells and flow gauges (Chapter 2). Other water collection systems at various scales were installed in tall three test piles (Chapter 2) but did not report water during the 2007 field season, or did not have sufficient analyses completed to permit geochemical interpretation.

4.3   Methods

4.3.1   Drainage sampling and water chemistry

Samples for basal drain water chemistry were obtained from a 500 mL dedicated geochemical sampling flow-through cell (Chapter 2). New, clean nylon tubing was inserted into the access port at the sample cell and attached to a 60 mL syringe. Successive aliquots of sample were drawn from the sample cell, as required, to obtain sufficient sample volume.

All sample bottles were new and were triple-rinsed with sample water before filling the bottle with sample water. The parameters pH, Eh, electrical conductivity and temperature were measured in an unfiltered aliquot in the field immediately following sample collection. The pH was measured with an Orion Ross combination electrode (model 815600) calibrated with standard buffer solutions of pH 10, 7 and 4. Eh was measured using an Orion Pt redox electrode (model 96-78B) calibrated in Zobell's solution (Nordstrom, 1977) and Light's solution (Light 1972). Electrical conductivity was measured using an Orion 3-Star Plus Conductivity meter. Aliquots for field alkalinity measurements were filtered through 0.45 μm cellulose-acetate syringe filters. Field alkalinity was measured using a Hach digital titrator and bromocresol green/methyl red indicator. Separate aliquots for spectrophotometer analyses were filtered through 0.45 um cellulose-acetate syringe filters. A Hach Spectrophotometer DR/2400 was used for determinations of P (Method 8048), Fe(II) (Method 8146), NH_3 (Method 10031), S(-II) (Method 8131), and Cl (Method 8113) for selected samples. Separate aliquots for dissolved cations, anions and nutrient analyses were filtered immediately using a 0.45 μm cellulose-acetate syringe filter. Separate aliquots for total cations, nutrients, isotopes, microbiology analyses were not filtered. The aliquots designated for dissolved and total cation analyses were acidified to pH <1 with 12 N trace-metal grade HNO_3, and the aliquots designated for dissolved and total nutrient analyses were acidified to pH <1 with H_2SO_4. The aliquots designated for dissolved and total anion analyses were not preserved. All cation, anion and nutrient samples were refrigerated and shipped to the University of Waterloo for analysis. Dissolved and total cation determinations for Al, A, B, Ba, Be, Ca, Cd, Co, Cr, Cu, Fe, K, Mg, Mn, Mo, Na, Ni, Pb, Si, Sr, V and Zn were by inductively coupled plasma optical emission

spectrometry (ICP-OES) and inductively coupled plasma mass spectrometry (ICP-MS). The concentrations of the anions SO_4 and Cl were determined by ion chromatography.

4.3.2 Geochemical modelling

The equilibrium mass transfer model MINTEQA2 (Allison et al., 1990) was used to calculate the saturation indices for discrete mineral phases. The MINTEQA2 database was modified to make it consistent with the WATEQ4F (Ball and Nordstrom, 1991) database. Field-measured Eh and alkalinity were used for speciation calculations thus only samples for which these measurements were taken were included in the speciation calculations. Geochemical equilibrium calculations were conducted for Type III basal drain samples with a complete suite of field and laboratory analyses.

4.4 Results and discussion

The geochemical response from the 2007 field season characterizes the initial flushing response of blasting residues and oxidation products derived from newly-exposed sulfides in waste rock exposed to the atmosphere for less than one year. The response represents a portion of the initial wetting-up phase of the test piles with increasing water-rock interaction and limited infiltration reaching sampling points. Although basal drain samples were collected from mid-May 2007, cation analyses were completed only for samples collected after July due to delays at the analytical laboratory.

4.4.1 Sulfide oxidation

Sulfide concentrations in samples of the < 50 mm fraction of Type III waste rock collected during the Type III pile construction ranged from 0.0085 wt. % S to 0.27 wt. % S (μ = 0.053 wt. % S and σ = 0.037 wt. % S; Chapter 3). Based on the conservative assumption that

the <50 mm fraction is the most reactive fraction of the Diavik waste rock and the <50 mm

fraction constitutes up to 40% of the total Type III pile volume (Chapter 2), the Type III pile

contains an estimated 20.8 tonnes of S in the < 50 mm fraction that may oxidize. Direct

observations of Type III pile waste rock mineralogy have not been completed however the

initial mineralogical study by Jambor (1997) provides rigorous analyses of the granite and

biotite schist lithologies that comprise Type III rock. The principal sulfide mineral in Diavik

waste rock is pyrrhotite, with occasional traces of pyrite, chalcopyrite and sphalerite. The

sulfides occur in the biotite schist lithology at concentrations ranging from 0.02 to 0.42 wt.% S.

The pyrrhotite occurs as locally disseminated anhedral to irregular grains. The composition

was determined to be $Fe_{0.85}S$ [$Fe_{17}S_{20}$] and was found to contain Co and Ni with an average

pyrrhotite composition of [$(Fe_{0.852}Ni_{0.004}Co_{0.001})_{\Sigma 0.857}S$] (Jambor, 1997). Pyrrhotite oxidizes

rapidly when exposed subaerially producing dissolved Fe, sulfate and acidity by the

bacterially-mediated reaction for pyrrhotite with $Fe_{0.85}S$ [$Fe_{17}S_{20}$]:

$$Fe_{17}S_{20(s)} + \frac{77}{2} O_2 + 3\ H_2O \rightarrow 17\ Fe^{2+} + 20\ SO_4^{2-} + 6\ H^+ \tag{1}$$
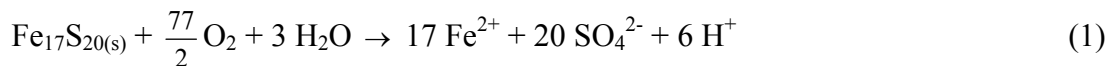
In circumneutral pH conditions the Fe(II) released during sulfide oxidation may be oxidized to

Fe(III) and precipitate Fe(III) oxyhydroxides, such as ferrihydrite [nominally $Fe_2O_3 \cdot 9H_2O$ but

represented here as $Fe(OH)_3$], and goethite [$\alpha FeOOH_3$]:

$$Fe^{2+} + \frac{1}{4} O_2 + \frac{5}{2} H_2O \rightarrow Fe(OH)_{3(s)} + 2H^+ \tag{2}$$

$$Fe^{2+} + \frac{1}{4} O_2 + \frac{3}{2} H_2O \rightarrow \alpha FeOOH_{3(s)} + 2H^+ \tag{3}$$

Marcasite pseudomorphic replacement of pyrrhotite was noted in samples with delayed

mineralogical analysis, but no significant alteration of pyrrhotite in samples analysed shortly

after collection (Jambor, 1997). These observations emphasize the rapid oxidation rate of pyrrhotite when exposed to the atmosphere from mining activities.

Several studies have shown that dissolution reactions are proportional to surface area: finer material with large surface area dissolves at a faster rate than the same material with a smaller surface area (e.g. Berner, 1980; Stumm, 1992; Lasaga, 1998). Particle size affects the rate at which oxygen and other reactants and products diffuse through alteration rims that surround particles to reach a reaction site. This process is transport-limited and can be described conceptually and mathematically by the shrinking core model for sulfide mineral oxidation (Levenspiel, 1972; Cathles, 1979; Davis and Ritchie, 1986,1987; Wunderly et al., 1996; Mayer et al., 2002). Brookfield et al. (2006) reported a rate expression for pyrrhotite oxidation based on the shrinking core model for oxidation by O_2 and Fe(III) and a calibrated effective rate coefficient:

$$R = -\max\left[\left(\frac{r^p}{(r^p - r^r)r^r}\right)\left(10^{-9.62}\{O_2(aq)\} + 10^{-11.92}[Fe(III)]^{0.06}\right)\left[1 - \frac{IAP}{10^{-135.7}}\right], 0\right] \qquad (4)$$

Where R [mol dm^{-3} sediment s^{-1}] is the reaction rate, r^p [m] is the radius of an average particle, r^r [m] is the radius of the unreacted portion of the mineral grain, and $\left[1 - \frac{IAP}{10^{-135.7}}\right]$ is the affinity term where IAP is the ion-activity product of the reaction and $10^{-135.7}$ is the value of the equilibrium constant K. The sulfur concentration of the < 10 mm fraction of Type III pile material showed an increasing trend of wt. % S with decreasing particle size (Chapter 3), which suggests the smaller particle sizes could contribute a higher proportion of mineral dissolution products.

Oxygen supply in the test piles is not anticipated to limit sulfide mineral oxidation rates. The average porosity of Type III material is 0.25 based on several different measurement

techniques (Neuner et al., 2009) and the average air permeability is 1.4 x 10^{-9} m^2, which is on the high end of the range measured at other waste rock piles (Amos et al., 2009). Test pile pore gas oxygen and carbon dioxide concentrations remain at atmospheric levels (20.9 vol. % O_2 and <0.01 vol. % CO_2) at all > 200 sampling points in the Type III test piles, and do not change seasonally. The constancy of atmospheric levels of O_2 and CO_2 within the test pile indicates atmospheric O_2 supply is not limiting sulfide mineral oxidation rates.

Pyrrhotite oxidation has shown to be temperature-dependent following Arrhenius behavior, similar to pyrite oxidation (Janzen, 2000) and consistent with the general temperature-dependence of reaction rates (e.g. Pauling, 1970). Reactions that follow Arrhenius behavior, including pyrrhotite oxidation, typically decrease by a factor of 2 for each 10 °C decrease in temperature when the reaction occurs near to 25 °C. Mean daily ambient temperature at the research site fluctuated from 21°C in July, 2007 to -30°C in November, 2007 (Figure 4-3).

Microbiological activity, which mediates sulfide mineral oxidation, can have an appreciable effect on sulfide mineral oxidation rates (e.g. Singer and Stumm, 1970, Olson, 1991), and microbiological activity is temperature dependent. The bacterial species *A. thiooxidans* and *A. ferrooxidans* have been found to be effective catalysts for sulfide mineral oxidation in mine wastes and have an optimal growth temperature range of 25 °C to 35 °C (Gould and Kapoor, 2003). However, *A. ferrooxidans* growth has been observed at temperatures as low as 2 °C (Leduc et al., 1993). Neutrophilic sulfur-oxidizing bacteria and, to a lesser extent acidophilic sulfur-oxidizing bacteria have been observed in the test pile laboratory column experiments conducted at 22 °C with lower numbers observed in experiments conducted at 4 °C (Moore, 2009).

4.4.2   Sulfate

Sulfate concentrations in the effluent from 3BNXdrn15 and 3BSXdrn15 exhibit a seasonal trend with a correlation to temperature. Higher SO_4 concentrations in warmer months (up to 1995 mg L^{-1} at 3BNXdrn15 and up to 1507 mg L^{-1} at 3BSXdrn15) and lower concentrations in colder months (minima of 111 mg L-1 at 3BNXdrn15 and 654 mg L^{-1} at 3BSXdrn15; Figure 4-4). The slight lag in peak sulfate concentrations compared to mean daily temperatures can be attributed to conductive and convective heat transfer warming the waste rock from the surface inward (Pham et al., 2009). The temperature-dependence of SO_4 concentrations in Type III pile effluent is consistent with the laboratory-scale experiments that illustrate higher SO_4 and lower pH in columns at 25°C compared to columns at 4°C (Moore, 2009, Smith et al., 2009; Figure 4-5).

Fluctuations in SO_4 concentrations also may be influenced by increasing water-rock interactions as field saturation is achieved along longer flow paths as infiltrating snowmelt and rain contact sulfide oxidation reaction products from previously unflushed waste rock. The average initial moisture content of the matrix fraction of the test piles was measured to be 0.025, compared to the estimated field capacity of 0.1 to 0.15 for the matrix material (Neuner, 2009). The discrepancy indicates a wetting-up phase is required before a wetting front can propagate through the pile. The wetting front was estimated to have reached a maximum depth of 7 m by the end of the 2007 field season (Neuner, 2009), suggesting water reporting to 3BNXdrn15 and 3BSXdrn15 is infiltrated snowmelt and rainfall on the pile batters moving by matrix flow and reporting from increasingly long flow paths as the 2007 field season progressed to a maximum height of 7 m of the outer slopes.

Geochemical equilibration calculations indicate few potential mineralogical controls on SO$_4$ during the 2007 field season (Figure 4-6). Saturation index values for basaluminite [Al$_4$SO$_4$(OH)$_{10}$·5H$_2$O] indicate supersaturation for the duration of the field season except a brief time in late August. The saturation indices for alunite [KAl$_3$(SO$_4$)$_2$(OH)$_6$], gypsum [CaSO$_4$·2H$_2$O] and jarosite [KFe$_3$ (SO$_4$)$_2$(OH)$_6$] show a distinct difference at 3BNXdrn15 compared to 3BSXdrn15. Samples collected from 3BSXdrn15 are undersaturated with respect to alunite but samples from 3BNXdrn15 were supersaturated with respect to alunite for the duration of the field season. Samples collected at 3BNXdrn15 approach equilibrium with respect to gypsum but those collected at 3BSXdrn15 remain undersaturated. Samples collected from both locations are undersaturated with respect to jarosite but the 3BNXdrn15 samples have higher saturation indices compared to 3BSXdrn15 (Figure 4-6). The differences in saturation indeces between 3BSXdrn15 and 3BNXdrn15 are attributed to higher SO$_4$ concentrations at 3BNXdrn15 as a result of lower flow rates (Figure 4-7).

4.4.3   pH and alkalinity

No appreciable amounts of carbonate minerals were detected in the biotite schist or granite mineral assemblages during the initial mineralogical investigation (Jambor, 1997). The carbon content of the <50 mm fraction of Type III material collected during test pile construction ranged from 0.008 wt. % C to 0.32 wt. % C with an average of 0.031 wt. % C (Chapter 3). Ratios of neutralizing potential (NP) to acid-generating potential (AP) using a modified Sobek test (Sobek et al., 1978) indicated the <50 mm fraction of Type III pile waste rock collected during pile construction was potentially acid-generating with little neutralization potential. Smaller size fractions have a higher acid-generating potential. The mean calculated NP for the Type III material was 0.28 kg tonne^{-1} CaCO$_3$ with a range of 0.12 to 1.16 kg tonne^{-1}

CaCO$_3$ (Chapter 3). Similarly, NP:AP ratios calculated for Type III material collected in 2004 for the laboratory experiments indicate the Type III material is potentially acid generating with little neutralization potential (Chapter 3).

The sampling points 3BNXdrn15 and 3BSXdrn15 show circumneutral pH rising slightly to a maximum of 7.5 in early July followed by a pH decrease to a minimum of 4.8 at both sample locations in late August. After reaching the minimum, pH increases slightly and stabilizes at about pH 5.5 at 3BNXdrn15 and pH 5.0 at 3BSXdrn15 in October (Figure 4-4). Alkalinity levels are low with a weak decreasing trend, reaching < 1.5 mg L^{-1} (as total CaCO$_3$) at both sample points in late August followed by stabilization at concentrations ~ 10 mg L^{-1} (as total CaCO$_3$) (Figure 4-4). The alkalinity minimum correlates to the pH minimum, which suggests available alkalinity is consumed in acid-neutralizing reactions. The increase in pH and alkalinity after the minimum in late August may be related to a decrease in ambient temperature and reduction in sulfide mineral oxidation rates, secondary mineral precipitation and/or increasing water-rock interactions as longer flow paths are activated. Activating longer flow paths would liberate sulfide mineral oxidation products and alkalinity sources from previously unflushed waste rock.

4.4.4 Aluminum

Concentrations of Al at 3BNXdrn15 increased steadily to a maximum of 0.38 mg L^{-1} in late August and remained at about 0.3 mg L^{-1} until mid-November when the measured concentration was 0.05 mg L^{-1}. Aluminum concentrations at 3BSXdrn15 increased rapidly in late July to 0.54 mg L^{-1} and remained in the range of 0.26 to 0.47 mg L^{-1} for the duration of the field season (Figure 4-4).

MINTEQA2 calculations for the Type III pile basal drain shows supersaturation with respect to gibbsite but undersaturation with respect to amorphous $Al(OH)_3$ (Figure 4-6). Saturation index values for diaspore [α-AlOOH] indicate supersaturation for the duration of the 2007 field season, and saturation index values for boehmite [γ-AlOOH] indicate a decline from supersaturation to undersaturation in early August. The Al hydroxysulfate species basaluminite and alunite may also influence Al concentrations in both 3BNXdrn15 and 3BSXdrn15 samples. Trends in Al concentrations appear to have an ambient temperature control, similar to SO_4.

Secondary Al-bearing precipitates were not observed directly in the initial mineralogical study of fresh waste rock samples (Jambor, 1997) or from samples collected from kinetic tests, which were operated for more than eight months (Blowes and Logsdon, 1998). Mineralogical studies of reacted waste rock in the laboratory column material and Type III pile have not been conducted but are planned after the completion of the laboratory study and field study, respectively. Furthermore, the presence of gibbsite and other secondary $Al(OH)_3$ minerals has not been confirmed in other geochemical studies of mining waste because of difficulties in identifying $Al(OH)_3$ or because other Al-bearing minerals were present (Blowes et al., 2003a). Similar to $Al(OH)_3$, diaspore and boehmite are common Al-species inferred from geochemical model calculations but there are few documented occurrences in mine waste studies (Blowes et al., 2003b).

4.4.5 Iron

Iron is released from primary mineral weathering, such as sulfide mineral oxidation and kinetically-controlled aluminosilicate weathering. Concentrations remain low throughout the field season. Concentrations of Fe at 3BNXdrn15 show a steady increase to a maximum of 0.37 mg L^{-1} in early September when the pH values were lowest, followed by a decrease to

0.02 mg L^{-1} in mid-November. The 3BSXdrn15 concentrations are lower, with Fe increasing to

a maximum of 0.09 mg L^{-1} in early August. Concentrations then decrease to < 0.04 mg L^{-1}

after September (Figure 4-4). Low Fe(II) concentrations compared to Fe(total) concentrations,

low Fe(total) concentrations compared to SO$_4$ levels (Figure 4-4), and pore-gas compositions

in the Type III pile of 20.9 vol. % for the duration of the 2007 field season (Amos et al., 2009),

suggest that Fe is predominantly Fe(III) and Fe is being controlled by secondary mineral

precipitation.

Equilibrium calculations using MINTEQA2 also suggest Fe is controlled by secondary

precipitates. Both 3BNXdrn15 and 3BSXdrn15 samples are supersaturated with respect to

several Fe(III) oxyhydroxide and oxide phases (Figure 4-6). The Fe oxyhydroxide phases

ferrihydrite, goethite and lepidocrocite [γ-FeOOH] represent the typical ferric precipitation

sequence in AMD waters (e.g. equation (3)) where Fe(III) hydroxide/ferrihydrite precipitates

with poorly crystalline goethite. These ferric hydroxides are more soluble and preferentially

dissolve and transform to the more thermodynamically stable crystalline minerals goethite and

lepidocrocite (Langmuir and Whittemore 1971). The 3BNXdrn15 and 3BSXdrn15 samples are

near saturation with respect to ferrihydrite in July but become undersaturated with a minimum

saturation index values occurring in late August. These samples are supersaturated with respect

to goethite and lepidocrocite for most of the field season but saturation index values also

decrease to a minimum in late August. Saturation index values for the Fe oxides hematite

[Fe$_2$O$_3$], maghemite [γ-Fe$_2$O$_3$] and magnetite [Fe$_3$O$_4$] exhibit similar trends to the Fe

oxyhydroxides with saturation at a minimum in late August. Saturation index values for

hematite and magnetite indicate supersaturation for all but a short time period in late August

when saturation indices are at a minimum, whereas saturation index values indicate

undersaturation with respect to maghemite for all but early time calculations. These observations suggest that Al-bearing phases persist, and that the pH becomes sufficiently low in late August to initiate dissolution of some Fe oxyhydroxides.

4.4.6 Neutralization sequence

A sequence of mineral-dissolution and precipitation reactions has been observed to neutralize the pH of pore water in mill tailings impoundments. The pH-buffered plateaus have distinct pH decreases as one mineral is depleted and dissolution of the mineral in the sequence with the next-highest solubility becomes the dominant pH buffer (Blowes and Ptacek, 1994; Jurjovec et al., 2002; Blowes et al., 2003a; Moncur et al., 2006). Typically the buffering sequence progresses from carbonate dissolution to Al hydroxide dissolution to Fe(III) hydroxide dissolution (Table 4-1). Kinetically-limited aluminosilicate mineral dissolution proceeds concurrent to these equilibrium pH buffering reactions and can lead to an increase in pH and the release of Al. Precipitation of Al as secondary Al hydroxides (e.g. gibbsite [crystalline $Al(OH)_3$]) is a source of acidity by consuming base and lowing pH. However, the dissolution of Al hydroxides is an important pH-buffering reaction in AMD waters that consumes acidity and maintains pH in the range of 4 to 4.5 (Blowes et al., 2003b). The equilibrium reaction can be expressed as:

$$Al^{3+} + 3H_2O \leftrightarrow Al(OH)_3 + 3H^+ \tag{5}$$

Where the forward reaction illustrates the production of acidity by $Al(OH)_3$ formation and the reverse reaction illustrates the consumption of acidity by $Al(OH)_3$ dissolution.

MINTEQA2 equilibrium calculations are consistent with the mineralogical and NP data. Water samples are calculated to be undersaturated with respect to calcite [$CaCO_3$], siderite [$FeCO_3$] and all other carbonate minerals for the duration of the 2007 field season

(Figure 4-6). Geochemical equilibration calculations for 3BNXdrn15 and 3BSXdrn15 indicate decreasing gibbsite, goethite saturation index values, concomitant with decreasing pH and alkalinity values. Samples are undersaturated with respect to gibbsite and goethite when pH decreases below 5 (Figure 4-8). Similar trends are evident with other Al and Fe oxide and oxyhydroxide phases (Figure 4-6). Both Al and Fe concentrations increase as saturation index values for Al and Fe oxyhydroxide and oxide phases decrease, respectively. These trends suggest pH is being buffered by the dissolution of Al oxyhydroxide and Fe oxyhydroxide phases as pH drops below 5. Buffering by $Al(OH)_3$ is also inferred to be occurring in the laboratory column experiments for Type III rock (Moore, 2009; Figure 4-5).

Although aluminosilicate mineral dissolution consumes H^+ throughout the pH sequence, the dissolution of aluminosilicate minerals continues to contribute to acid neutralization after the more soluble phases have been depleted. Aluminosilicate mineral dissolution, however, is kinetically-limited. Type III material is a combination of biotite schist and granite lithologies. The biotite schist aluminosilicate mineral assemblage consists mainly of quartz (20 to 50%), albite (35 to 55%) and biotite (10 to 25%) in proportions that vary between samples. The granite consists mainly of K-feldspar, albite and quartz, with <5% each of biotite and muscovite (Jambor, 1997). Type III material aluminosilicate mineral assemblage is expected to consume acid by the dissolution of biotite and plagioclase in the biotite schist and K-feldspar and albite in the granite. These reactions are expected to contribute to acid neutralization in the test piles after the Al and Fe hydroxide phases have been depleted.

4.4.7 Trace metals

The dissolved metals Mn, Cd, Cu, Zn, Co and Ni are present in the Type III basal drain effluent at elevated concentration (Figure 4-4). Concentrations of these metals show similar trends in both 3BNXdrn15 and 3BSXdrn15, and exhibit a seasonal trend with higher concentrations in warmer months and lower concentrations in colder months, similar to SO_4 concentrations. Dissolved metal concentrations at 3BNXdrn15 increase steadily to a maximum on August 20, 2007 then immediately decrease to approximately half of the maximum on August 22, 2007. Concentrations then increase steadily until the end of the intense sampling period in mid-September approaching or attaining to concentrations equal to the maximum values observed in August. The final two concentrations measured in October and November show a decreasing trend with concentrations less than half of the maximum. Most dissolved metal concentrations at 3BSXdrn15 are less than those at 3BNXdrn15 and local maxima occur on different sample days. Concentrations increase through August 10, 2007, with a single sample date (July 30, 2007) recording the maximum observed concentration. Concentrations decrease to approximately half of the maximum on August 24, 2007 and then increase again to a local maximum on September 5, 2007. Concentrations then decrease steadily until late November to concentrations similar to those measured at the beginning of the field season. Gradual increasing and decreasing trends can be attributed to increasing and decreasing test pile temperature in response to ambient temperature fluctuations (Figure 4-3). Abrupt changes in concentrations may be caused by preferential flow paths being activated causing dilution, however the extent of macropore flow in the test piles requires verification (Neuner, 2009). Differences between concentrations of dissolved phases at 3BNXdrn15 and 3BSXdrn15 can be

attributed to lower outflow by an order of magnitude at 3BNXdrn15 compared to 3BSXdrn15 (Figure 4-7).

The concentration of Mn in 3BNXdrn15 increases from < 1 mg L^{-1} in mid-July to a maximum of 19.2 mg L^{-1} on August 20, 2007. The next sample point after the maximum shows a rapid decrease to 8.6 mg L^{-1} and then the concentration increases to a local maximum of 16.3 mg L^{-1} on September 10, 2007. The final two sample points in October and November are < 6 mg L^{-1}. The 3BSXdrn15 effluent Mn concentration reaches 9.5 mg L^{-1} in mid-August and then declines with a concentration of < 7.5 mg L^{-1} for the remainder of the field season (Figure 4-4). The increasing Mn is attributed to dissolution of the aluminosilicate mineral assemblage of the biotite schist. Whole rock analysis of biotite schist samples indicated an average concentration of 0.07 wt. % MnO, and no Mn was detected in sulfide samples (Jambor, 1997). There is no apparent secondary mineral control for Mn based on MINTEQA2 calculations for 3BNXdrn15 and 3BSXdrn15 samples. Saturation index values indicated all of the Type III basal drainage water samples were undersaturated with respect to all Mn secondary species in the database including rhodocrosite, a common mineral found in waters impacted by mining (Figure 4-9).

The concentration of Ni attains a maximum of 10.4 mg L^{-1} at 3BNXdrn15 on August 20, 2007, the Ni concentration then decreases to 4.4 mg L^{-1} on August 22, 2007 and subsequently increases to 8.8 mg L^{-1} on September 10. The final two 3BNXdrn15 samples in the 2007 field season have Ni < 3 mg L^{-1}. The Ni concentration of the 3BSXdrn15 drainage water increases from 2.0 mg L^{-1} in mid-July to 4.1 mg L^{-1} on August 10, 2007 with the local maximum concentration occurring on July 30, 2007 (4.3 mg L^{-1}). The Ni concentration remains < 3 mg L^{-1} at 3BSXdrn15 for the remainder of the field season (Figure 4-4). The Co

concentration at 3BNXdrn15 increases to 1.8 mg L^{-1} on August 20, 2007, drops to 0.75 mg L^{-1} on August 22, 2007 and increases to 1.5 mg L^{-1} through to September 10, 2007. The Co concentrations measured on the October and November sample dates were 0.44 mg L^{-1} and 0.24 mg L^{-1}, respectively. Cobalt concentrations at 3BSXdrn15 increase to a season maximum of 0.70 mg L^{-1} on August 10, 2007, decrease to < 0.4 mg L^{-1} in late August and follow a slight decreasing trend for the remainder of the field season with concentrations in the range of 0.4 to 0.5 mg L^{-1} (Figure 4-4).

Nickel and Co concentrations are highly correlated ($r^2 > 0.98$) but Co concentrations are lower by an order of magnitude. Both Co and Ni are derived from substitutions for Fe in the pyrrhotite [$(Fe_{0.852}Ni_{0.004}Co_{0.001})_{\Sigma 0.857}S$] contained in the Diavik biotite schist. In solution chemistry $Ni(OH)_2$ is a common control for Ni (Alpers et al., 1994) but MINTEQA2 calculations indicate that the drainage water remains undersaturated with respect to $Ni(OH)_2$ for the duration of the 2007 field season (Figure 4-9). However, Ni has been found to adsorb to the surface or be incorporated into the structure of Fe oxyhydroxides (e.g. Cornell, 1991; Webster et al., 1998; Lee et al., 2002; Galan et al., 2003; Gunsinger et al., 2006). Cobalt does not typically form secondary precipitates but may co-precipitate with Fe (oxy)hydroxides, or adsorb to Fe oxyhydroxides (Cornell, 1991). MINTEQA2 calculations indicated that the drainage water remained undersaturated with respect to secondary Co phases.

The Zn concentration is on the same order of magnitude as Co concentrations and reaches 0.95 mg L^{-1} at 3BNXdrn15 on August 20, 2007, decreases to 0.47 mg L^{-1} on August 22, 2007 and then increases to 0.88 mg L^{-1} at the end of the intensive sampling period on September 10, 2007. Concentrations of 0.38 mg L^{-1} and 0.14 mg L^{-1} were measured at 3BNXdrn15 in October and November, respectively. The concentration of Zn measured at

3BSXdrn15 increases from 0.31 mg L^{-1} in mid-July to 0.56 mg L^{-1} in mid-August, with a single sample reaching 0.73 mg L^{-1}. Concentrations remain in the range of 0.5 to 0.4 mg L^{-1} and illustrate a slight decreasing trend for the remainder of the field season. Whereas Zn can substitute for Fe^{2+} in biotite, the low Zn concentration and trends consistent with Co, Ni and SO$_4$ suggests sphalerite oxidation is the source of Zn. Zinc hydroxide [Zn(OH)$_2$] precipitation is a common control for Zn in solution chemistry (Alpers et al., 1994) but MINTEQA2 calculations indicate that both 3BNXdrn15 and 3BSXdrn15 remain undersaturated with respect to Zn secondary minerals for the duration of the 2007 field season (Figure 4-9). Zinc has been found to have a higher propensity to adsorb onto metal oxide surfaces as pH increases (Blowes and Jambor, 1990) and Zn has been observed in Fe oxyhydroxide samples from mill tailings impoundments (Moncur et al., 2005).

Cadmium concentrations are low at both 3BNXdrn15 and 3BSXdrn15 but show trends consistent with Ni, Co and Zn associated with sulfide minerals in the Type III material. Concentrations of Cd at 3BNXdrn15 increase from < 0.002 mg L^{-1} to 0.015 mg L^{-1} on August 20, 2007, drop to 0.010 mg L^{-1} on August 22, 2007 and then increase to 0.015 mg L^{-1} on September 10, 2007. Concentrations for the October sample and the November sample were measured to be 0.007 and 0.006 mg L^{-1}, respectively. 3BSXdrn15 Cd concentrations are lower, increasing from 0.006 mg L^{-1} in mid July to 0.011 mg L^{-1} in mid-August. From mid-August to the end of the sampling season, concentrations steadily decrease to < 0.01 mg L^{-1} (Figure 4-4). Cadmium was not detected in the initial mineralogical study by Jambor (1997) but Cd can substitute for Zn in sphalerite. Geochemical calculations indicate undersaturation with respect to all Cd-bearing secondary minerals in the MINTEQA2 database including otavite, a Cd-bearing carbonate found in other mine waste AMD waters (Figure 4-9).

Copper is released to the Type III pile drainage water by the oxidation of chalcopyrite. Concentrations of Cu show a similar trend to other metals and ions for each 3BNXdrn15 and 3BSXdrn15. Copper, however, is the only metal where 3BNXdrn15 concentrations do not exceed those of 3BSXdrn15 (Figure 4-4). The Cu concentration at 3BNXdrn15 increases from 0.005 mg L^{-1} in mid-July to 0.05 mg L^{-1} on August 20, 2007, decreases to 0.03 mg L^{-1} on August 22, 200, increases to 0.07 mg L^{-1} in September and subsequently decreases to 0.02 mg L^{-1} at the end of the field season in November. The 3BSXdrn15 drainage has higher Cu concentrations. Copper concentrations increasefrom 0.03 mg L^{-1} in mid July to 0.11 mg L-1 on August 10, 2007. After mid-August, the Cu concentration follows a decreasing trend with the effluent concentration in the range of 0.07 to 0.08 mg L^{-1}. MINTEQA2 calculations indicate there is no tendency for covellite [CuS] or chalcocite [CuS$_2$] to become saturated in the drain water (Figure 4-9). Covellite and chalcocite are two common copper precipitates in mine-impacted water.

Maximum concentrations for Mn, Ni, Co, Zn, Cd and Cu correlate to a pH minimum, and are consistent with SO$_4$ behavior. This observation suggests that these metals are released by sulfide-mineral oxidation and acid neutralization reactions and that pH-dependent adsorption reactions control dissolved trace metal concentrations, rather than precipitation of discrete secondary mineral. Type III basal drain samples show a general trend of decreasing concentrations of Ni > Co > Zn > Cu > Cd. This order is consistent with the order of dissolved metal concentrations and mobility observed in several mill tailing impoundments, including the Nordic Main tailings impoundment with Co = Ni > Zn > Pb > Cu (Dubrovsky, 1984), the Waite Amulet tailings with Zn > Ni ≥Co>Pb >Cu (Blowes and Jambor, 1990), and the Lynn Lake tailings area with Zn >Ni = Co > Cr >Al >Cu (Gunsinger et al., 2006).

4.5   Summary and conclusions

Decreasing pH and increasing concentrations of SO_4, Mn, Ni, Co, Zn, Cd and Cu in the Type III pile basal drain samples suggest sulfide mineral oxidation is occurring in the low-sulfide waste rock. Ambient temperature fluctuations and flow path length are inferred to influence concentrations in drainage water. The pH decrease to < 5 in both 3BNXdrn15 and 3BSXdrn15, and alkalinity decrease to < 1 mg L^{-1} (as total $CaCO_3$) suggest acid generation from sulfide mineral oxidation is overwhelming the neutralization capacity of the waste rock and pH acid neutralization is occurring by the dissolution of carbonate minerals and Al and Fe oxyhydroxides. Concentrations of SO_4 up to 1995 mg L^{-1} suggest sulfide mineral oxidation is occurring in the Type III waste rock pile. Concentrations up to 0.54 mg L^{-1} of Al, and calculated saturation index values that indicate a tendency for dissolution of Al (oxy)hydroxides and Al hydrosulfates, suggest that pH-buffering by the dissolution of the Al (oxy)hydroxides is occurring. Low Fe concentrations (<0.37 mg L^{-1}) compared to SO_4 concentrations and calculated saturation index values indicating supersaturation with respect to Fe (oxy)hydroxide phases suggest the dissolved Fe concentration is controlled by Fe(III) (oxy)hydroxide precipitation. Dissolved Mn released from aluminosilicate weathering showed an increasing trend with concentrations up to 19 mg L^{-1} and MINTEQA2 calculations indicated no secondary mineral controls. Nickel and Co released from pyrrhotite oxidation are highly correlated, with maximum concentrations of 10.4 mg L^{-1} and 1.8 mg L^{-1}, respectively. Zinc and Cd released from oxidative dissolution of sphalerite have maximum concentrations of 0.9 mg L^{-1} and 0.015 mg L^{-1}, respectively. Copper concentrations reach 0.13 mg L^{-1} as a result of chalcopyrite oxidation. Equilibrium calculations for 3BNXdrn15 and 3BSXdrn15 indicate undersaturation with respect to Ni, Co, Zn, Cd and Cu-bearing phases.

Superimposed on pH controls of solution chemistries in Type III pile basal drain effluent are ambient temperature variations, which affect sulfide-mineral oxidation rates, and changes to flow path lengths as the wetting front propagates downward through the pile. Changes in sulfide-mineral oxidation rates affect the release of acidity, SO_4, Fe, Co, Ni, Zn, Cd, and Cu. Increases in flow path lengths introduce previously unflushed waste rock into the system, which affects reaction product and alkalinity replenishment. Al is not directly affected by changes in sulfide mineral oxidation rates or reaction path lengths because the Al source is kinetically-limited aluminosilicate mineral dissolution. However, fluctuations in pH will affect whether Al is controlled by $Al(OH)_3$ precipitation or dissolution. Similarly, the solubility control of ferric (oxy)hydroxides, with which Ni, Zn, Co and/or Cd may co-precipitate, decreases with increasing pH.

4.6   Tables

Table 4-1: The pH buffering o fminerals observed in acid-neutralizing sequences (after Blowes and Ptacek, 1994).

Phase	pH range
Calcite	6.5-7.5
Siderite	4.8 – 6.3
Al(OH)3	4.0 – 4.3
Fe(OH)3	2.5 < 3.5

4.7 Figures

Figure 4-1: Location of Diavik diamond mine

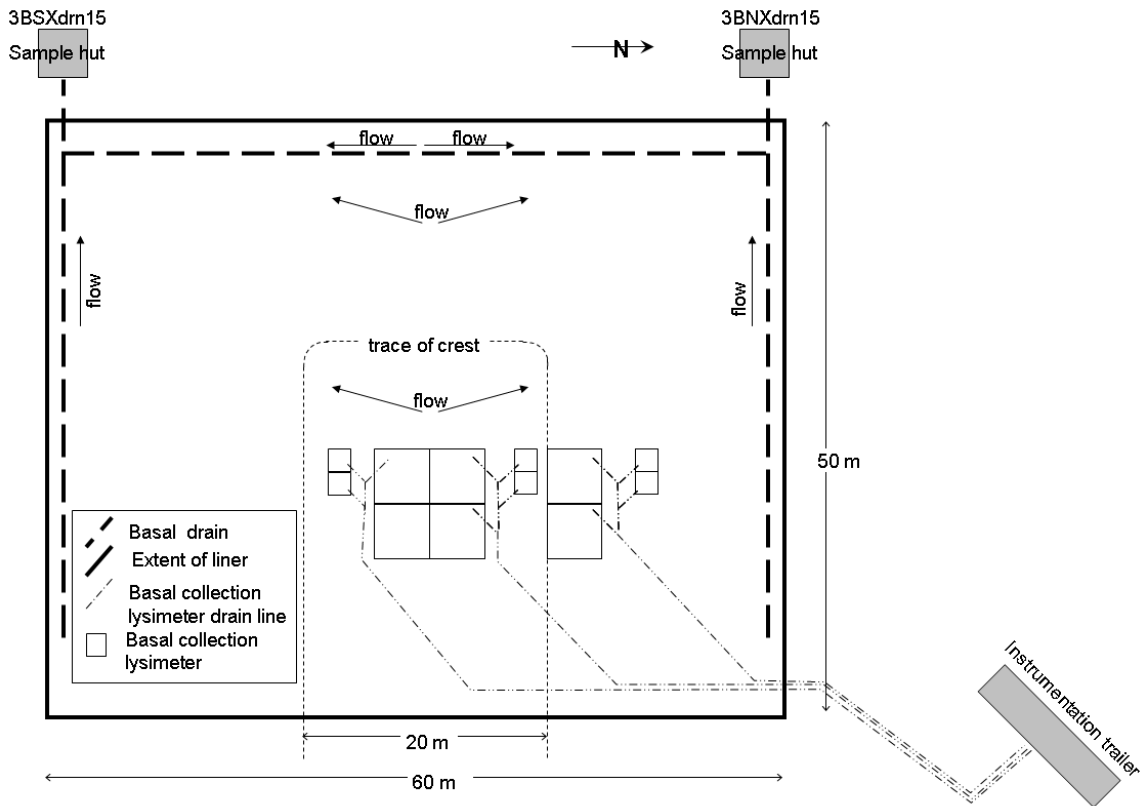**Figure 4-2: Type III pile basal drain configuration**

Figure 4-3: Mean daily temperature from July to November, 2007. Data for October were not available (Environment Canada, 2008).
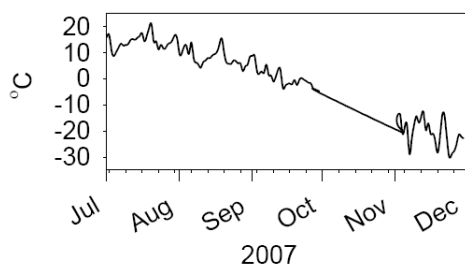
Figure 4-4: Time-series of field parameters, SO₄ and dissolved cations in 3BNXdrn15 (open symbols) and 3BSXdrn15 (closed symbols).
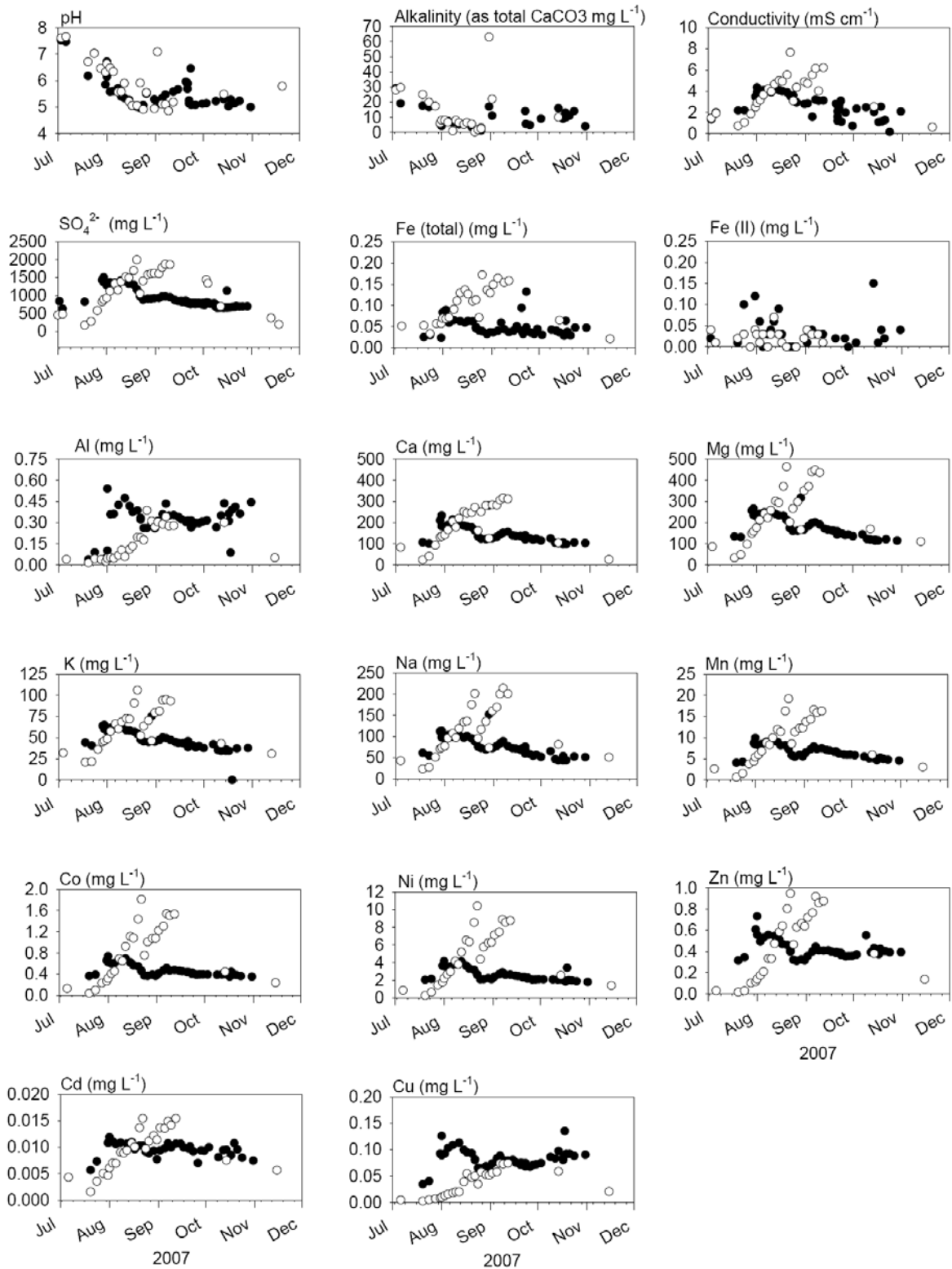
Figure 4-5: Type III material lab results at room temperature (black line) and at 4ºC (grey line)

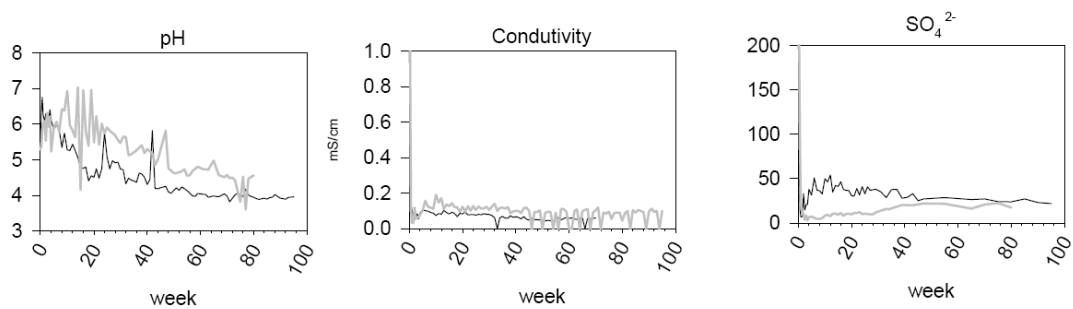**Figure 4-6: Time-series of modeled saturation indices for selected sulfate, carbonate, aluminum and iron species in 3BNXdrn15 (open symbols) and 3BSXdrn15 (closed symbols).**
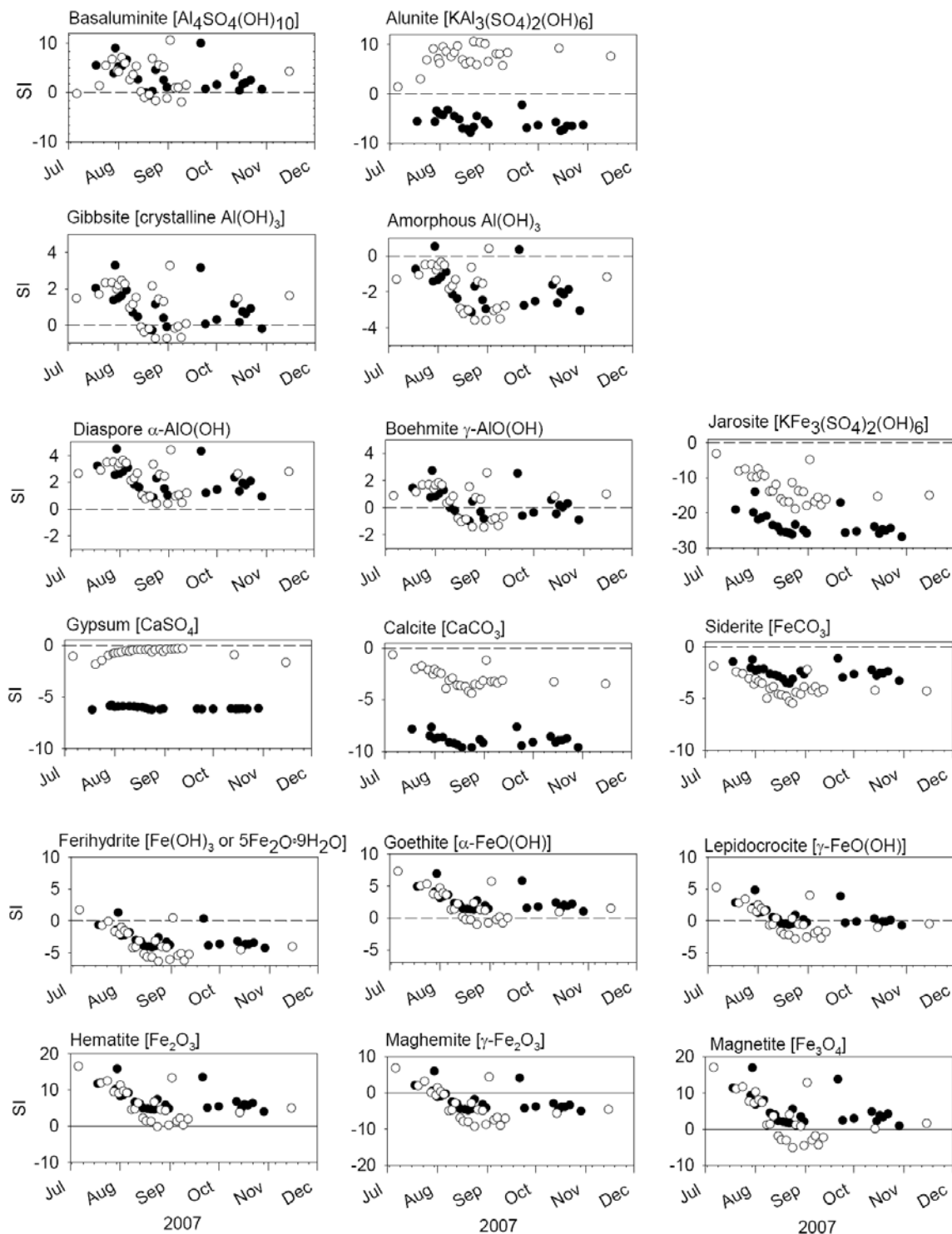
Figure 4-7: Outlfow for (a) 3BSXdrn15 and (b) 3BNXdrn15. Outflow measurement were not recorded from July to August, 2007. Line plot and symbols in (a) represent manual measurements, but manual measurements were not available for 3BNXdrn15.
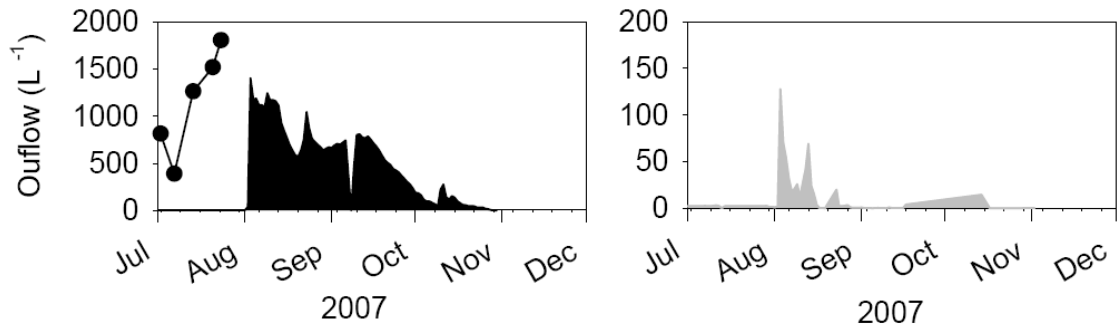
Figure 4-8: pH buffering sequence for 3BNXdrn15 (open symbols) and 3BSXdrn15 (closed symbols).

Minima for pH, alkalinity, and saturation indices for gibbsite and goethite are coincident.
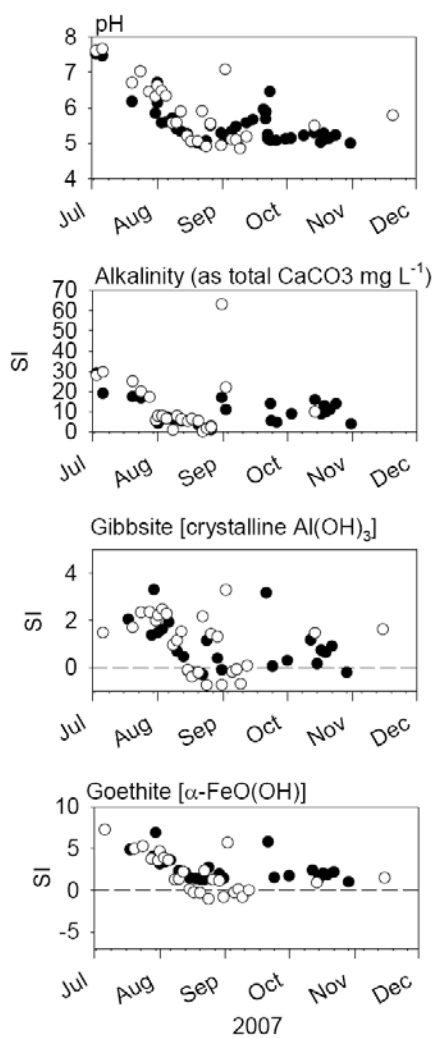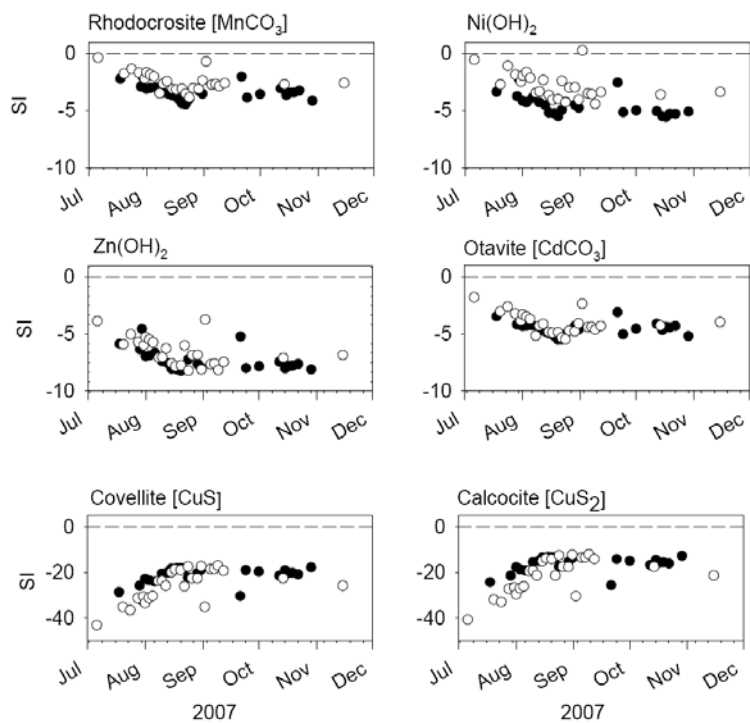
Figure 4-9: Time-series of modeled saturation indices for selected secondary minerals containing Mn, Ni, Zn and Cu in 3BNXdrn15 (open symbols) and 3BSXdrn15 (closed symbols).

Chapter 5: Summary and conclusions

Three large-scale instrumented waste rock piles were constructed at an operating diamond mine in the Canadian Arctic to measure water flow, thermal conductivity, gas evolution and transport, and geochemical and microbiological processes. Instruments were installed on the base of each pile, four angle of repose faces in each pile, and within the covers of the Covered pile. Sufficient instrumentation survived the construction phase in all piles such that measurements will allow the quantification of coupled physicochemical processes occurring in the test piles at various scales and the evolution of those processes over time. A 2 m scale experiment was also installed to measure physicochemical processes in the active freeze-thaw layer and to compare results from the 2 m scale to those obtained from the larger-scale test piles.

One pile was constructed from Type I waste rock, the second pile was constructed from Type III waste rock, and the third Covered pile consisted of a Type III core that was contoured and covered by 1.5 m of till and 3 m of Type I rock. Waste rock types were classified by Diavik as part of the operational waste management procedures. The Type I pile contained an average of 0.035 wt. % S, towards the high end of the Type I waste rock classification. The Type III pile contained an average of 0.053 wt% S, which is below the target sulfur range for Type III waste rock classification. The Covered pile Type III core contained an average of 0.082 wt. % S, which is at the low end of Type III waste rock classification.

Sulfur concentrations of Type I and Type III material suggest higher sulfur concentrations in smaller size fractions. Blast pattern averages were lower than the < 50 mm size fraction, and discrete size fractions < 10 mm had higher sulfur concentrations in smaller particles than larger particles. Particle size distributions of test pile material showed little

variation between the piles and suggest the test piles will behave as rock-like rather than soil-like piles. Rock-like piles may permit channelized flow, which can influence solute flushing rates.

Acid-base accounting suggest AP values calculated using site-specific pyrrhotite composition better predicts the acid-generating behaviour of Diavik Type I and Type III material. However, NP:AP calculations are conservative when NP:AP ratios for column material are compared to column effluent pH and alkalinity levels. The sulfur and particle size data presented in this paper provide a basis for further characterization of the reactive particle size fraction and hydrologic flow regimes.

Effluent samples collected during the first field season in 2007 from the Type III basal drain show decreasing pH and increasing concentrations of SO_4, Mn, Ni, Co, Zn, Cd and Cu. These trends suggest sulfide mineral oxidation is occurring. Ambient temperature fluctuations and flow path lengths are inferred to influence concentrations in drainage water. The pH decreases to < 5, and alkalinity is depleted to < 1 mg L^{-1} (as total $CaCO_3$), suggesting acid generation from sulfide mineral oxidation is overwhelming the neutralization capacity of the waste rock. These findings are consistent with the NP:AP calculations for Type III material. Aluminum and Fe concentrations and geochemical equilibrium calculations suggest that Al (oxy)hydroxide dissolution is buffering the pH. Geochemical calculations also indicate that Fe (oxy)hydroxide phases are controlling the Fe concentration in solution. Aluminosilicate weathering is releasing Mn to solution at concentrations up to 19 mg L^{-1}. No secondary mineral controls on Mn concentrations are indicated by the results of geochemical modelling. Oxidation of pyrrhotite releases Ni and Co to the effluent in concentrations that reach 10.4 mgL^{-1} and 1.8 mg L^{-1}, respectively. Zinc and Cd are released by sphalerite oxidation and have

maximum concentrations of 0.9 mg L^{-1} and 0.015 mg L^{-1}, respectively. Copper released from chalcopyrite oxidation reaches 0.13 mg L^{-1}. Geochemical calculations indicate that the concentrations of these metals are not controlled by secondary mineral precipitation, but Ni, Co and Cd may be adsorbing to Fe oxyhydroxide surfaces and removed from solution. Mineralogical analyses of Type III material is required to confirm the presence of secondary mineral formation.

References

Chapter 1: Introduction

Al, T., Blowes, D.W., Martin, C., Cabri, L., Jambor, J.L. 1997. Aqueous geochemistry and analysis of pyrite surfaces in sulfide-rich mine tailings. Geochim. Cosmochim. Acta, 61, 2353-2366.

Blowes, D.W., Jambour, J.L. 1990. The pore-water chemistry and mineralogy of the vadose zone of sulfide tailings, Waite Amulet, Quebec. Appl. Geochem. 5, 327-346.

Blowes, D.W., Reardon, E.J., Jambor, J.L., Cherry J.A., 1991. The formation and potential importance of cemented layers in inactive sulfide mine tailings. Geochim. Cosmochim. Acta. 55, 965-978.

Blowes, D.W., Logsdon, M.J., 1998. Diavik Geochemistry Baseline Report. Report to Diavik Diamond Mines Inc.

Blowes, D., Smith, L., Sego, D., Smith, L., Neuner, M., Gupton, M., Moncur, M., Klassen, R., Deans, T., Garvie, A., Reinson, J., 2007. Prediction of effluent water quality from waste rock piles in a continuous permafrost region. In Cidu, R. and Frau, F. (eds) Water in Mining Environments. p 3-9, Cagliari (Mako Edizioni).

DDMI, 2006. Interim Closure and Reclamation Plan, Version 2, September 2006. Internal Report.

Environment Canada., 2008. Monthly data report for Ekati A, Northwest Territories, Bulk Data 1998-2007. Accessible at: http://climate.weatheroffice.ec.gc.ca/climateData/canada_e.html

Gunsinger, M.R., Ptacek, C.J., Blowes, D.W. 2006. Evaluation of long-term sulfide oxidation processes within pyrrhotite-rich tailings, Lynn Lake, Manitoba. J. Contam. Hydrol. 83, 149-170.

Johnson, R., Blowes, D.W., Robertson, W., Jambor, J.L. 2000. The hydrogeochemistry of the Nickel Rim mine tailings impoundment, Sudbury, Ontario. J. Contam. Hydrol. 41, 49-80.

Lefebvre, R., Hockley, D., Smolensky, J., Gelinas, P., 2001a. Multiphase transfer processes in waste rock piles producing acid mine drainage 1. Conceptual model and system characterization. J. Contam. Hydrol. 52, 137-164.

Lefebvre, R., Hockley, D., Smolensky, J., Lamontagne, A., 2001b. Multiphase transfer processes in waste rock piles producing acid mine drainage 2. Applications of numerical simulation. J. Contam. Hydrol. 52, 165-186.

Linklater, C.M., Sinclair, D.J., Brown, P.L., 2005. Coupled chemistry and transport modelling of sulphidic waste rock dumps at the Aitik mine site, Sweden. Appl. Geochem. 20, 275-293.

Moncur, M.C., Ptacek, C.J., Blowes, D.W., Jambor, J.L., 2005. Release, transport and attenuation of metals from an old tailings impoundment. Appl. Geochem. 20, 639-659.

Nichol, C., Smith, L., Beckie, R., 2005. Field-scale experiments of unsaturated flow and solute transport in a heterogeneous porous medium. Water Resour. Res. 41, W05018.

Nordstrom, D.K., Alpers, C.N., 1999. Negative pH, efflorescent mineralogy, and consequences for environmental restoration at the Iron Mountain Superfund site, California. Proc. Natl. Acad. Sci. 96, 3455-3462.

Sracek, O., Choquette, M., Gélinas, P., Lefebvre, R., and Nicholson, R.V. 2004. Geochemical characterization of acid mine drainage from a waste rock pile, Mine Doyon, Québec, Canada. J. Contam. Hydrol. 69, 45-7.

Stockwell, J., Smith, L., Jambor, J.L., Beckie, R., 2006. The relationship between fluid flow and mineral weathering in heterogeneous unsaturated porous media: A physical and geochemical characterization of a waste-rock pile. Appl. Geochem. 21, 1347-1361.

Strömberg, B., Banwart, S., 1994. Kinetic modelling of geochemical processes at the Aitik mining waste rock site in northern Sweden. Appl. Geochem. 9, 583-595.

Strömberg, B., Banwart, S., 1999a. Weathering kinetics of waste rock from the Aitik copper mine, Sweden: scale dependent rate factors and pH controls in large column experiments. J. Contam. Hydrol. 39, 59-89.

Strömberg, B., Banwart, S., 1999b. Experimental study of acidity-consuming processes in mining waste rock: some influences of mineralogy and particle size. Appl. Geochem. 14, 1-16.

Chapter 2: Design and Construction of Field-Scale Instrumented Waste Rock Piles in the Canadian Arctic

ADI and ANSTO, 1997. Assessment of gas transfer – ANSTO model at Heath Steele Mines. MEND report 1.21.1b, July 1997, 199 pp.

ANSTO, 1997. Reduction in the overall sulfate generation rate by a low oxygen diffusion coefficient cover. Report to Diavik Diamond Mines Inc.

ANSTO, 1998. The feasibility of maintaining an ice-filled cover layer in an oxidizing stockpile in the Lac de Gras basin. Report to Diavik Diamond Mines Inc.

ASTM D5744-96 Standard Test Method, 2000. Standard test method for accelerated weathering of solid materials using a modified humidity cell. In: Annual Book of ASTM Standards, American Society for Testing and Materials.

Benner, S.G., Blowes, D.W., Ptacek, C.J., and Mayer, K.U., 2002. Rate of sulphate removal and metal sulfide precipitation in a permeable reactive barrier. Appl. Geochem. 17, 201-320.

Bennett, J.W., Ritchie, A.I.M., 1993. Field procedures manual: Measurement of gas permeability. MEND report 1.21.1a, April 1993, 15 pp.

Bennett, J.W., Comarmond, M.J., Clark, N.R, Carras, J.N., Day, S., 1999. Intrinsic oxidation rates of coal reject measured in the laboratory. Proc. Sudbury '99 Mining Environ.1, pp 9-17.

Blackford, M.G., Harries, J.R., 1985. A heat source probe for measuring thermal conductivity in waste rock dumps. AAEC Report No. E609, ANSTO.

Blowes, D.W., Reardon, E.J., Jambor, J.L., Cherry J.A., 1991. The formation and potential importance of cemented layers in inactive sulfide mine tailings. Geochim. Cosmochim. Acta. 55, 965-978.

Blowes, D.W., Logsdon, M.J., 1998. Diavik Geochemistry Baseline Report. Report to Diavik Diamond Mines Inc.

Blowes, D., Moncur, M., Smith, L., Sego, D., Bennet, J., Garvie, A., Linklater, C., Gould, D., Reinson, J., 2006. Construction of two large-scale waste rock piles in a continuous permafrost region. Presented at 2006, 7th International Conference on Acid Rock Drainage, March 26-30, St. Louis, MO.

Brown, P., Luo, X-L., Mooney, J., Pantelis, G., 1999. The modelling of flow and chemical reactions in waste piles. In Second International Conference on CFD in the Minerals and Process Industries, CSIRO, Melbourne, Australia, December 6-8. pp 169 – 174.

Brown, P.L., Crawford, J., Irannejad, P., Miskelly, P.C., Noël, M.M., Pantelis, G., Pltnikoff, W.W., Sinclair, D.J., Stpanyants, Y.A., 2001. SULFIDOX: Version 1.1 A tool for modelling the temporal and spatial behaviour of heaps containing sulfidic minerals. ANSTO Technical Report, ANSTO/ED/TN01-03.

Cathles, L.M., 1979. Predictive capabilities of a finite difference model of copper leaching in low grade industrial sulfide waste dumps. Math. Geol. 11, 175-191.

DDMI, 2006. Interim Closure and Reclamation Plan, Version 2, September 2006. Internal Report.

DDMI, 2007. Meterological Report, March 2007. Internal Report.

Davis, G.B., Ritchie, A.I.M., 1986. A model of oxidation in pyretic mine wastes. 1. Equations and approximate solution. Appl. Math. Modell. 10, 314-322.

Davis, G.B., Ritchie, A.I.M., 1987. A model of oxidation in pyretic mine wastes. 3. Import of the particle size distribution. Appl. Math. Modell. 10, 417-422.

Davis, G.B., Doherty, G., Ritchie, A.I.M., 1986. A model of oxidation in pyretic mine wastes. 2. Comparison of numerical and approximate solution. Appl. Math. Modell. 19, 323-329.

Environment Canada., 2008. Monthly data report for Ekati A, Northwest Territories, Bulk Data 1998-2007. Accessible at: http://climate.weatheroffice.ec.gc.ca/climateData/canada_e.html

Ericksson, N., Gupta, A., Destouni, G., 1997. Comparative analysis of laboratory and field tracer tests for investigating preferential flow and transport in mining waste rock. J. Hydrol. 194, 143-163.

Harries, J.R., Ritchie, A.I.M., 1981. The use of temperature profiles to estimate the pyritic oxidation rate in a waste rock dump from an opencut mine. Water Air Soil Pollut. 15, 405-423.

Harries, J.R., Ritchie, A.I.M., 1983. Runoff fraction and pollution levels in runoff from a waste rock dump undergoing pyritic oxidation. Water Air Soil Pollut. 19, 155-170.

Hubert, W.A., Ferroni, G.D., Leduc, L.G. 1994. Temperature-dependent survival of isolates of *Thiobacillus ferrooxidans*. Current Microbiol. 28, 179-183.

Janzen, M.P., Nicholson, R.V., Scharer, J.M., 2000. Pyrrhotite reaction kinetics: reaction rates for oxidation by oxygen, ferric iron, and for nonoxidative dissolution. Geochim. Cosmochim. Acta 64, 1511-1522.

Lamontagne, A., Lefebvre, R, Poulin, R. Leroueil, S., 1999. Modelling of acid mine drainage physical processes in a waste rock pile with layered co-mingling. Proceedings, 52nd Canadian Geotechnical conference, Regina, Saskatchewan, Oct 24-27, pp 479-485.

Lapakko, K.A., 2003. Developments in humidity-cell tests and their applications. In: Jambor, J.L., Blowes, D.W. and Ritchie, A.I.M. (Eds.), Environmental Aspects of Mine Wastes, Mineral. Assoc. Can. Short Course, 31, pp 147-164.

Leduc, L.G., Trevors, J.T., Ferroni, G.D. 1993. Thermal characterization of different isolates of *Thiobacillus ferrooxidans*. Microbiol. Letters. 108, 189-194.

Lefebvre, R., Gélinas, P., Isabel, D., 1993. Heat transfer during acid mine drainage production in a waste rock dump, La Mine Doyon (Québec). MEND report 1.14.2c, March 1994, 106 pp.

Lefebvre, R., Hockley, D., Smolensky, J., Gelinas, P., 2001a. Multiphase transfer processes in waste rock piles producing acid mine drainage 1. Conceptual model and system characterization. J. Contam. Hydrol. 52, 137-164.

Lefebvre, R., Hockley, D., Smolensky, J., Lamontagne, A., 2001b. Multiphase transfer processes in waste rock piles producing acid mine drainage 2. Applications of numerical simulation. J. Contam. Hydrol. 52, 165-186.

Levenspiel, O., 1972. Chemical Reaction Engineering. J. Wiley, New York.

Litaor, M.I., 1988. Review of Soil Solution Samplers. Water Resour. Res. 24, 727-733.

Linklater, C.M., Sinclair, D.J., Brown, P.L., 2005. Coupled chemistry and transport modelling of sulphidic waste rock dumps at the Aitik mine site, Sweden. Appl. Geochem. 20, 275-293.

Malström M.E., Destouni, G., Banwart, S.A., Strömberg, B.H.E., 2000. Resolving the scale-dependence of mineral weathering rates. Env. Sci Technol. 34, 1375-1378.

Marcoline, J., 2007. Investigations of water and tracer movement in covered and uncovered unsaturated waste rock. PhD Thesis. University of British Columbia, Canada. 292 pp.

Mayer, K.U., Frind, E.O., Blowes, D.W., 2002. Multicomponent reactive transport modeling in variably saturated porous media using a generalized formulation for kinetically controlled reactions. Water Resour. Res. 38, 1174-1195.

Mayer, K.U., Frind, E.O., Blowes, D.W., 2003. Advances in reactive-transport modelling. In: Jambor, J.L., Blowes, D.W. and Ritchie, A.I.M. (Eds.), Environmental Aspects of Mine Wastes, Mineral. Assoc. Can. Short Course, 31, pp. 383-302.

Moncur, M.C., Ptacek, C.J., Blowes, D.W., Jambor, J.L., 2005. Release, transport and attenuation of metals from an old tailings impoundment. Appl. Geochem. 20, 639-659.

Nichol, C., Smith, L., Beckie, R., 2005. Field-scale experiments of unsaturated flow and solute transport in a heterogeneous porous medium. Water Resour. Res. 41, W05018.

Nichol, C., Smith, L., Beckie, R., 2003. Time domain reflectrometry measurements of water content in coarse waste rock. Can. Geotech. J. 40, 137-148.

Nichol, C., Beckie, R., Smith, L., 2002. Evaluation of uncoated and coated TDR probes for high electrical conductivity systems. Soil Sci. Soc. Am. J. 66, 1454-1465.

Nordstrom, D.K., Alpers, C.N., 1999. Negative pH, efflorescent mineralogy, and consequences for environmental restoration at the Iron Mountain Superfund site, California. Proc. Natl. Acad. Sci. 96, 3455-3462.

Parker, J.C., van Genuchten, M. Th., 1984. Flux-averaged and volume-averaged concentrations in continuum approaches to solute transport. Water Resour. Res., 20, 866-872.

Ritchie, A.I.M., 1994. The waste rock environment In: Jambour, J.L. and lowes, D.W. Eds), Environmental Geochemistry of Sulfide Mineral Wastes, Mineral. Assoc. Can. Short Course, 22, pp 201-245.

Ritchie, A.I.M., 2003. Oxidation and gas transport in piles of sulfidic material. In: Jambor, J.L., Blowes, D.W. and Ritchie, A.I.M. (Eds.), Environmental Aspects of Mine Wastes, Mineral. Assoc. Can. Short Course, 31, pp 73-94.

Smith, L., Beckie, R., 2003. Hydrologic and geochemical transport processes in mine waste rock. In: Jambor, J.L., Blowes, D.W. and Ritchie, A.I.M. (Eds.), Environmental Aspects of Mine Wastes, Mineral. Assoc. Can. Short Course, 31, pp 51-72.

Smith, L., Lopez, D.L., Beckie, R., Morin, K., Dwason, R., Price, W., 1995. Hydrogeology of waste rock dumps. Contract report, Natural Resources Canada, Ottawa.

Stockwell, J., Smith, L., Jambor, J.L., Beckie, R., 2006. The relationship between fluid flow and mineral weathering in heterogeneous unsaturated porous media: A physical and geochemical characterization of a waste-rock pile. Appl. Geochem. 21, 1347-1361.

Strömberg, B., Banwart, S., 1999. Weathering kinetics of waste rock from the Aitik copper mine, Sweden: scale dependent rate factors and pH controls in large column experiments. J. Contam. Hydrol. 39, 59-89.

Tan, Y., Ritchie, A.I.M., 1997. In situ determination of thermal conductivity of waste rock dump material. Water, Air and Soil Poll. 98, 345-359.

Velbel, M.A., 1993. Constancy of silicate-mineral weathering-rate ratios between natural and experimental weathering: implications for hydrologic control of differences in absolute rates. Chem. Geol. 105, 89-99.

Wunderly, M.D., Blowes, D.W., Frind, E.O., Ptacek, C.J., 1996. Sulfide mineral oxidation and subsequent reactive transport of oxidation products in mine tailings impoundments: A numerical model. Water Resour. Res. 32, 3173-3187.

Chapter 3: Particle Size and Sulfur Characteristics of Low Sulfide Waste Rock

Amos, R.T., D.W., Blowes, L., Smith, and D.C., Sego., 2009. Measurement of wind induced pressure gradients in a waste rock pile. Accepted; Vadose Zone Journal.

ASTM D422-63 Standard Test Method, 2002. Standard test method for particle-size analysis of soils. In: Annual Book of ASTM Standards, American Society for Testing and Materials.

Blowes, D.W., Ptacek, C.J., Jambor, J.L., Weisener, C.G., 2003. The geochemistry of acid mine drainage. In: Sherwood Lollar, B., Holland, H.D., and Turekian, K.K. (Eds.), Treatise on Geochemistry, Volume 9, 149-204, Elsevier.

Blowes, D.W., Logsdon, M.J., 1998. Diavik Geochemistry Baseline Report. Report to Diavik Diamond Mines Inc.

Cathles, L.M., 1979. Predictive capabilities of a finite difference model of copper leaching in low grade industrial sulfide waste dumps. Math. Geol. 11, 175-191.

Davis, G.B., Ritchie, A.I.M., 1986. A model of oxidation in pyretic mine wastes. 1. Equations and approximate solution. Appl. Math. Modell. 10, 314-322.

Davis, G.B., Ritchie, A.I.M., 1987. A model of oxidation in pyretic mine wastes. 3. Import of the particle size distribution. Appl. Math. Modell. 10, 417-422.

Davis, G.B., Doherty, G., Ritchie, A.I.M., 1986. A model of oxidation in pyretic mine wastes. 2. Comparison of numerical and approximate solution. Appl. Math. Modell. 19, 323-329.

Dawson, R., Morgenstern, N., 1995. Liquifaction flowslides in Rocky Mountain coal waste dumps, Phase 3, Final Report. Natural Resources Canada, Ottawa, Ontario. Contract Report 23440-3-9135/01.

Environment Canada., 2008. Monthly data report for Ekati A, Northwest Territories, Bulk Data 1998-2007. Accessible at: ttp://climate.weatheroffice.ec.gc.ca/climateData/canada_e.html

Jambor, J.L., Dutrizac, J.E., Raudsepp, M., 2007. Measured and computed neutralization potentials from static tests of diverse rock types. Environ. Geol. 52, 1173-1185.

Jambor, J.L., 2003. Mine-waste mineralogy. In: Jambor, J.L., Blowes, D.W. and Ritchie, A.I.M. (Eds.), Environmental Aspects of Mine Wastes, Mineral. Assoc. Can. Short Course, 31, pp. 117-145.

Jambor, J.L., Dutrizac, J.E., Raudsepp, M., Groat, L.A., 2003. Effect of peroxide on neutralization-potential values of siderite and other carbonate minerals. J. Environ. Qual. 32, 2373-2378.

Jambor, J. 1997. Mineralogy of the Diavik Lac de Gras kimberlites and host rocks. Report to Diavik Diamond Mines Inc.

Johnson, R., Blowes, D.W., Robertson, W., Jambor, J.L. 2000. The hydrogeochemistry of the Nickel Rim mine tailings impoundment, Sudbury, Ontario. J. Contam. Hydrol. 41, 49-80.

Lamontagne, A., Lefebvre, R, Poulin, R. Leroueil, S., 1999. Modelling of acid mine drainage physical processes in a waste rock pile with layered co-mingling. Proceedings, 52nd Canadian Geotechnical conference, Regina, Saskatchewan, Oct 24-27, pp 479-485.

Lefebvre, R., Hockley, D., Smolensky, J., Lamontagne, A., 2001a. Multiphase transfer processes in waste rock piles producing acid mine drainage 2. Applications of numerical simulation. J. Contam. Hydrol. 52, 165-186.

Lefebvre, R., Hockley, D., Smolensky, J., Gelinas, P., 2001b. Multiphase transfer processes in waste rock piles producing acid mine drainage 1. Conceptual model and system characterization. J. Contam. Hydrol. 52, 137-164.

Levenspiel, O., 1972. Chemical Reaction Engineering. J. Wiley, New York.

Linklater, C.M., Sinclair, D.J., Brown, P.L., 2005. Coupled chemistry and transport modelling of sulphidic waste rock dumps at the Aitik mine site, Sweden. Appl. Geochem. 20, 275-293.

Mayer, K.U., Frind, E.O., Blowes, D.W., 2003. Advances in reactive-transport modelling. In: Jambor, J.L., Blowes, D.W. and Ritchie, A.I.M. (Eds.), Environmental Aspects of Mine Wastes, Mineral. Assoc. Can. Short Course, 31, pp. 383-302.

Mayer, K.U., Frind, E.O., Blowes, D.W., 2002. Multicomponent reactive transport modeling in variably saturated porous media using a generalized formulation for kinetically controlled reactions. Water Resour. Res. 38, 1174-1195.

Moore, M.L. 2009. Laboratory column experiments of low sulfide waste rock. M.Sc. Thesis, University of Waterloo, in preparation.

Neuner, M., 2009. Water flow through unsaturated mine waste rock in a region of permafrost. MSc Thesis, University of British Columbia, Vancouver, BC, Canada.

Nichol, C., Smith, L., Beckie, R., 2005. Field-scale experiments of unsaturated flow and solute transport in a heterogeneous porous medium. Water Resour. Res. 41, W05018.

Skousen, J., Renton, J., Brown, H., Evans, P., Leavitt, B., Brady, K., Cohen, L., Ziemkiewicz, P., 1997. Neutralization potential of overburden samples containing siderite. J. Environ. Qual. 26, 673-681.

Sobek, A.A., Schuller, W.A., Freeman, J.R., Smith, R.M. 1978. Field and laboratory methods applicable to overburdens and minesoils. EPA report no. EPA-600/2-78-054.

Stockwell, J., Smith, L., Jambor, J.L., Beckie, R., 2006. The relationship between fluid flow and mineral weathering in heterogeneous unsaturated porous media: A physical and geochemical characterization of a waste-rock pile. Appl. Geochem. 21, 1347-1361.

Strömberg, B., Banwart, S., 1999. Experimental study of acidity-consuming processes in mining waste rock: some influences of mineralogy and particle size. Appl. Geochem. 14, 1-16.

Velbel, M.A., 1993. Constancy of silicate-mineral weathering-rate ratios between natural and experimental weathering: implications for hydrologic control of differences in absolute rates. Chem. Geol. 105, 89-99.

Weber, P.A., Thomas, J.W., Skinner, W.M., Smart, R.St.C., 2004. Improved acid neutralization capacity assessment of iron carbonates by titration and theoretical calculation. Appl. Geochem. 19, 687-694.

White, W.W. III, Lapakko, K.A., Cox, R.L., 1999. Static test methods most commonly used to predict acid-mine drainage: Practical guidelines for use and interpretation. In: Plumlee, G.S., Logsdon, M.J. (Eds.), The Environmental Geochemistry of Mineral Deposits. Part A: Processes, techniques and health issues. Rev. Econ. Geol. 6A, 325-338.

Wunderly, M.D., Blowes, D.W., Frind, E.O., Ptacek, C.J., 1996. Sulfide mineral oxidation and subsequent reactive transport of oxidation products in mine tailings impoundments: A numerical model. Water Resour. Res. 32, 3173-3187.

Chapter 4: Initial Geochemical Response from a Low Sulfide Waste Rock Pile

Al, T., Blowes, D.W., Martin, C., Cabri, L., Jambor, J.L., 1997. Aqueous geochemistry and analysis of pyrite surfaces in sulfide-rich mine tailings. Geochim. Cosmochim. Acta, 61, 2353-2366.

Allison, J.D., Brown, D.S., Nova-Gardac, K.L., 1990 MINTEQA2/PRODEFA2, A geochemical assessment model for environmental systems, Version 3.0 User's Manual. Environmental Research Laboratory, Office of Research and Development, U.S. EPA, Athens, Ga. Pp 106.

Alpers, C.N., Blowes, D.W., Nordstrom, D.K., Jambor, J.L., 1994. Secondary minerals and acid mine-water chemistry. In: Jambor, J.L., Blowes, D.W. (Eds.), Environmental Geochemistry of Sulfide Mine-Wastes, Mineral. Assoc. Can. Short Course, 22, 245-270.

Amos, R.T., D.W., Blowes, L., Smith, and D.C., Sego., 2009. Measurement of wind induced pressure gradients in a waste rock pile. Accepted; Vadose Zone Journal.

Ball, J.W., Nordstrom, D.K., 1991. User manual for WATQF4 with revised thermal dynamic database and test cases for calculating speciation of major, trace, and redox elements in natural waters. Open-file report, USGS. P. 91-183.

Berner, R.A., 1980. Early Diagenesis: A Theoretical Approach. Princeton, NJ: Princeton University Press.

Blowes, D.W., Jambor, J.L., 1990. The pore-water geochemistry and the mineralogy of the vadose zone of sulfide tailings, Waite Amulet, Quebec, Canada. Appl. Geochem. 5, 327-346.

Blowes, D.W., Reardon, E.J., Jambor, J.L., Cherry J.A., 1991. The formation and potential imoratnace of cemented layers in inactive sulfide mine tailings. Geochim. Cosmochim. Acta. 55, 965-978.

Blowes, D.W., Jambor, J.L., Appleyard, E.C., Reardon, E.J., Cherry, J.A., 1992. Temporal observations of the geochemistry and mineralogy of a sulfide-rick mine-tailings impoundment, Heath Steele Mines, New Brunswick. Explor. Mining Geol. 1, 251-264.

Blowes, D.W., Ptacek, C.J., 1994. Acid neutralization reactions in mine tailings. In: Jambor, J.L., Blowes, D.W. (Eds.), Environmental Geochemistry of Sulfide Mine-Wastes, Mineral. Assoc. Can. Short Course, 22, 271-292.

Blowes, D.W., Logsdon, M.J., 1998. Diavik Geochemistry Baseline Report. Report to Diavik Diamond Mines Inc.

Blowes, D.W., Ptacek, C.J., Jurjovec, J., 2003a. Mill tailings: Hydrogeology and geochemistry. In: Jambor, J.L., Blowes, D.W. and Ritchie, A.I.M. (Eds.), Environmental Aspects of Mine Wastes, Mineral. Assoc. Can. Short Course, 31, 95-116.

Blowes, D.W., Ptacek, C.J., Jambour, J.L., Weisener, C.G., 2003b. The geochemistry of acid mine drainage. In: Sherwood Lollar, B., Hooland, H.D., and Turekian, K.K. (Eds.), Treatise on Geochemistry, Volume 9, 149-204, Elsevier.

Brookfield, A.E., Blowes, D.W., Mayer, K.U., 2006. Integration of field measurements and reactive transport modelling to evaluate contaminant transport to a sulfide mine tailings impoundment. J. Contam. Hydrol 88, 1-22.

Cathles, L.M., 1979. Predictive capabilities of a finite difference model of copper leaching in low grade industrial sulfide waste dumps. Math. Geol. 11, 175-191.

Cornell, R.;M., 1991. Simultaneous incorporation of Min, Ni and Co in the goethite structure. Clay Minerals 26, 427-430.

Davis, G.B. and Ritchie, A.I.M., 1986. A model of oxidation in pyretic mine wastes. 1. Equations and approximate solution. Appl. Math. Modell. 10, 314-322.

Davis, G.B., Doherty, G. and Ritchie, A.I.M., 1986. A model of oxidation in pyretic mine wastes. 2. Comparison of numerical and approximate solution. Appl. Math. Modell. 19, 323-329.
Davis, G.B. and Ritchie, A.I.M., 1987. A model of oxidation in pyretic mine wastes. 3. Import of the particle size distribution. Appl. Math. Modell. 10, 417-422.

Dubrovsky, N.M., Cherry, J.A., Reardon, E.J., Vivyurka, A.J., 1984. Geochemical evolution of inactive pyritic tailings in the Elliot Lake Uranium Districts: The groundwater zone. Can. Geotech. J. 22, 110-128.

Environment Canada., 2008. Monthly data report for Ekati A, Northwest Territories, Bulk Data 1998-2007. Accessible at: http://climate.weatheroffice.ec.gc.ca/climateData/canada_e.html

Galan, E., Gomez-Hriza, J.L., Gonzales, I., Fernandez-Caliani, J.C., Morales, E., Giraldez, I., 2003. Heavy metal partitioning in river sediments severly polluted by acid mine drainage in the Iberian Pyrite Belt. Appl. Geochem. 18, 409-421.

Gould, W.D., Kapoor, A., 2003. The microbiology of acid mine drainage. In: Jambor, J.L., Blowes, D.W. and Ritchie, A.I.M. (Eds.), Environmental Aspects of Mine Wastes, Mineral. Assoc. Can. Short Course, 31, 203-226.

Gunsinger, M., Ptacek, C.J., Blowes, D.W., Jambor, J.L., 2006. Evaluation of long-term sulfide oxidation processes within pyrrhotite-rich tailings, Lynn Lake, Manitoba. J. Contam. Hydrol. 83, 149-170.

Jambor, J.L., 1997. Mineralogy of the Diavik Lac de Gras kimberlites and host rocks. Report to Diavik Diamond Mines Inc.

Janzen, M.P., Nicholson, R.V., Scharer, J.M., 2000. Pyrrhotite reaction kinetics: Reaction rates for oxidation by oxygen, ferric iron and for nonoxidative dissolution. Geochim. Cosmochim. Acta. 64, 1511-1522.

Johnson, R., Blowes, D.W., Robertson, W., Jambor, J.L., 2000. The hydrogeochemistry of the Nickel Rim mine tailings impoundment, Sudbury, Ontario. J. Contam. Hydrol. 41, 49-80.

Jurjovec, J., Ptacek, C.J., Blowes, D.W., 2002. Acid neutralization mechanisms and metal release in mine tailings: A laboratory column experiments. Geochim. Cosmochim. Acta 66, 1511-1523.

Langmuir, S., Whittemore, D.O., 1971. Variations in the stability of precipitated ferric oxyhydroxides. In: Hem, J.D. (Ed.) Variations in the stability of precipitated ferric oxyhydroxides. Advances in Chemistry Series, no. 106.

Lasaga, A.C., 1998. Kinetic Theory in Earth Sciences. Princeton, NJ: Princeton University Press.

Leduc, L. G., Trevors, J.T., Ferroni, G.D., 1993. Thermal characterization of different isolates of *Thiobacillus ferrooxidans*. FEMS Microbiol. Lett. 18, 189-194.

Lee, G., Bigham, J.M., Faure, G., 2002. Removal of trace metals by coprecipitation with Fe, Al and Mn from natural waters contaminated with acid mine drainage in the Ducktown Mining District, Tennessee. Appl. Geochem. 17, 569-581.

Lefebvre, R., Hockley, D., Smolensky, J. Gelinas, P., 2001. Multiphase transfer processes in waste rock piles producing acid mine drainage 1. Conceptual model and system characterization. J. Contam. Hydrol. 52, 137-164.

Levenspiel, O., 1972. Chemical Reaction Engineering. J. Wiley, New York.

Mayer, K.U., Frind, E.O., Blowes, D.W., 2002. Multicomponent reactive transport modeling in variably saturated porous media using a generalized formulation for kinetically controlled reactions. Water Resour. Res. 38, 1174-1195.

Moncur, M.C., Ptacek, C.J., Blowes, D.W., Jambor, J.L., 2005. Release, transport and attenuation of metals from an old tailings impoundment. Appl. Geochem. 20, 639-659.

Moncur, M.C., Ptacek, C.J., Blowes, D.W., Jambor, J.L., 2006. Spatial variations in water composition at a northern Canadian lake impacted by mine drainage. Appl. Geochem. 20, 639-659.

Moore, M.L., 2009. Laboratory column experiments of low sulfide waste rock. M.Sc. Thesis, University of Waterloo, in preparation.

Neuner, M., Gupton, M., Smith L., Pham, N., Smith, L., Blowes, D., Sego, D., 2009. Diavik waste rock project: Unsaturated water flow. Proceedings of the 8th International Conference on Acid Rock Drainage, June 22-26, Skellefteå, Sweden.

Neuner, M., 2009. Water flow through unsaturated mine waste rock in a region of permafrost. MSc Thesis, University of British Columbia, Vancouver, BC, Canada.

Nichol, C., Smith, L. and Beckie, R., 2005. Field-scale experiments of unsaturated flow and solute transport in a heterogeneous porous medium. Water Resour. Res. 41, W05018.

Olson, G.J., 1991. Rate of pyrite bioleaching by *Thiobacillus ferrooxidans* - results of an interlaboratory comparison. Appl. Environ. Microbiol. 57, 642-644.

Pauling, L. 1970. General Chemistry, 2nd Ed. New York: Dover.

Pham, N., Sego, D.C., Arenson, L.U., Blowes, D., Smith, L., Smith, L., Gupton, G., Neuner, M., Amos, R., 2009. Diavik waste rock project: Heat transfer in experimental waste rock piles under permafrost environment. Proceedings of the 8th International Conference on Acid Rock Drainage, June 22-26, Skellefteå, Sweden.

Singer, P.C., Stumm, W., 1970. Acid mine drainage-rate determining step. Science 167, 1121-1123.

Smith, L.J.D., Neuner, M., Gupton, M., Moore, M., Bailey, B.L., Blowes, D.W., Smith, L., Sego, D.C., 2009. Diavik waste rock project: From the laboratory to the Canadian Arctic. Proceedings of the 8th International Conference on Acid Rock Drainage, June 22-26, Skellefteå, Sweden.

Sobek, A.A., Schuller, W.A., Freeman, J.R., Smith, R.M., 1978. Field and laboratory methods applicable to overburdens and mine soils. EPA report no. EPA-600/2-78-054.

Stockwell, J., Smith, L., Jambor, J.L., Beckie, R., 2006. The relationship between fluid flow and mineral weathering in heterogeneous unsaturated porous media: A physical and geochemical characterization of a waste-rock pile. Appl. Geochem. 21, 1347-1361.

Strömberg, B., Banwart, S., 1999. Experimetnal study of acidity-consuming processes in mining waste rock: some influences of mineralogy and particle size. Appl. Geochem. 14, 1-16.

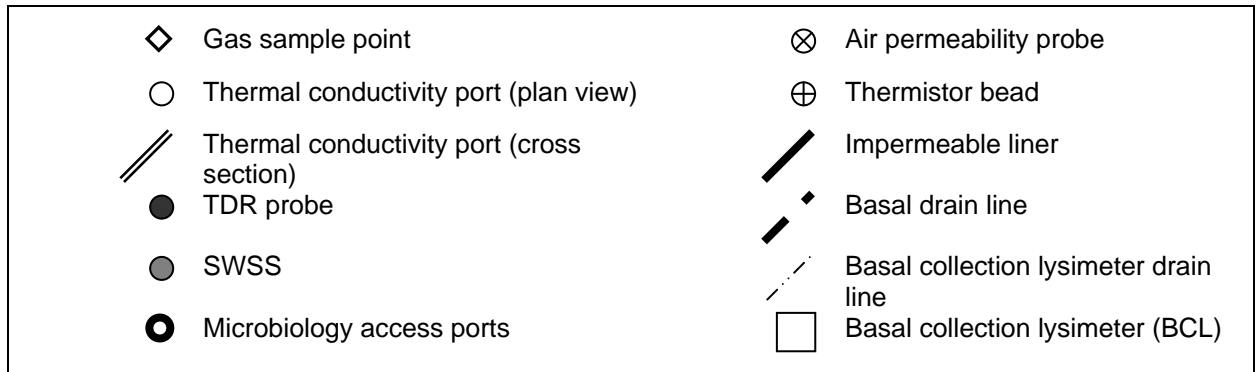Stumm, W., 1992. Chemistry of the Solid-Water Interface. New York: John Wiley & Sons.

Webster, J.G., Swedlund, P.J., Webster, K.S., 1998. Trace metal adsorption onto an acid mine drainage iron(III) oxy hydroxyl sulphate. Environ. Sci. Technol. 32, 1361-1368.

Wunderly, M.D., Blowes, D.W., Frind, E.O. and Ptacek, C.J., 1996. Sulfide mineral oxidation and subsequent reactive transport of oxidation products in mine tailings impoundments: A numerical model. Water Resour. Res. 32, 3173-3187.

Appendix A   Instrument distribution figures

A.1 Legend for figures

◇	Gas sample point	⊗	Air permeability probe
○	Thermal conductivity port (plan view)	⊕	Thermistor bead
⫽	Thermal conductivity port (cross section)	—	Impermeable liner
●	TDR probe	┄	Basal drain line
◓	SWSS	╱	Basal collection lysimeter drain line
◉	Microbiology access ports	☐	Basal collection lysimeter (BCL)

A.2 Type I pile

Figure A-1: Type I pile base dimensions and instrument distributions

118
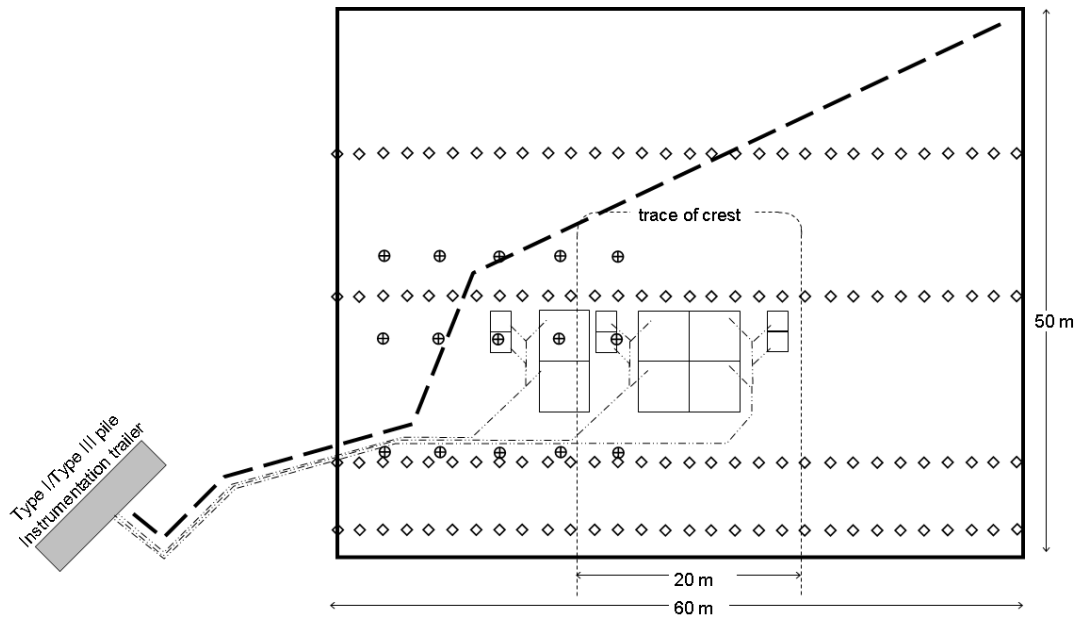
Figure A-2: Type I pile crest dimensions and instrument distributions
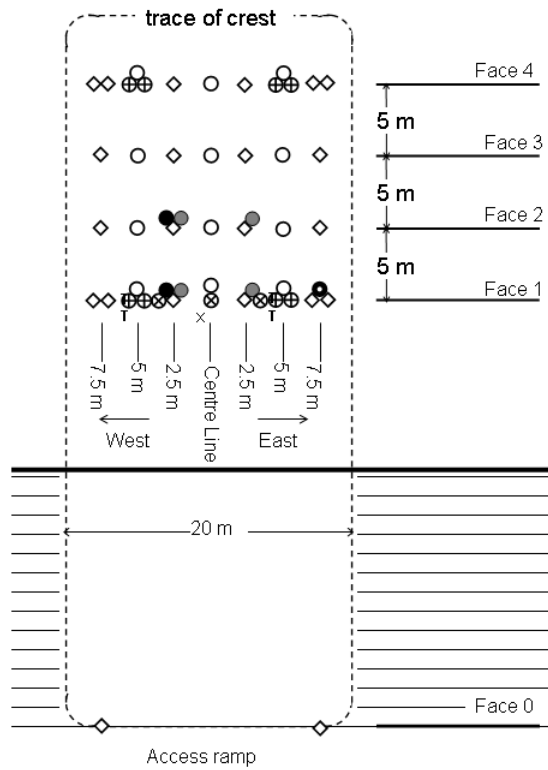
Figure A-3: Type I pile Face 0 (transition between access ramp and pile) dimensions and instrument distributions
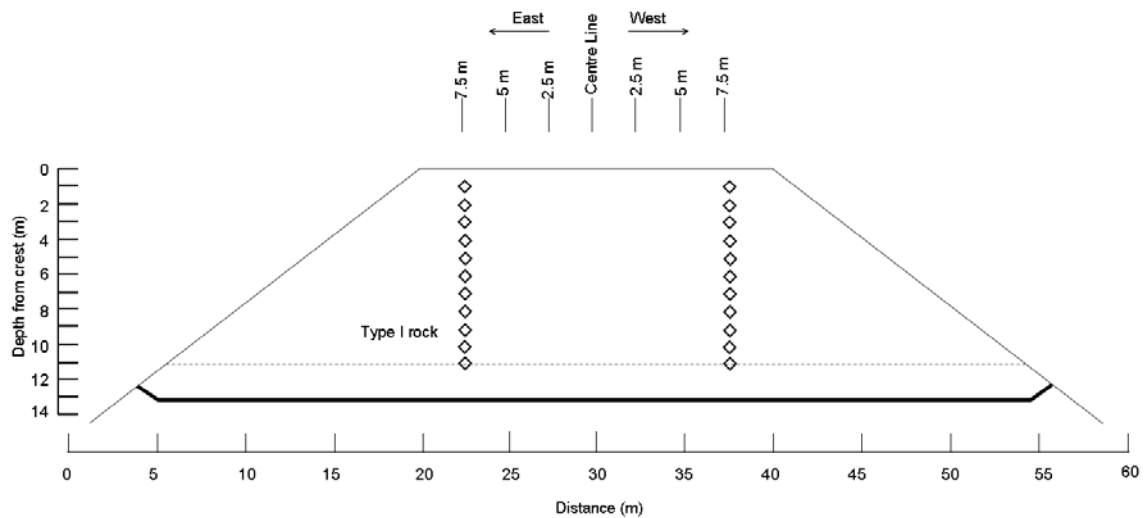
Figure A-4: Type I pile Face 1 dimensions and instrument distributions
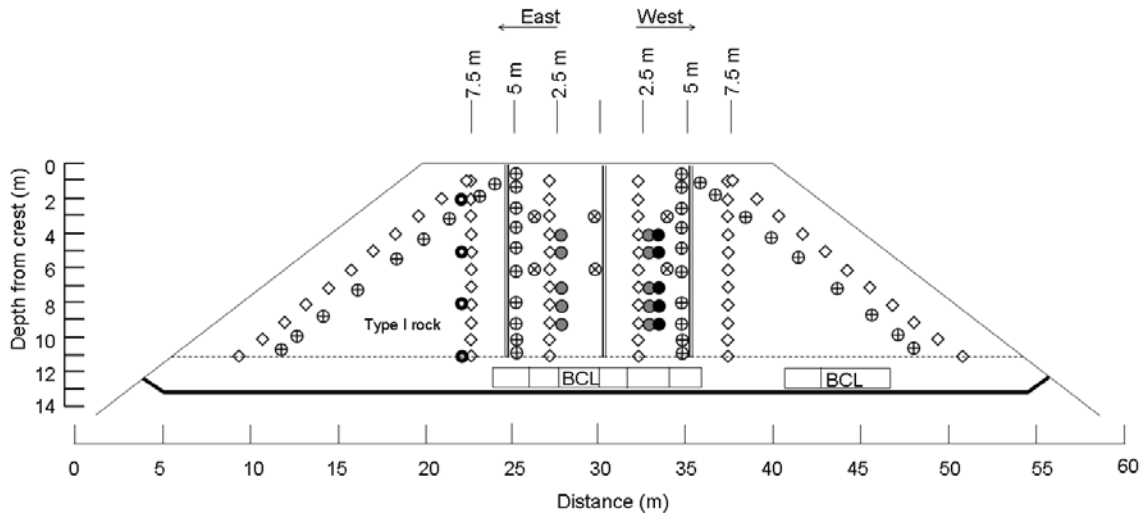
Figure A-5: Type I pile Face 2 dimensions and instrument distributions
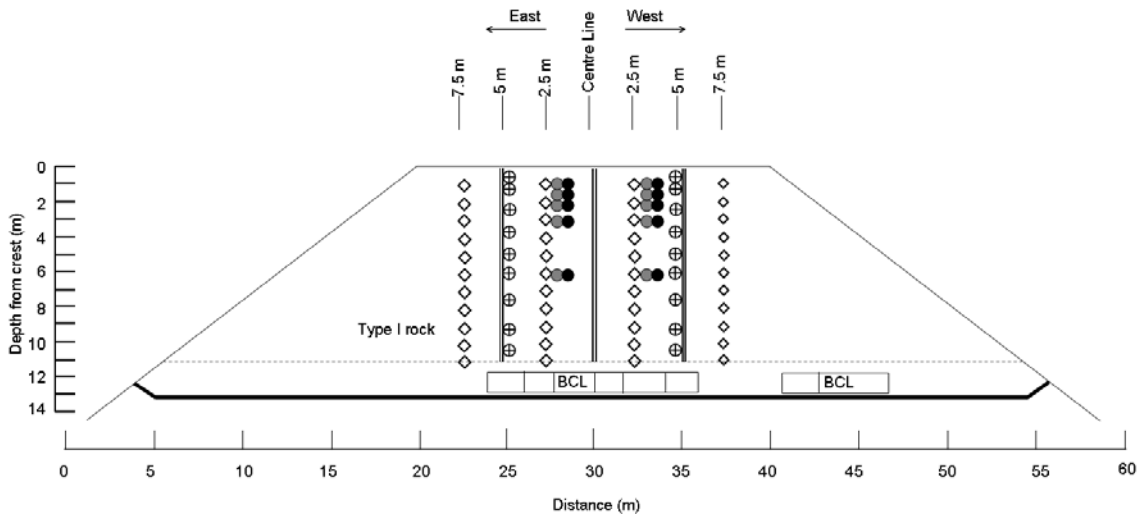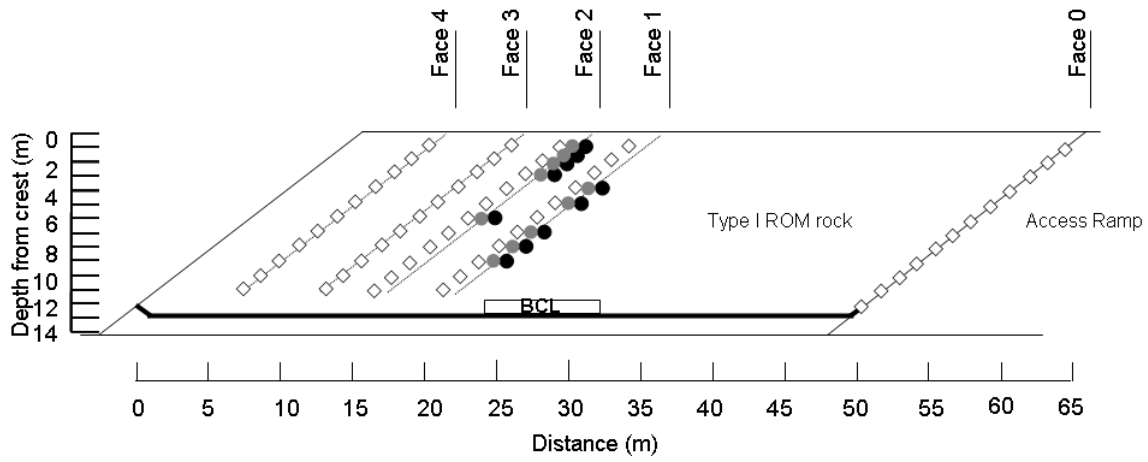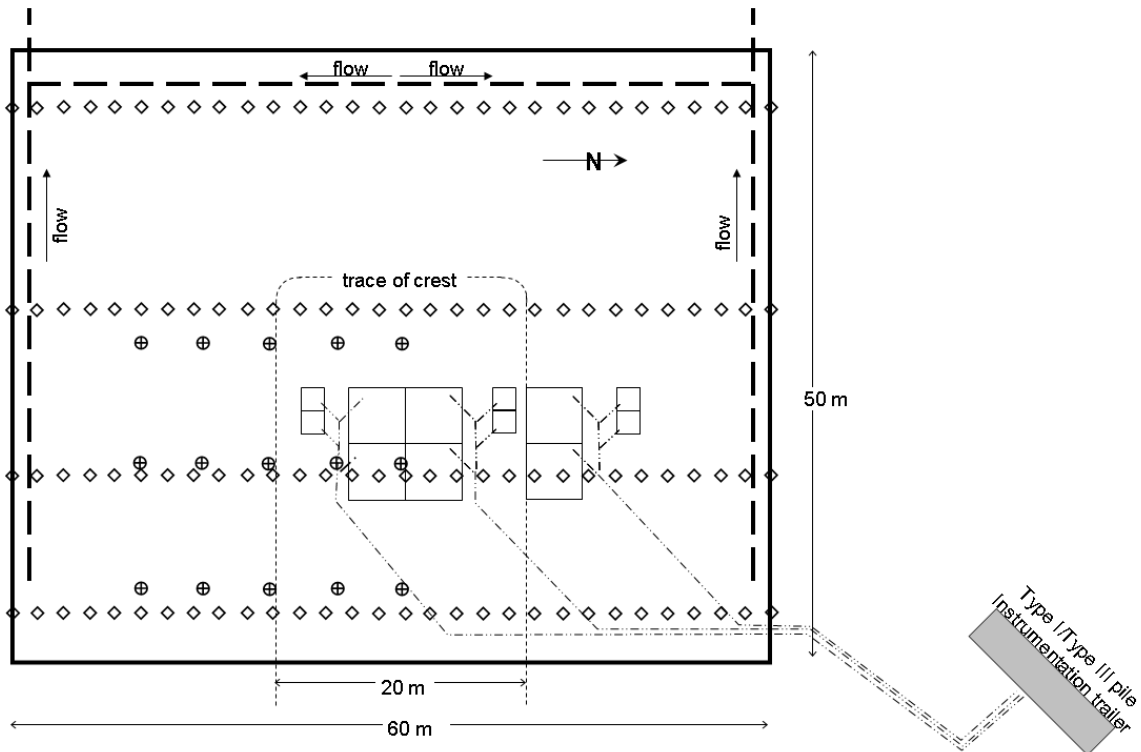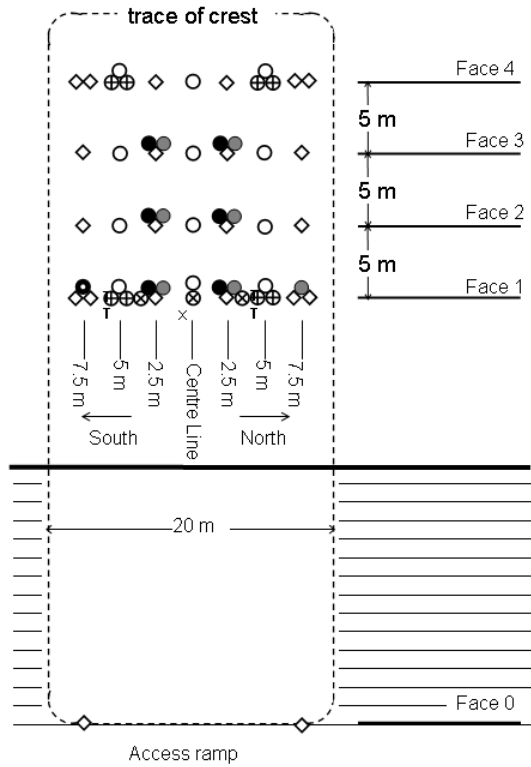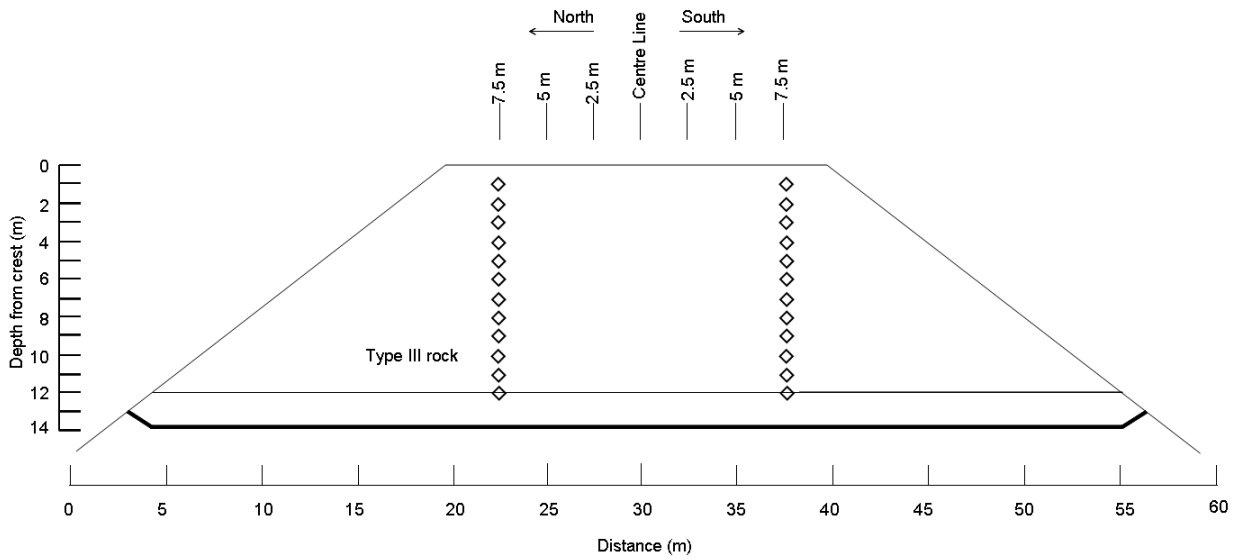
Figure A-6: Type I pile Face 3 dimensions and instrument distributions
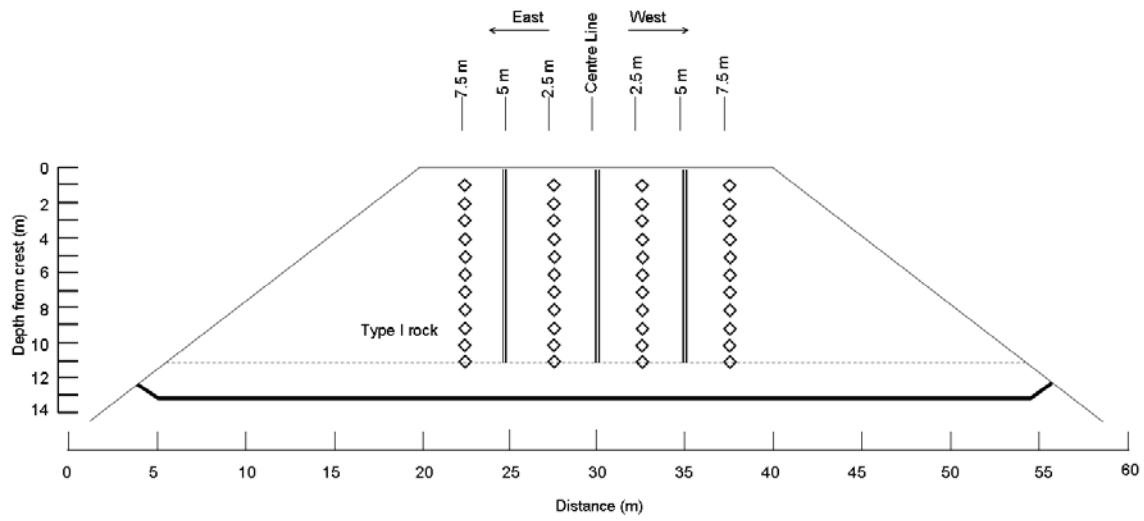
Figure A-7: Type I pile Face 4 dimensions and instrument distributions
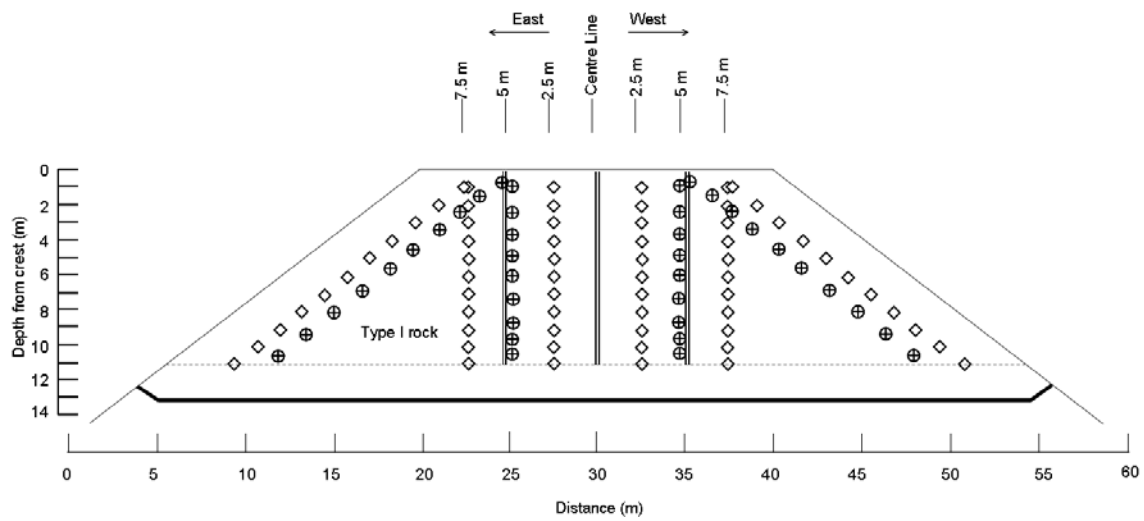
Figure A-8: Type I pile profile of SWSS, TDR and gas line distributions

A.3 Type III pile

Figure A-9: Type I pile base dimensions and instrument distributions

122

Figure A-10: Type III pile crest dimensions and instrument distributions

Figure A-11: Type I pile Face 0 (transition between access ramp and pile) dimensions and instrument distributions

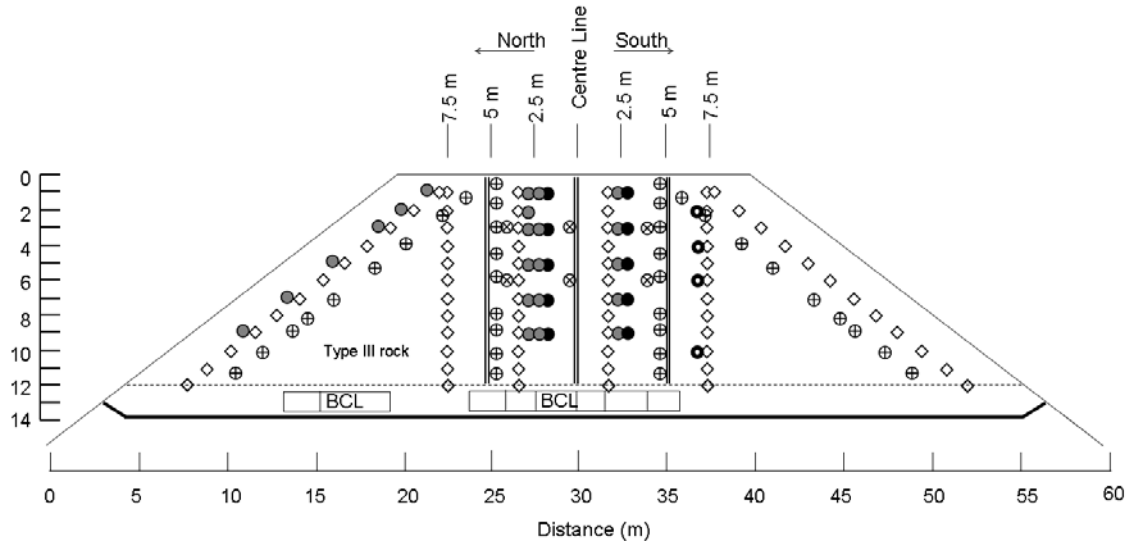**Figure A-12: Type III pile Face 1 dimensions and instrument distributions**

Figure A-13: Type III pile Face 2 dimensions and instrument distributions
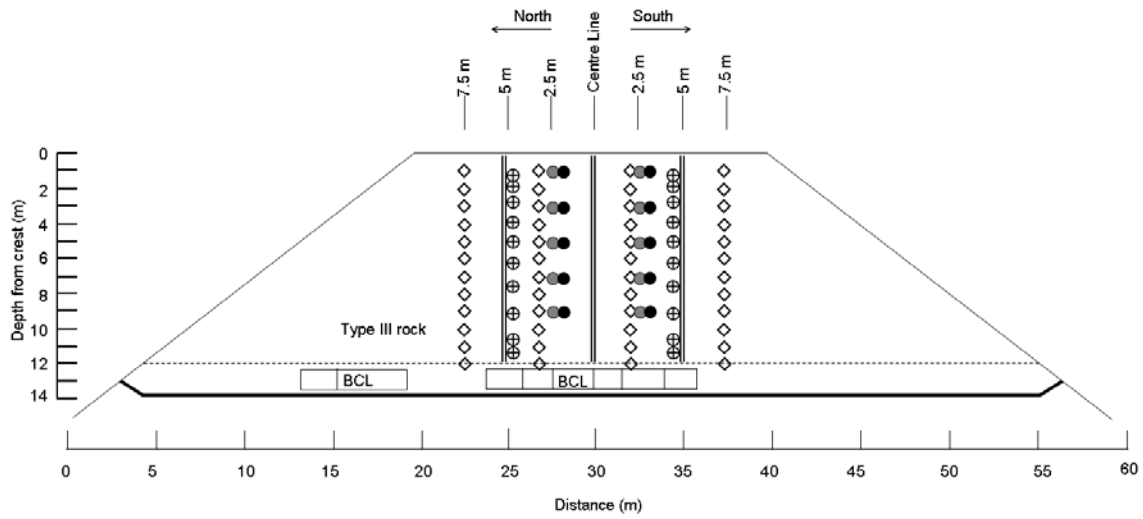
Figure A-14: Type III pile Face 3 dimensions and instrument distributions
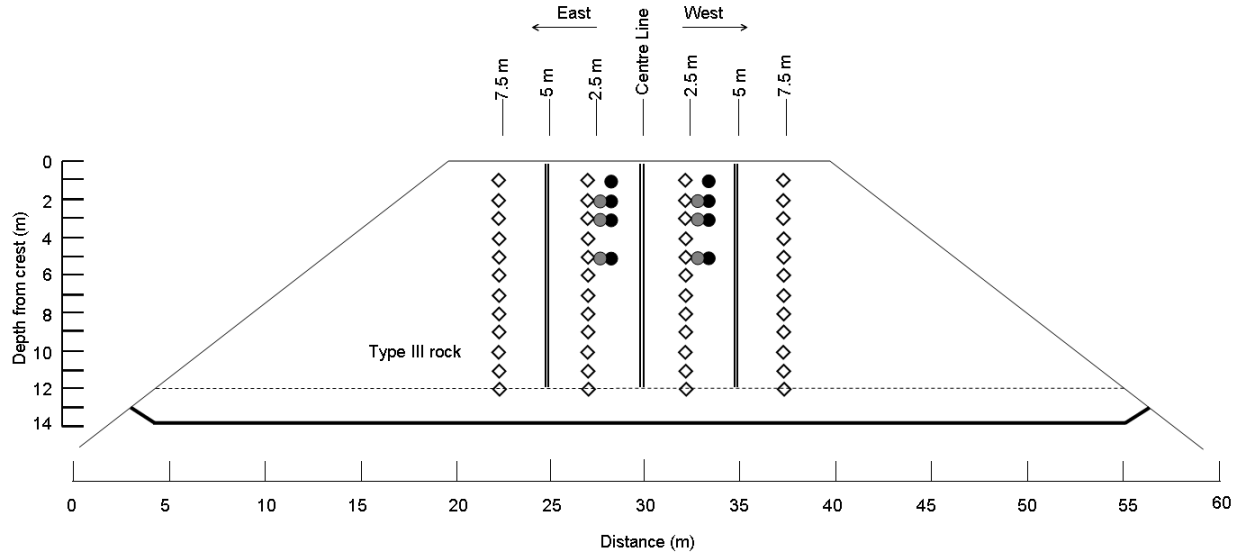

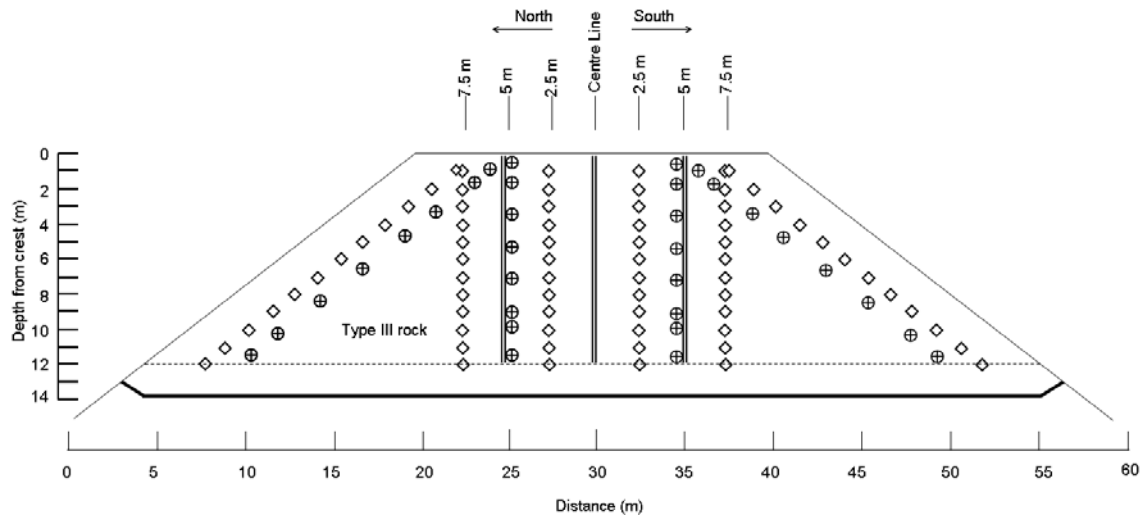**Figure A-15: Type III pile Face 4 dimensions and instrument distributions**
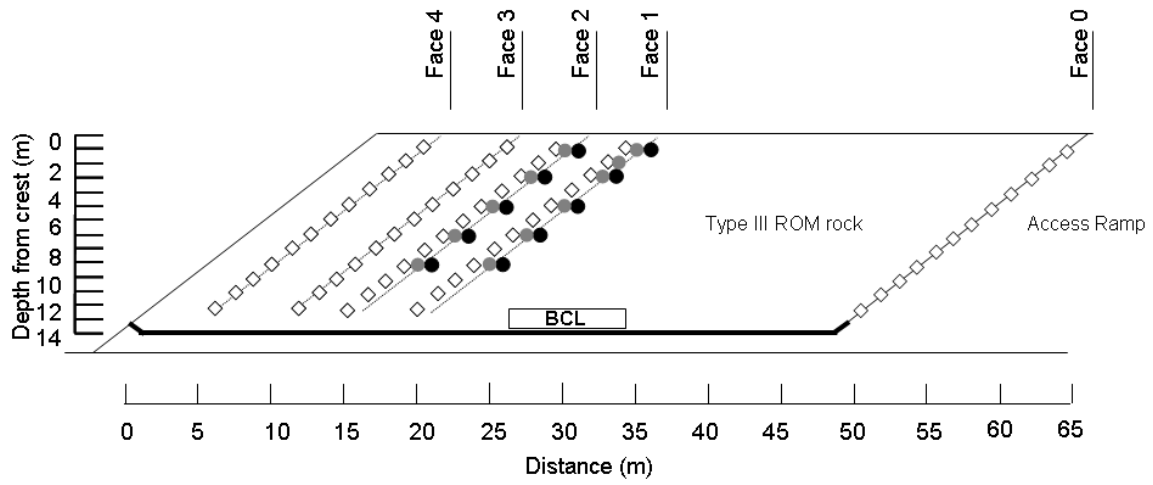
Figure A-16: Type III pile profile of SWSS, TDR and gas line distributions

A.4   Covered pile

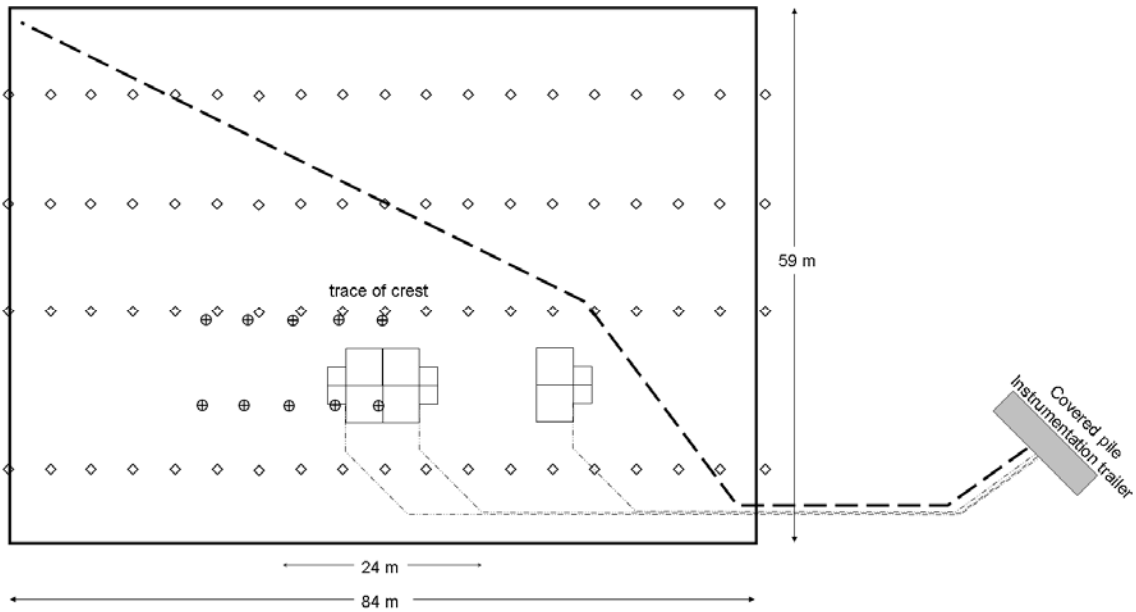**Figure A-17: Covered pile base dimensions and instrument distributions**

Figure A-18: Covered pile crest dimensions and instrument distributions
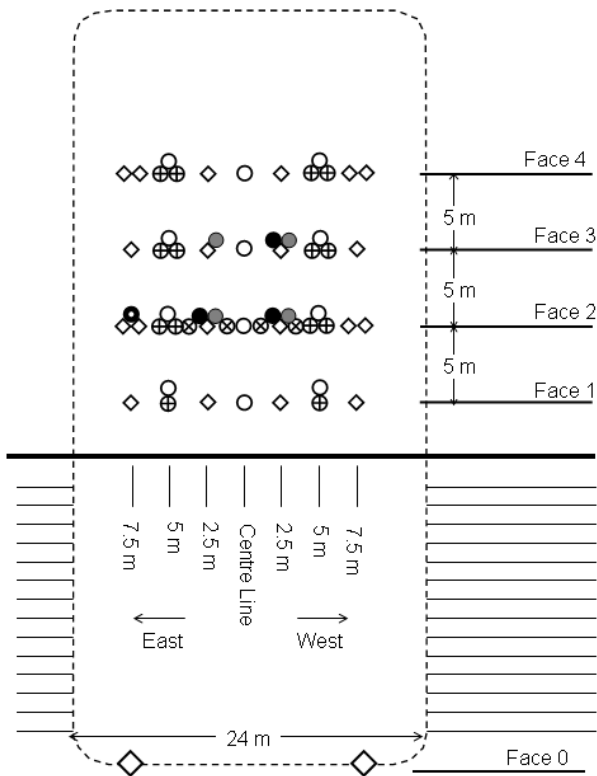

Figure A-19: Covered pile Face 0 (transition between access ramp and pile) dimensions and instrument distributions

Figure A-20: Covered pile Face 1 dimensions and instrument distributions

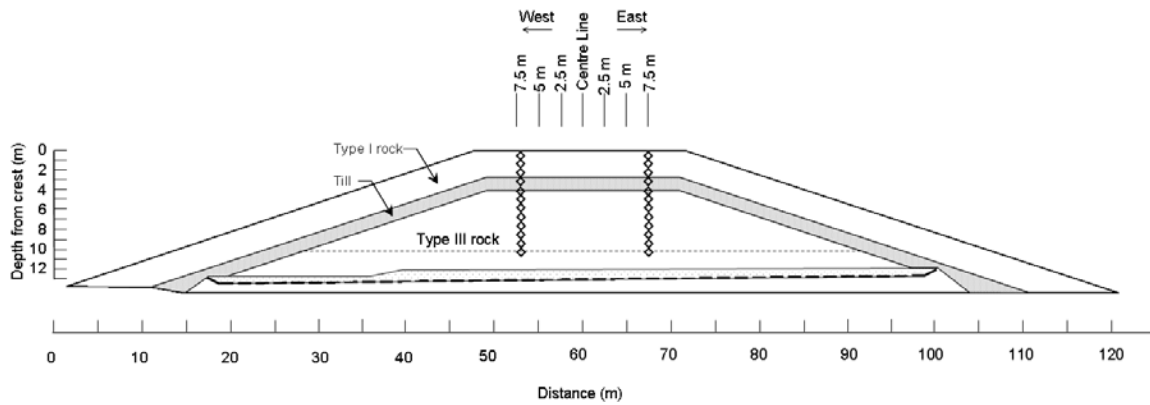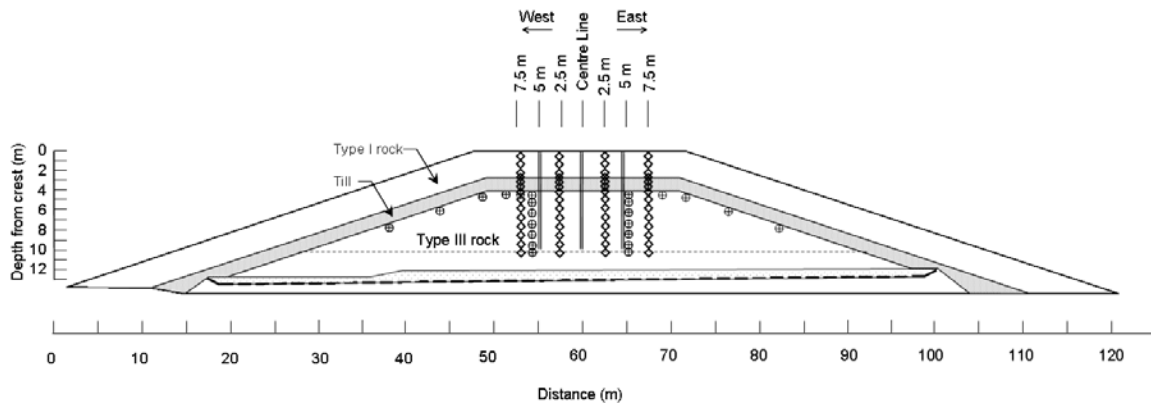**Figure A-21: Covered pile Face 2 dimensions and instrument distributions**
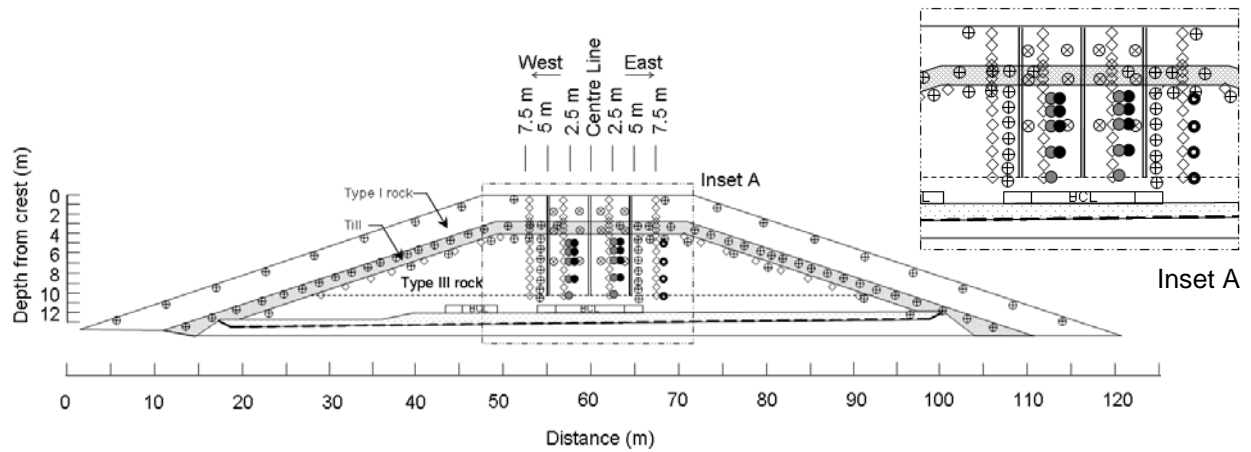

Figure A-22: Covered pile Face 3 dimensions and instrument distributions
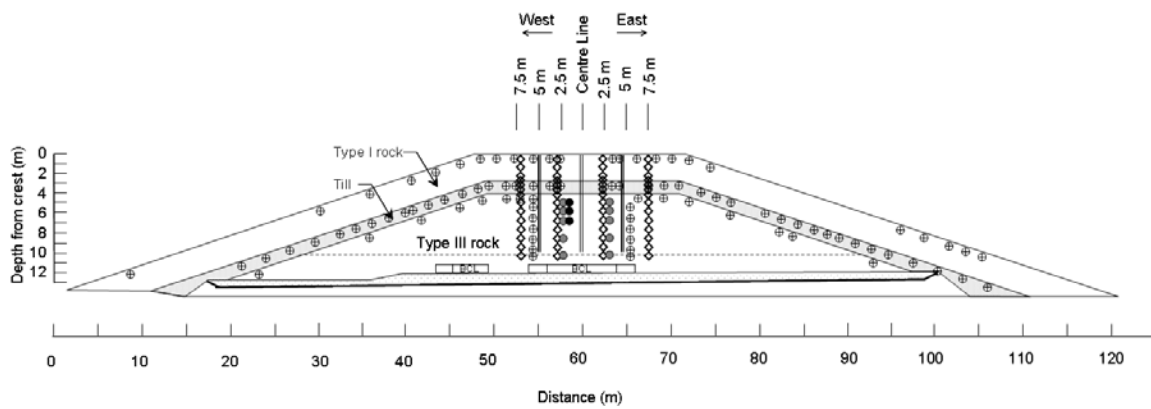
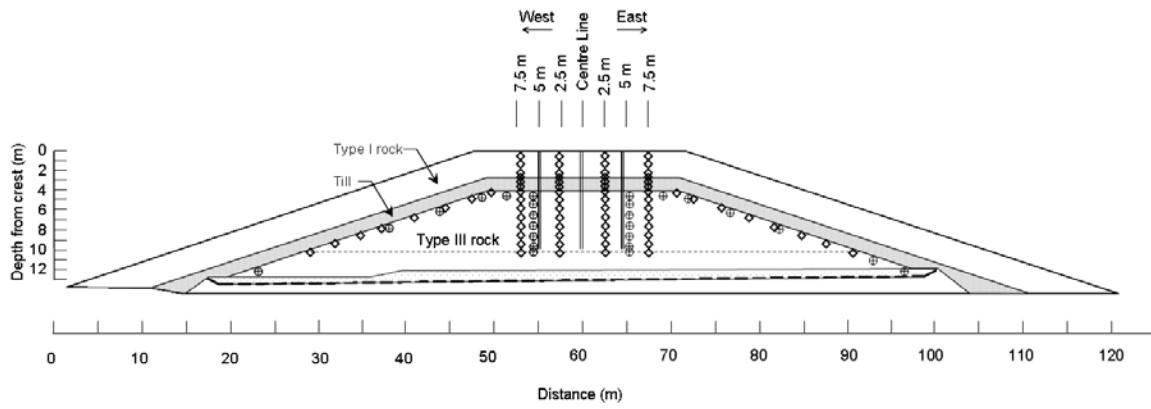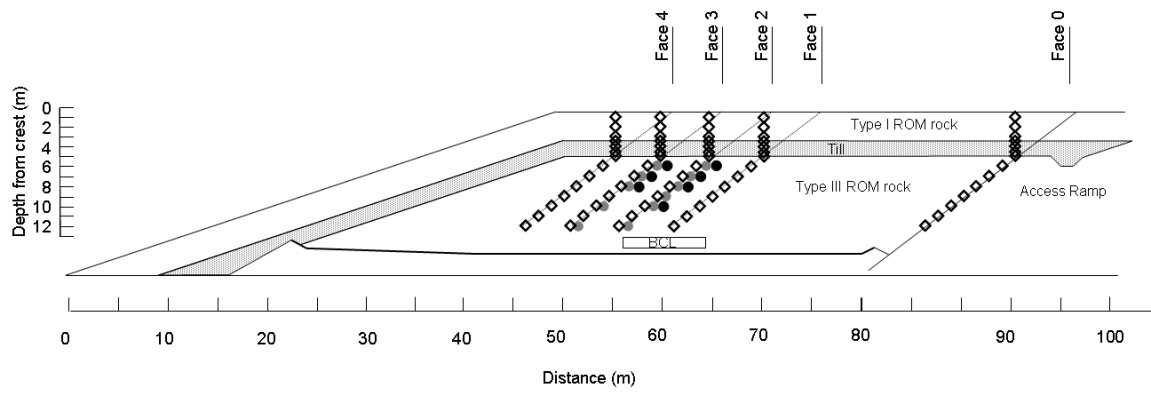**Figure A-23: Covered pile Face 4 dimensions and instrument distributions**

Figure A-24: Covered pile profile of SWSS, TDR and gas line distributions

Appendix B   **Blast pattern sulfur calculation method**

B.1 Introduction

At the Diavik mine site, the waste rock is segregated operationally based on target sulfur content into Type I (target <0.04 wt % S), Type II (target 0.04 to 0.08 wt % S) or Type III (target >0.08 wt % S), and stockpiled in separate areas. To determine mineable units of waste rock type depth integrated samples of blast hole cuttings from each blast hole in a blast pattern is assayed on-site. Samples are dried in an oven at 105°C for 2 to 4 hours. Cooled samples are crushed and homogenized. Aliquots of 0.26 +/- 0.01 g of pulverized samples are analysed using a LECO IR-432 Sulfur Determinator. The equipment is calibrated using seven calibration standards with the three closest to the average sulfur content used for calibration. A minimum of seven sulfur blanks are run per day. Sulfur standards are run every tenth sample run and sample duplicates are run randomly.

Site geological technicians produce dig maps of waste rock type based on the spatially-distributed sulfur assay results (Figure B-1). Operations loads and hauls the wastes rock to the designated storage or construction area, depending on waste rock type. Both 240 tonne (average of 90 tonne or 80 m^3 payload) and 100 tonne (40 tonne or 32 m^3 payload) trucks are used to haul waste rock.

B.2 Calculation method

Blast pattern average sulfur concentrations were calculated from best available data. Data required to calculate blast pattern average sulfur concentration for a test pile instrumentation face included maps delineating waste rock type areas within blast patterns ("dig maps"), sulfur analyses for individual blast holes within each waste rock type area of the dig map, and haul tracking sheets to determine the volume of material from each blast pattern delivered to the test piles.

The assayed sulfur concentration for each blast hole in the target area of the dig map was averaged to provide an average sulfur concentration for the waste rock type area in the blast pattern (Figure B-1). Haul loads from 220 tonne and 100 tonne trucks were used to calculate the volume hauled to the test pile face from the dig area. Where two or more blast patterns provided material for construction of a test pile face, the weighted average was calculated from the number of loads from each blast pattern and the average sulfur concentration of the dig area within the blast pattern. Where a single blast pattern had two target areas of the same waste rock type the average sulfur concentration of the two areas was used as the blast pattern average sulfur concentration. Where no haul load information or blast hole sulfur information was available the available data only was used to calculate the average (Table B-1 and Table B-2)

B.3 Tables

Table B-1: Haul load tracking and dig area wt. % S for blast pattern dig areas by Pile and instrumentation face. The dig area wt. % S was calculated from blast hole assay data for a given dig area(s) in the specified blast pattern.

Pile/Face	Pattern number	No. Loads from 240 tonne haul trucks	No. loads from 100 tonne haul trucks	Total m^3	Dig area wt. % S
Type I pile					
Base	A21 portal	0	54	1728	not available
Base	290-034	64	2	5184	0.0158
Base	300-049	4	0	320	0.0134
Base	300-051	4	0	320	0.0142
Base	300-052	12	0	960	0.0089
Face 1	280-040	4	0	320	0.0147
Face 1	280-018	22	1	1792	0.0153
Face 1	290-037	3	0	240	0.0101
Face 2	280-047	14	5	1280	0.0094

Face 2	290-039	16	1	1312	0.0169
Face 3	290-047	10	0	800	0.0139
Face 3	280-051	11	3	976	0.0123
Face 4	No record	No record	No record	-	-
Face 5	280-061	40	0	3200	0.0073
Face 5	290-044	2	0	160	0.0342
Face 5	290-049	12	0	960	0.00614
Type III pile					
Base	300-050	55	38	5616	0.0555
Base	300-048	0	12	384	0.0121
Base	300-BENCH	0	23	736	not available
Face 1	290-035	11	0	880	0.0422
Face 1	290-037	99	0	7920	0.0680
Face 2	280-044	18	0	1440	0.0713
Face 2	290-040	12	0	960	0.0393
Face 3	290-041	11	0	880	0.0372
Face 3	290-043	2	0	160	0.0242
Face 4	280-051	10	0	800	0.0606
Face 4	290-047	12	5	1120	0.0670
Face 4	290-034	4	0	320	0.0507
Face 5	280-058	36	12	3264	0.0143
Face 5	280-059	6	0	480	0.0629
Covered pile					
Base	290-041	41	0	3280	0.0372
Base	290-043	24	0	1920	0.0242
Base	280-036	27	0	2160	0.0210
Face 1	260-003	0	5	160	0.0790
Face 1	280-051	1	0	80	0.0606
Face 1	280-052	41	16	3792	0.0744
Face 1	290-047	0	45	1440	0.0670
Face 2	260-003	0	4	128	0.0790
Face 2	280-054	0	4	128	0.0385
Face 3	270-003	0	15	480	0.0623
Face 4	280-064	13	0	1040	0.0684
Face 5	270-009	31	3	2576	0.0482

Table B-2: Weighted average wt. % S by instrumentation face based on dig area and blast hole sulfur data

Pile/Face	Weighted wt. % S
Type I pile	
Base	0.0146
Face 1	0.0147
Face 2	0.0132
Face 3	0.0130
Face 4	not available
Face 5	0.0080
Type III pile	
Base	0.0528
Face 1	0.0654
Face 2	0.0585
Face 3	0.0352
Face 4	0.0624
Face 5	0.0205
Covered pile	
Base	0.0290
TCF1	0.0724
TCF2	0.0588
TCF3	0.0623
TCF4	0.0684
TCF5	0.0482

B.4   Figures

Figure B-1: Plan dig map for blast pattern number 280-044. All blast patterns in waste rock are 10 m in vertical extent. The size (volume) of the blast pattern and dig areas are typical of operational blast patterns and dig maps. Alpha-numeric codes are blast hole identification numbers and indicate blast hole location. Pink represents Type I sulfur range (< 0.04 wt. % S), blue represents Type II sulfur range (0.04 to 0.08 wt. % S), and yellow represents Type III sulfur range (> 0.08 wt. % S). Notice the two areas of Type I within one blast pattern. The average of all Type I material was calculated for any Type I loads delivered to the test piles from this pattern, consistent with other blast patterns that had two Type I or Type III areas within a single blast pattern.